Photo-electrochemical processes at the triple phase boundary

Collins, Andrew

Award date:
2012

Awarding institution:
University of Bath

Photo-Electrochemical Processes at the Triple Phase Boundary

Andrew Martin Collins

A thesis submitted for the degree of Doctor of Philosophy

University of Bath
Department of Chemistry

March 2012

Copyright

Andrew M Collins

“Facts are stubborn things; and whatever may be our wishes, our inclinations, or the dictates of our passion, they cannot alter the state of facts and evidence.”

John Adams, December 1770.

US Diplomat, Politician and President, 1735 - 1826

Outlook

The main aim and ultimate final goal of the work carried out in this thesis is a drive towards a feasible system for light harvesting, which is in short, using the Sun's energy to create electricity or a fuel for our energy requirements here on Earth. This work will see an approach using the triple phase boundary afforded by a microdroplet array. Although light harvesting is an ambition which has seen decades of work and uncountable man-hours, approaching it from the angle of utilizing the triple phase boundary between two immiscible liquids and a solid electrode is a new, and novel concept.

Before any attempts towards a light harvesting technique can be made, we will need to have characterized and fully understood the mechanisms and nuances, both for dark and light processes, that are observed at the triple phase boundary. This initial process will start by selection of a suitable redox molecule, and exploring its reactivity in microdroplets under dark conditions. Once this has been achieved, an attempt can be made to use this knowledge, and implement it towards light harvesting. This will eventually include an attempt to couple photo-excited states with other molecules, this will be an important step if energy is ever able to be stored from such a system.

This early phase will also see the need to employ many other techniques other than electrochemistry in an effort to aid in the understanding and characterization of the triple phase boundary at microdroplets. This will include travelling to other laboratories in search of specialized scientific skills and apparatus, such as electron paramagnetic resonance, or photocurrent spectroscopy. It will also see the need to build new equipment needed to conduct tests such as surface tension visualization, or new electrochemical cells for photocurrent measurement.

In summary, this report will see initial characterization of the processes, both light and dark, that occur within the triple phase boundary of a microdroplet for a given redox molecule dissolved within. Early attempts at coupling excited states with other molecules are also explored. Serendipity has always played a part in scientific discovery and the work outlined in this report was no different. The choice of oil used for the organic phase microdroplet deposits yielded some interesting and unexpected results, and has been implicated as one of the key aspects of the photoreactions that have been explored.

Chapter 1 - Introduction

Chapter 1

Introduction

1.1 - Introduction to Electrochemistry

Let us first consider the question, "what is electrochemistry?"

Deceptively simple in nature, this question would likely require volumes to adequately answer, but we can start by saying that it is a division of science concerned with the study of the combining of electricity and chemical systems. These can range from the more obvious avenues such as batteries[(1)(2)(3)] and blood glucose meters[(4)], to more specialized fields such as solar cells[(5)(6)(7)], electro-deposition[(8)(9)], extraction of metals[(ni10)], sensing devices -medical[(11)(12)] and industrial[(13)]-, corrosion analysis[(14)(15)], kinetic studies[(16)] and water purification[(17)(18)] to name a few.

Essentially, electrochemistry is the study of charge transfer reactions. This charge transfer normally occurs as transfer of an electron between an electrode in the solid state, and the species that undergoes oxidation and/or reduction; this species is normally in the solution phase, which would typically contain an ionic species. The ionic species is present in order to be able to conduct charge and provide a path of little electrical resistance in order to allow the desired electrochemical reactions to take place[(19)]. The electrode can be made up of a variety of conducting materials, from metals -both solid[(20)] and liquid[(21)]- carbon based such as graphite[(22)] or

diamond[23] to semiconductors[24]. Once an oxidation or reduction takes place, there is an imbalance of charge, and in order for electro neutrality to be conserved a total of two half reactions must occur[25]. Generally speaking, only one of these half-reactions is of experimental interest and this one is said to occur at the working electrode[25]

1.2 – Electrode Potential

Let us first consider the effects that occur when a metal is exposed to an electrolyte under no other external influences such as application of potential.

If we consider a metal, M, immersed in an aqueous electrolyte solution containing metal ions of the metal (M^{z+}), an exchange will occur between the metal lattice atoms and ions in solution. At first, before equilibrium is established, one of these exchanges could occur at a faster rate than the other. For this example, let it be assumed that metal ions leaving the lattice occurs at a faster rate than M^{z+} entering the lattice [26]

(Equation 1)[26] $M \rightleftarrows M^{z+} + ze^-$

As a result of the metal leaving, z electrons are left behind in the lattice; this builds up a negative charge on the metal. Proceeding with the assumption that the solution is the metal salt MA, the M^{z+} ions will be attracted to the interface of the metal, and consequently repels the A^- ions. As a result of the imbalance of charge at the interface, the solution therefore acquires a charge of opposite sign, but equal

magnitude and this is given the symbol q_s^+, and is defined as "the charge per unit area on the solution side of the interface" [26]. Consequently this positive charge has the effect of slowing the release of M^{z+} ions from the metal and also increasing the rate at which M^{z+} ions enter the metal lattice; thus a dynamic equilibrium is reached [26].

(Equation 2) $$M^{z+} + ze^- \rightleftharpoons M$$

The interface is neutral at equilibrium. This means the charge of the metal lattice and solution are of equal magnitude, but opposite signs [26].

(Equation 3) $$q_M = -q_S$$

The change in potential across the metal and solution as a result of the electron transfers - termed a potential difference- is given the symbol $\Delta\phi$ (M, S) [26]

(Equation 4) $$-\Delta\phi\ (M, S) = \phi_M - \phi_S$$

In order for a value for this potential to be recorded it must be measured with reference to another potential interface as part of a whole circuit. A problem with this arises in that the other electrode necessary to provide the completed system will also include a potential drop, thus the voltage value will include both potential drops. One is generally only interested in the reaction occurring at one of the electrodes, therefore the system is standardized by the utilization of a reference electrode, which has a constant and known potential [26] [27]. As the potential of the reference is constant, we

can therefore correctly assign any observed changes in current to the working electrode -where the reaction of interested in occurs-[27].

The reference is given by a variety of methods, and involves the reference electrode being its own half-cell where the known processes can occur[27]. One such method is the standard hydrogen electrode (SHE) and by convention the potential of the system is taken as 0V relative to SHE. The SHE is utilized due to the fact that it is very consistent, and variances between different hydrogen electrodes are only in the order of approximately 10μV[25].

One of the other popular reference electrodes utilized, and the one utilized throughout most of this report, is the saturated calomel electrode (SCE)[25]. The SCE uses a potassium chloride solution as the electrolyte of the cell, in which the reference reactions occur. These are between Hg(vi) (as part of the mercury(vi) chloride compound) and free elemental mercury[25]. It has a potential of 0.242V *vs.* SHE.

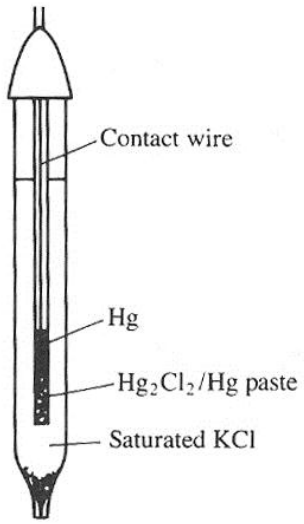

Figure 1 - Representation of a saturated calomel reference electrode (SHE) [25].

The potential of the system is measured in volts (V). If the value is large, it indicates that a given number of electrons are able to do a large amount of electrical work, whereas if the value is small, a small amount of work is done by the same number of electrons[26] (given no other variables).

If the metal ions are the only source of electrical current, i.e. no current is being passed through the system, then the Nernst equation shows that the equilibrium potential is governed by the composition of the cell [28].

(Equation 5) $E = E^0 + (RT/zF) \ln a(M^{z+})$

E^0 = Standard electrode potential
R = Gas constant
F = Faraday constant
$a(M^{z+})$ = Activity of the ion

This equation is related to the Gibbs free energy of the cell potential, and can be used to calculate thermodynamic properties [28].

The Gibbs free energy is given by[25] -

(Equation 6) $\Delta G = -nFE$

Where n is the stoichiometric number of electrons transferred.

1.3 - Application of Potential

It can be seen that the ΔG term in equation 6, can be influenced by the electrode potential and hence controlled by the application of potential to the system. Up until now we have discussed the system with no current flowing through it as a result of outside intervention. The reference allows one to accurately drive the working electrode to more negative or positive potentials than the equilibrium potential of the cell; this can then allow an exchange of electrons to be facilitated to redox active molecules at the electrode. This can proceed in both oxidative or reductive directions -molecules in solution can either lose or gain electrons from the metal working electrodes-[27].

1.3.1 - Fermi Levels

By applying a potential to the electrode we are altering its Fermi level, and it is because of this that the transfer of electrons can take place so readily. A metal consists of an ordered array of atoms. In this lattice the electron orbitals overlap and this has the effect of allowing the electrons of the metal ions to move freely within the lattice. The electrons reside in the energy states of the metal up to a finite point that is referred to as a Fermi level. The act of applying a potential to the metal can either raise or lower this energy level [27].

Let us take a generic electrochemical example to illustrate these points and how they influence the reactions. A reactant R is in solution, and has a highest occupied molecular orbital (HOMO) below the metal electrodes Fermi level, and a lowest

unoccupied molecular orbital (LUMO) above the metals Fermi level, this situation is shown in figure 2a. In order for the reactant molecule R to be reduced and gain an electron, the Fermi level of the metal must be at a higher energy level than that of the LUMO of the reactant[27]. By the application of a negative potential to the metal (figure 2b) the metals Fermi level is increased to a point where the electron transfer is thermodynamically favourable. This then causes a reduction current that passes from the electrode to the reactant in the electrolyte, causing reduction of the R. If a more negative potential is applied to the metal, the rate at which the reduction of the reactant takes place will increase[27].

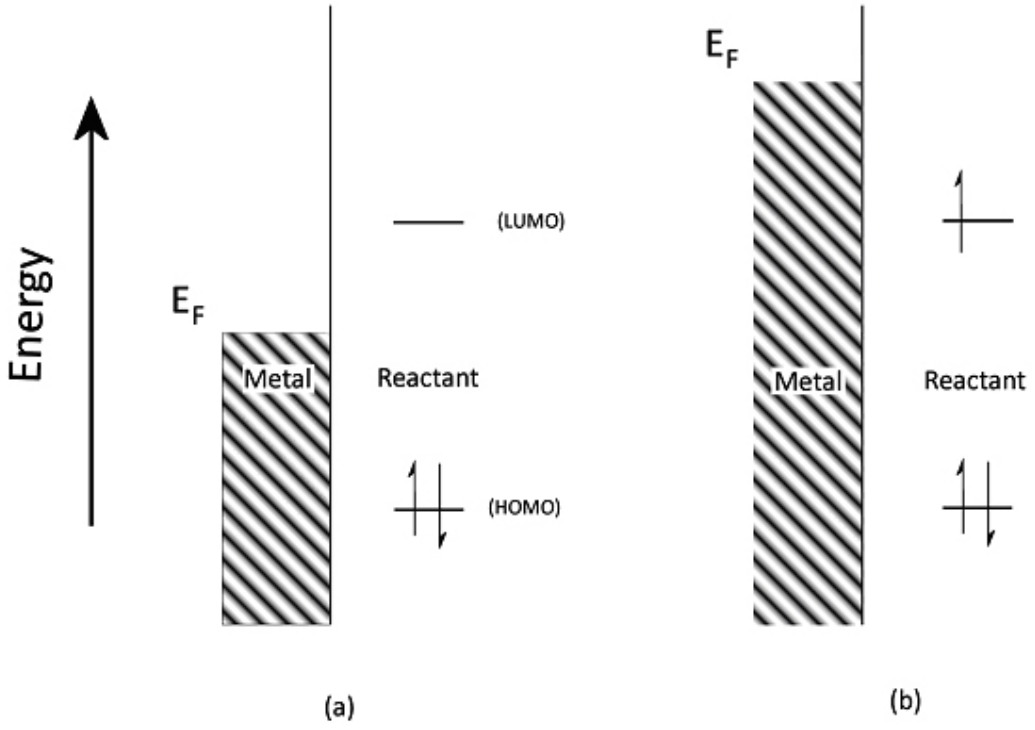

Figure 2 – Illustration of how application of a reductive potential can alter the Fermi level of an electrode and therefore facilitate electron transfer.

If we were to take a different scenario with a reactant that can be oxidized, then the application of a positive potential to the electrode would effectively lower the energy level of the electrons in the electrode, and thus induce a movement of electrons from the reactant in the solution phase to the electrode. This creates an oxidation current and the reactant molecule will be oxidized at the electrode surface[29].

The total current (I) produced as a result of this oxidation or reduction is given by equation 7, where A is the electrode area (cm^2), F is the faraday constant and j is the flux[27]. Flux is a quantity that can be described as the amount of substance reacting at the area of the electrode per second, and thus the rate at which the electrochemical reaction proceeds. As such, it is ‘‘described by a rate law, not dissimilar in form from those commonly encountered in homogenous kinetics’’[27]. This is shown in equation 8. It is important to remember that the concentration term in equation 8 refers only to the surface concentration of the electro-active species; this is because the electrochemical reaction converts the reactive species at the electrode surface and thus the concentration therein becomes lower than that in the bulk solution [27].

(Equation 7) [27] $i = AFj$

(Equation 8) [27] $j = k_0[R]_0$

The value for current is essentially the rate of flow of electrons in the system. The SI unit for current is the Ampere (A) and one Amp, is given by a rate of flow of one coulomb per second. Coulombs are a measure of charge, and this can be used to measure the total number of electrons transferred in the system. One coulomb is equal to 6.24×10^{18} electrons, and Faraday’s law allows us to understand the connection

between the amount of product formed and the charge transferred, in that 96485 coulombs transferred will consume one mole of reactants to form one mole of products -assuming a one electron transfer- [29].

1.3.2 - Overpotential

As has been discussed earlier we know that if we apply a potential which is different to the equilibrium potential of the cell, we can induce a current flow and therefore electrolysis of the given species. The variance from the equilibrium potential as a result of the applied potential is termed the overpotential (η), and is given by equation 9 [27].

(Equation 9) $$\eta = E - E_0$$

The amount of electrochemically generated current as a result of overpotential is affected by whether the reaction is reversible or irreversible. For a reversible system relatively little overpotential is required to facilitate the reaction and current flows easily, compared to an irreversible system where comparatively more overpotential is needed to generate the same amount of current and make the reaction possible[27]. Reversibility of an electrochemical system is discussed in more detail in chapter 1.5.5 (*vide infra*).

1.3.3 – Butler-Volmer Model

The Butler-Volmer model is one of the most utilized models for the interpretation of electrode kinetics. The reaction coordinate for an electrochemical reaction, for example a reduction, can be viewed as two vibration parabolas (figure 3)[29].

Let us assume a generic oxidation for the purposes of this explanation:

(Equation 10)

$$O_{(aq)} + e^- \rightleftarrows R^-_{(aq)}$$

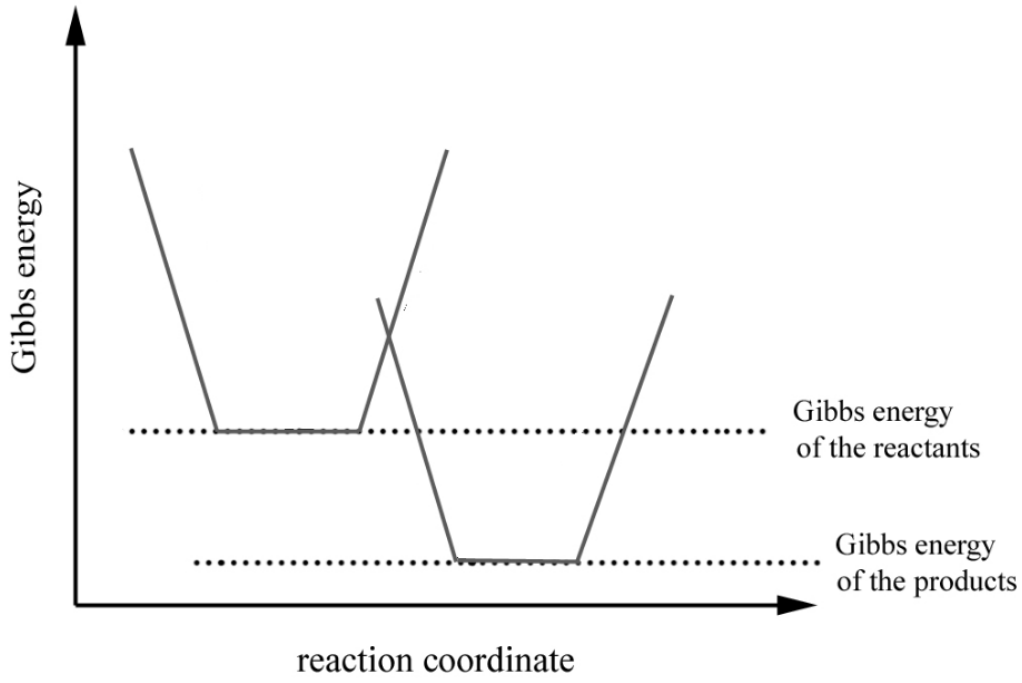

Figure 3 - Illustration of the reaction coordinate viewed as two parabolas showing the Gibbs energy of the reactants and the products.

The rate constant for the procession of this oxidation is given by equation 11[29].

(Equation 11)

$$k_{ox} = A_{ox}\, e\, (-\Delta G^{\neq} / RT)$$

Where G is the Gibbs energy, R the gas constant, T the temperature and A is a pre-exponential factor. The rate constant for the corresponding reduction would follow the same format but with its own pre-exponential factor and change in Gibbs energy.

The mathematical expression for the rate constant can be re-written if the activation parameter is known, by substitution of the Gibbs energy term, as equation 12[29].

(Equation 12)

$$k_{ox} = A_{ox}\, e - [\, (\lambda + F\eta)^2 / 4\lambda RT \,] \qquad \textit{for oxidation}$$

$$k_{red} = A_{red}\, e - [\, (\lambda + F\eta)^2 / 4\lambda RT \,] \qquad \textit{for reduction}$$

If we expand the square in the brackets of these equations we end up with the following.

(Equation 13)

$$(\lambda + F\eta)^2 = \lambda^2 + 2\lambda F\eta + F^2\eta^2 \approx \lambda^2 + 2\lambda F\eta$$

Using equation 13, it is possible to express the rate constants -both oxidation and reduction-. This leads to the following expressions, which form the basis for the Butler-Volmer expressions[27][29].

(Equation 14)

$$k^{ox} = A \times \exp\left[-\frac{\lambda^2 - 2\lambda F\eta}{4\lambda RT}\right] = A \times \exp\left[-\frac{\lambda}{4RT}\right] \times \exp\left[\frac{F\eta}{2RT}\right]$$

$$k^{red} = A \times \exp\left[-\frac{\lambda^2 + 2\lambda F\eta}{4\lambda RT}\right] = \underbrace{A \times \exp\left[-\frac{\lambda}{4RT}\right]}_{k_0} \times \exp\left[-\frac{F\eta}{2RT}\right]$$

Into these equations we can introduce a new term, α, known as the transfer coefficient, or symmetry factor. This is a measure of the shape of the parabolas. A value of less than 0.5 indicates a late transition state, whilst a value of more than 0.5 indicates an early transition state, this is shown in equation 15[29].

(Equation 15)

$$k^{red} = k_0 \times \exp\left[-\frac{1}{2}\frac{F\eta}{RT}\right] = k_0 \times \exp\left[-\frac{\alpha F\eta}{RT}\right]$$

$$k^{ox} = k_0 \times \exp\left[\frac{1}{2}\frac{F\eta}{RT}\right] = k_0 \times \exp\left[\frac{(1-\alpha)F\eta}{RT}\right]$$

The current obtained from one of these reactions is directly proportional to the rate constant for the electron transfer reaction. An expression for the current obtained is expressed in equation 16[29].

(Equation 16)

$$I^{red} = k^{red} F\, c_{ox}\, A$$

$$I^{ox} = k^{ox} F\, c_{red}\, A$$

Substituting into equation 15 for the rate constant gives equation 17. These expressions for current are commonly referred to as the Butler-Volmer equations[29].

(Equation 17)

$$I^{red} = AFc_{ox} \times k_0 \times \exp\left[\frac{-\alpha F \eta}{RT}\right]$$

$$I^{ox} = AFc_{red} \times k_0 \times \exp\left[\frac{(1-\alpha) F \eta}{RT}\right]$$

They can be combined to form the total current which is defined as equation 18

(Equation 18)

$$I = I^{ox} - I^{red} = AFc_{red} k_0 \exp\frac{(1-\alpha) F \eta}{RT} - AFc_{ox} k_0 \exp\frac{-\alpha F \eta}{RT}$$

1.4 - Interface at the Electrode Surface

The interface at the electrode surface between the electrode itself, and the aqueous electrolyte is said to be comparable to that of a capacitor, figure 4. A capacitor can be defined as a circuit with a break in it consisting of two conducting plates separated by a dielectric material. The behaviour of a capacitor can be described by equation 19 where q defines the charge stored across the capacitor (C), E describes the potential applied across the capacitor (V), and C being the capacitance which is measured in Farads, (F)[27].

(Equation 19) $q/E = C$

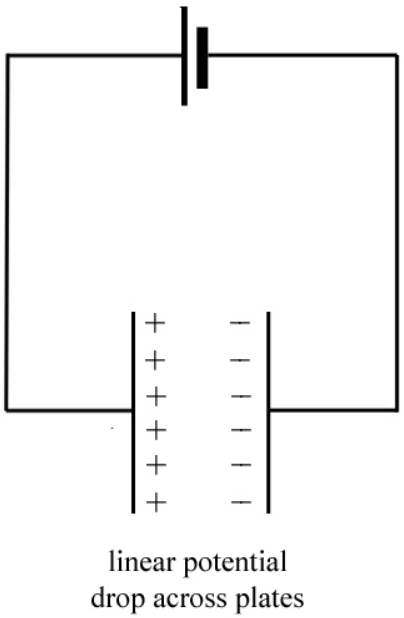

Figure 4 - Illustration of a capacitor showing two charged capacitor plates that incur a linear potential drop between them.

When charge is passed through a capacitor, there is a flow of current which will precipitate an imbalance on the plates, consisting of an excess of electrons on one side and a deficit electrons on the other plate[29]. The interface between the electrode and the solution can be shown to act in a similar fashion to that of a capacitor, as when a potential is applied at the electrode, a charge will be present on the electrode with an equal but opposite charge present in solution. The charge on the metal is defined as q_M and the charge in solution is defined as q_s, *vide ante*. Charge density (σ^M, C/cm^2) is calculated by dividing the charge present by the area of the electrode. The charge present in the solution will exist as an excess of cations or anions depending on whether the charge present at the electrodes surface is composed of an excess or lack of electrons.

This system, existing at the metal electrode | electrolyte solution, is referred to as the electrical double layer[29]. It is worth noting that unlike normal capacitors, the capacitance of the electrical double layer is seen to vary with applied potential, whereas with normal capacitors, capacitance values are independent of the potential applied to the circuit[29].

1.4.1 - Helmholtz Model

Helmholtz proposed the first model to describe the electrical double layer seen at the interface of the electrode-solution[27]. It is assumed that at the electrode itself, no electron transfer reactions occur. As a result of the increased or deficiency in charge on the electrode surface, a reorientation of dipoles of the molecules in the solution or a reorganization of the electrolyte ions at the interface itself will occur. Helmholtz predicted that the charge imbalance present at the electrode would be completely

counteracted by a single layer of counter ions situated at what is now known as the Outer Helmholtz Plane (OHP)[29]. These counter ions are assumed to have a monolayer of solvation present and thus can approach the electrode surface up to a distance as allowed by the solvation layer. For the purposes of this report, let us consider this distance $\chi_{OHP.}$ The Helmholtz model suggests that the ions from the solution completely balance out the charge present on the electrodes surface. The potential drop between the electrode and the OHP was assumed to be linear, as the electrolyte layer at the OHP balances out the charge on the electrode completely [27][29]. The Helmholtz double layer model is illustrated in figure 5[27].

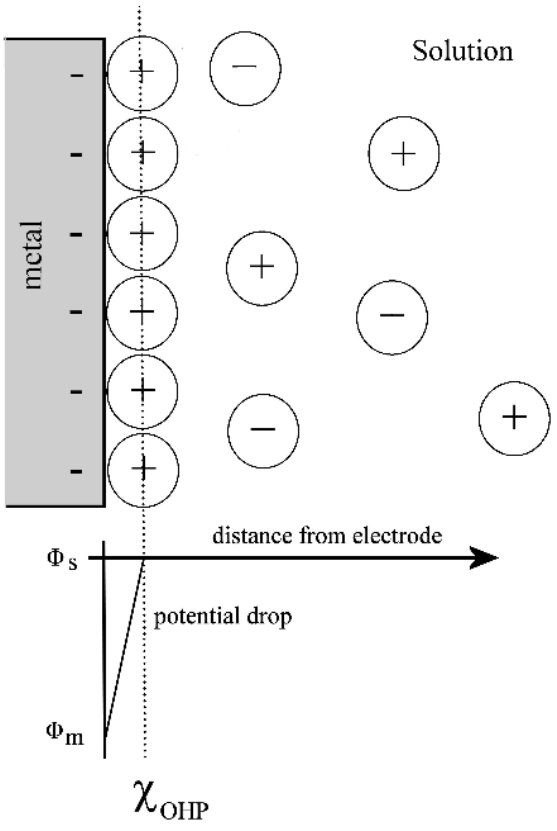

Figure 5[27]- Illustration of the Helmholtz model for the interface between a charged metal electrode and the electrolyte solution

1.4.2 - Gouy and Chapman Model

The model for the double layer proposed by Helmholtz was a simplistic one, and over the years from his initial proposition of the idea (in 1853) [27] revisions and new facts were added to the theory of the double layer. One of these was conducted by Gouy and Chapman, and was concerned with the effect that Brownian motion would have on the molecules of the solution. It was suggested that it was unlikely that the entire charge of the electrode would be balanced by solution ions present only at OHP.

The effect of Brownian motion within the solution would scatter some of the ions at the OHP leading to a gradual, but consistent, potential drop away from the electrode. This meant that the charge in the solution is spread over a larger volume than simply the OHP, the area at which the potential drop occurs in the solution layer could be viewed as a diffuse layer[27]. The actual thickness of this layer, would of course vary with concentration of the ions in solution, but for a electrolyte concentration of *ca.* 0.1M or above, the thickness would normally be in the order of approximately 100 x 10^{-10}m[29].

1.4.3 - Stern Model

A further revision on the these two models was proposed by Stern, this essentially taking the ideas of both theories and combining them. Stern accepted the effect that Brownian motion and thermal agitation would have on the solution ions at the OHP, but still retained the idea from Helmholtz theory that there would be a minimum distance of approach due to solvation of the ions in solution. He proposed that this would not lead to a steady potential drop from the surface of the electrode, but rather

one which would contain a linear drop up to the OHP, and then a gradual potential drop as we move away from the electrode and into the diffusion layer[27].

1.4.4 - Grahame Model

Yet another addition came from Grahame, and this was concerned with non-solvated ions present within the solution. He proposed that it was possible for a few solvated ions to loose their solvation shell therefore allowing these non-solvated ions to cross the threshold of the OHP, becoming specifically adsorbed onto the surface of the electrode at a closer distance. This new distance at which a non-solvated specifically adsorbed ion can approach is referred to as the Inner Helmholtz Plane (IHP). For the purposes of diagrams illustrating this, (see figure 6) the IHP is referred to as χ_{IHP}. This leads to a potential profile which includes two linear drops - one to the IHP, then one to the OHP- and then a gradual potential drop across the diffusion layer[29].

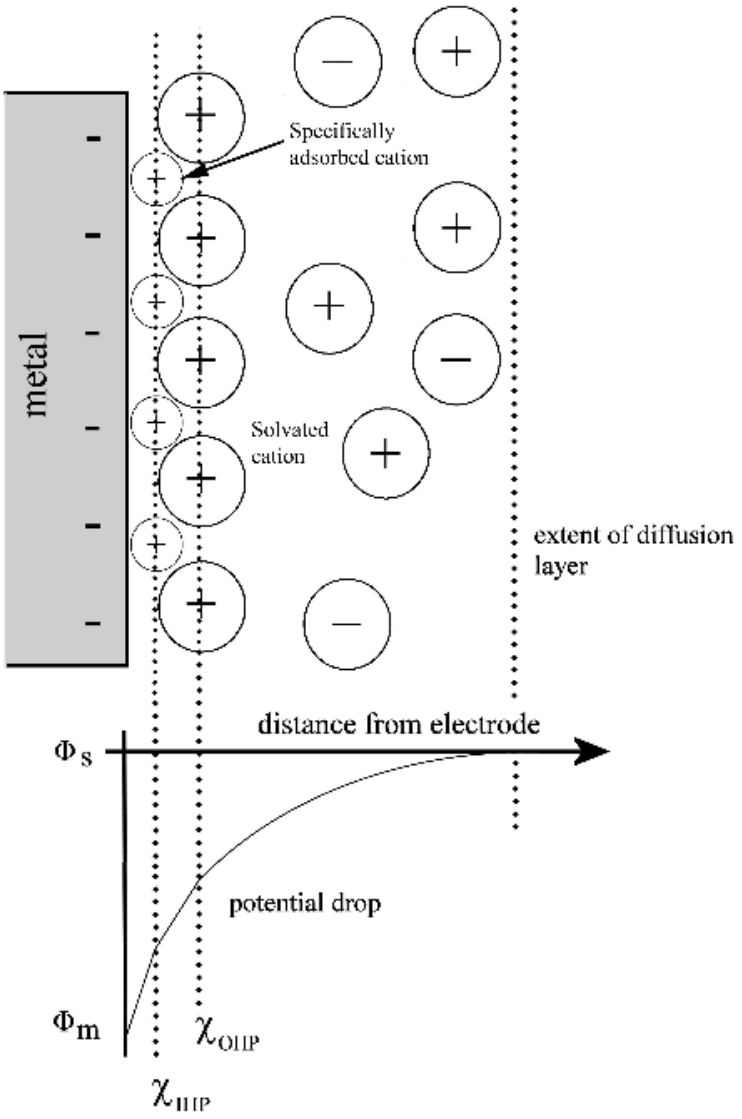

Figure 6[27] - Illustration of the Graham model of the electrode | electrolyte interface showing the electrical double layer and extent of the diffusion layer.

1.6 - Diffusion

Some 150 years ago, Adolf Fick was responsible for developing some of the first ground-breaking ideas on diffusion for species in a solution [30]. He showed that diffusion would take place down the concentration gradient (ie. from a high concentration to a low concentration) and that at any point (noted as *x*) along this one dimensional diffusion layer, there would be a diffusive flux, noted as *j*, (mole $cm^{-2}s^{-1}$), which is expressed in equation 20 and is known as Fick's First Law[31].

(Equation 20) $$j = -D (\delta c / \delta x)$$

The value for flux corresponds to the number of moles passing through a given unit area in a given time, $\delta c / \delta x$ denotes the concentration gradient at the point given by *x*. Finally D is the value for the diffusion coefficient (units of cm^2s^{-1}). The diffusion coefficient for the vast majority of solvents utilized during voltammetric processes has a magnitude in the region of 10^{-6} to 10^{-5} cm^2s^{-1} [31], although it should be noted that this value is temperature dependent. Another important point to note is that Fick's First Law assumes that no potential gradient effects exist, thus for the example illustrated for the diffusion layer, the diffusing species must be neutral for this equation to hold true [31].

Fick's Second Law delves into more detail, and considers what effect time will have on the concentrations of the diffusing species at point *x*. A way to visualize this is to imagine a stationary rectangular block within the solution with a width of δx. One can imagine a diffusing flux passing through this block in the plane of *x* [30].

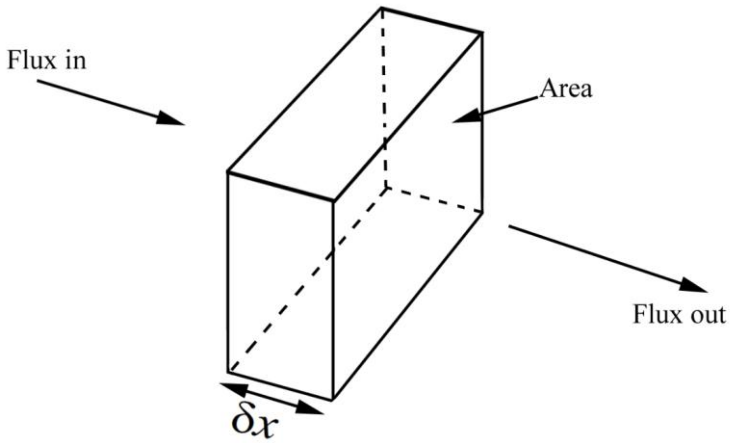

Figure 7 - Illustration of principles of Fick's second law, considering the effect of time upon the diffusion of a species through x.

If this idea is followed through mathematically, the expression for Fick's Second Law is eventually reached (for one dimension), as shown in equation 21[30]

(Equation 21) $(\delta c/\delta t) = D\,(d^2c/dx^2)$

It is possible to calculate the diffusion coefficient in a given system. Cottrell first considered this in 1902[30] with a potential step experiment. This is where we start an electrochemistry experiment with the electrode immersed in solution at a potential at which no charge transfer occurs. The potential is then instantly stepped to a potential well above the value at which the given species in solution will start to undergo oxidation/reduction. The oxidative or reductive process will occur at a very fast rate and thus the concentration at the electrode surface can be said to be zero. This will incur a diffusion layer through which fresh reactant from the bulk will need to diffuse through in order to reach the electrode. Cottrell devised an equation (equation 22) which showed that the current would fall during a potential step experiment in a

relationship that was inversely proportional to the square root of the time[30]. This relationship breaks down somewhat in the first few milliseconds of a potential step experiment, as the current at this stage is dominated by the fast electron transfer step. At this stage no diffusion needs to occur due to the plentiful supply of reactant at the electrode surface. In this equation, I refers to the current, A the electrode area, c^* the concentration of the solution[30].

(Equation 22) $$I = (nFA\sqrt{Dc^*})/\sqrt{\prod t}$$

In a potential step experiment as is described above, when the potential is driven to such a value that the concentration of the reactant species at or near the electrode surface falls to zero, the current reaches a limited value, as defined by the diffusion of the species shown in the Cottrell equation This limiting value is referred to as the limiting current[30]. An equation to describe the limiting current is shown as equation 23[27], where I_L is the limiting current, δ_d is the diffusion layer thickness and A the electrode area.

(Equation 23) $$I_L = (D_B FA[B]_{bulk}) / \delta_d$$

Nersnt was able to calculate a value for the diffusion layer thickness by extrapolation of the linear region of the diffusion layer thickness until this value reached the value of the bulk concentration. This is illustrated in figure 8[31].

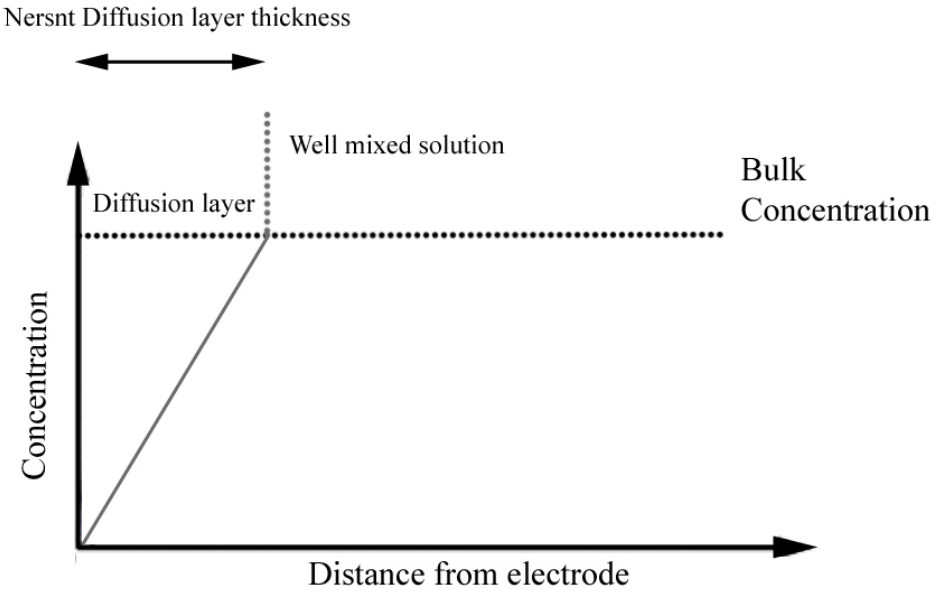

Figure 8 – Illustration of the Nernst Diffusion layer model

Nernst's model for the diffusion layer thickness is a basic one, as it assumes that the 'stagnant zone' of the diffusion layer and the well mixed bulk of the solution occur as two separate entities with a sharp transition between them, when in actual fact these are seen to merge into each other in a progressive fashion[(31)]. Nevertheless, this model can be used to calculate an estimate for the amount of flux approaching the electrode surface[(27)]. This is shown in equation 24[(27)]

(Equation 24) $$j_d = D_B ([B]_{bulk} - [B]_0) / \delta_d$$

1.6.1 - Forcing Diffusion

We have covered various aspects of voltammetry at stationary electrodes, and how the transport of fresh reactant to the electrode surface is perpetuated by diffusion through a concentration gradient set up by a diffusion layer. It is however, possible through convection -in this case forced- to minimize or almost completely remove the diffusion layer. For this type of effect a deliberate stirring or agitation of the electrolyte solution is performed in order to dominate the effects of mass transport through diffusion, and overwhelm these with forced convection. The term overwhelm, instead of replace, is deliberately used, as there will always be some mass transport diffusion type effects at very close distances to the electrode[31].

There are many ways to induce this forced convection, either by movement of the electrode itself or by inducing a movement in the electrolyte solution; these are known as hydrodynamic electrodes[27]. One of the most popular examples for illustrating this is the rotating disc electrode, but others include sono-voltammtery[32] and channel flow voltammetry[31]. Because the effects that are forcing these convections are controlled by the user (rotation speed and channel flow rate) the rates of convection can be altered, which will in turn alter the rate of mass transport to the electrode surface. This can provide diverse reaction timescales and give kinetic and mechanistic insights into the system. It also avoids problems that might occur at stationary electrodes in experiments such as running a very fast scan rate, which can create charging of the double layer capacitance, therefore resulting in warping of the data [31].

The rotating disc electrode set-up is simple, and incorporates an electrode immersed in solution, where the electrode is capable of being rotated along the axis of its length. Normally the rotation rate would be up to approximately 50Hz[31]. The diagram shown as figure 9 illustrates how the rotating disc creates a laminar hydrodynamic flow over the electrode surface.

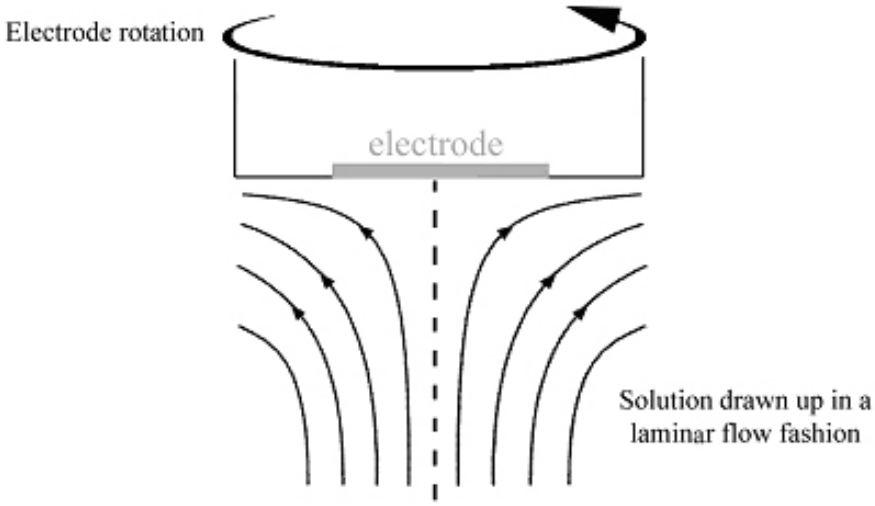

Figure 9- Schematic representation of a rotating disc hydrodynamic electrode. The rotation of the electrode causes a drawing up of the solution towards the disc and is then pushed outwards along the electrode surface. The flow of the solution is laminar.

1.5 – Electrochemical Cells and Voltammetry

There are two types of cell in which charge transfer reactions occur, one is the galvanic cell and the second is the electrolytic cell. In a galvanic cell, when the electrodes are connected by a conductor, the electrochemical reaction proceeds spontaneously. This type of cell is, for example, utilized when converting stored chemical energy directly to electricity[29]. The focus of this introduction will be concerned with the electrolytic cell. For this type of cell there is an application of potential at values greater than the open circuit potential (*vide ante*)[29].

Electrolytic experiments are normally conducted in a fashion that would normally consist of a three-electrode system, although this does not always have to be the case, and some alternatives are discussed in later chapters. The three electrodes consist of the working electrode (WE), counter electrode (CE) and reference electrode (RE) and these are immersed in an aqueous solution phase of conducting electrolyte [28]. Some other electrolytes are utilized in more specialized systems[28a], but for the purposes of this introduction we will consider an aqueous electrolyte.

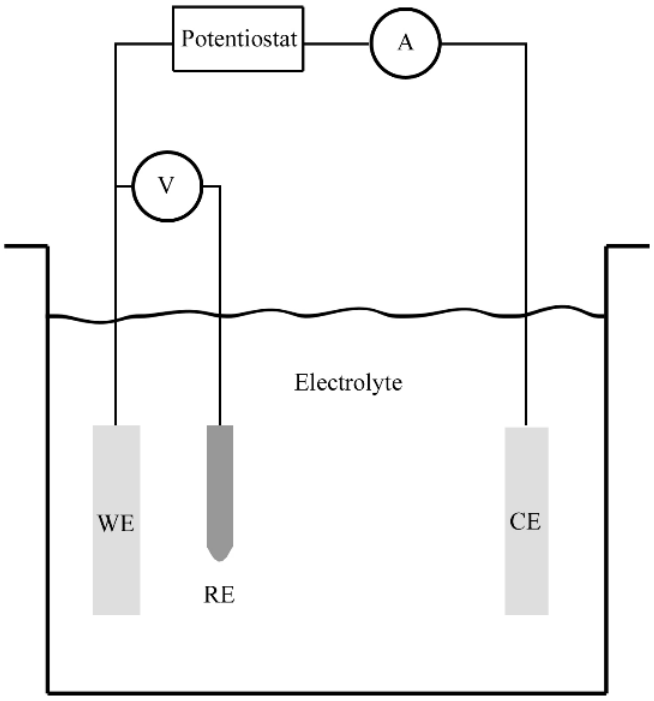

Figure 10 - A representation of a typical electrochemical cell, where WE, RE and CE refer to the working electrode, reference electrode and counter electrode respectively

Working electrodes must be chosen with the intended experiment in mind, as different materials have different properties, and one must select the working electrode that will best match the intended work. Such properties can include: what the range of useful potentials are, purity of the material, if anything will be immobilized on the surface and what solvent will be used in the experiment[(25)(31)]. The potential range to be used also influences other factors such as the stability of the supporting electrolyte under the desired conditions, solvent decomposition, and the possibility of electrode dissolution taking place [(25)].

1.5.1 - Cyclic Voltammetry

A very common method of electrochemical analysis is cyclic voltammetry. This is a technique that involves recording the current response of the system as a function of applied potential. This is a powerful analytical technique as it provides a large amount of data on a given system; from electron transfer data to kinetic processes occurring, and diffusion coefficients [29]. A linear sweep experiment is half of a cyclic voltammetry experiment. It begins at a starting potential E1 (this is normally chosen at a potential which does not incur a reduction or oxidation current for the species being studied) and ends at potential E2. At this point we will have arrived at a potential where electron transfer will occur rapidly for the system. Moving across the two potentials is undertaken over a set length of time, and this can be varied to suit the needs of the experiment and is referred to as the scan (or sweep) rate [25].

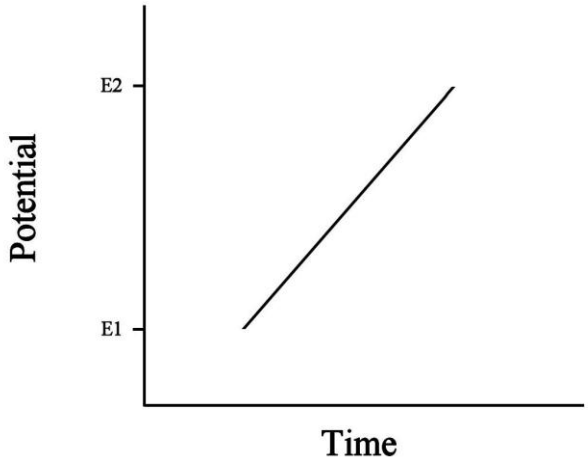

Figure 11 – Graph showing change in potential with time during a linear sweep voltammetry experiment.

Cyclic Voltammetry introduces a backwards sweep along the potential that was traversed in linear sweep voltammetry. After the potential reaches E2, it is then swept back to the starting potential, at the same rate as was used to traverse the forward direction. Figure 12 shows how potential varies with time under Cyclic Voltammetry.

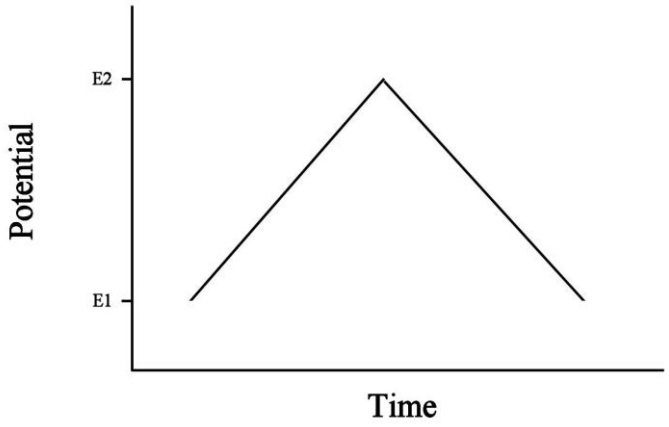

Figure 12- Graph illustrating how potential varies with time during a cyclic voltammetry experiment.

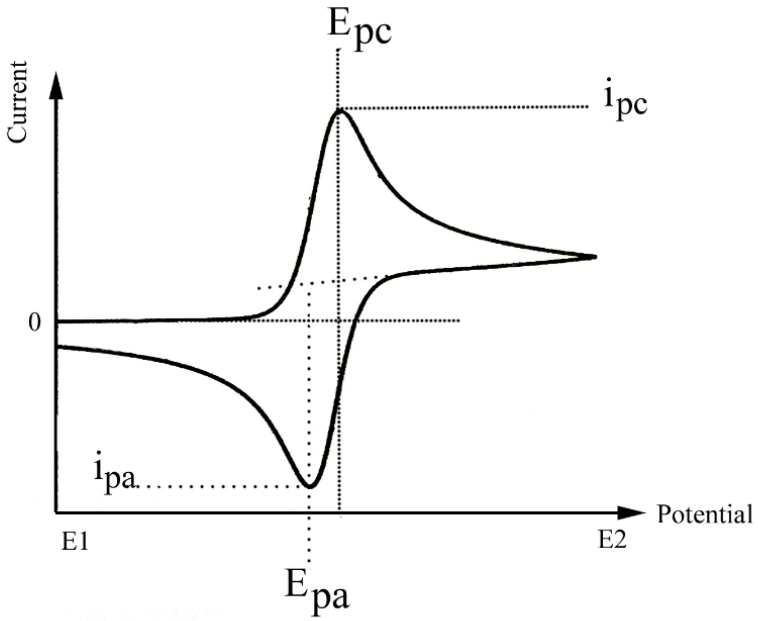

Figure 13 - A typical cyclic voltammogram of a reversible oxidation process. The values for the peak currents for both the oxidation and reduction (I_{pc} and I_{pa} respectively) are highlighted as well as the corresponding potential value at which these occur, E_{pc} and E_{pa}.

Figure 13 shows a typical cyclic voltammetry plot of current *vs.* potential for a reversible system. This is referred to as a voltammogram. There are many factors which influence the observed current[29], and an understanding of these is essential in order to be able to understand and interpret a cyclic voltammogram.

Typically there are three main[29] processes that will control the observed current during a such an electrochemical experiment:

Mass Transport – This is the transfer of the reacting material from the bulk of the solution to the electrode surface. There are three modes of mass transport, diffusion, migration and convection [27].

Electron Transfer – The transfer of electrons from the electrode to the molecule in solution or *vice versa.* This is a fast process [29].

Surface processes – This can include such processes as adsorption, desorption or other effects such as crystallisation or electrodeposition[29]

Figure 14 is an illustration of some of these processes, where a molecule of reactant, O, approaches the electrode surface via diffusion (a mass transport process) until it reaches the electrode, at which point it is reduced by an electron transfer reaction. The product R then discuses away from the electrode.

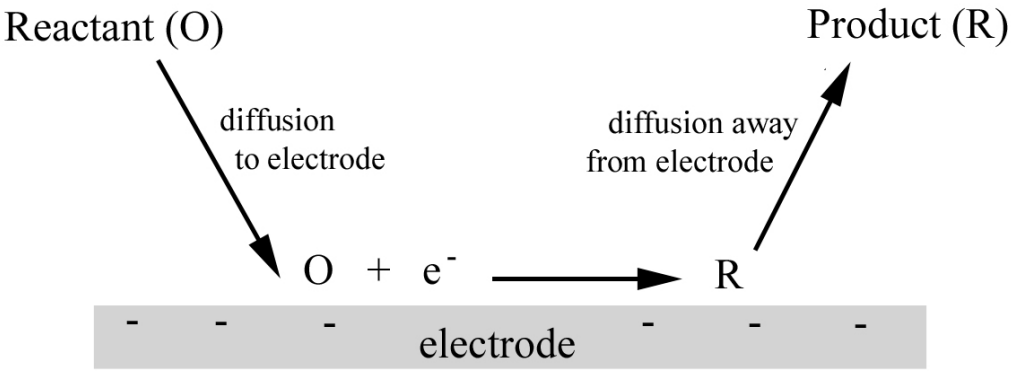

Figure 14 – Illustration of a reactant approaching and diffusing to an electrode surface, where it then undergoes a reduction. The product then diffuses away from the electrode.

1.5.2 The Shape of a Typical Reversible Cyclic Voltammogram for an Electrode in Solution

In order to show how these processes affect the voltammetry and the recorded voltammograms, we will review and go though the typical cyclic voltammogram shown earlier in figure 13, and explain why the trace recorded for current *vs* potential occurs in the way it does.

We start on the left at the potential marked E1, (the starting potential is not at a value which is capable of inducing electron transfer for the system being studied). As the potential is swept to more positive values we will start to approach the oxidation potential of the species being studied. At this point electron transfer from the species will start to occur. The rate constant of the electron transfer step will depend on the potential applied; a more positive potential will induce a higher oxidation current which in turn will mean a faster electron transfer[29]. As species X is oxidised to X^+,

the electron transfer is detected as a measurable increase in current at the electrode, which is plotted on the voltammogram. There is a rise in current as we go to more positive potentials due to the fact that more positive potentials precipitate a faster electron transfer, which is measured as a larger current. This rise in current will eventually reach a peak, and then start to decline, this peak is labelled i_{pc} in figure 13. Before this peak, the mechanism is under kinetic control, the limiting factor at this point is how quickly the electron transfer step can occur, and this is a fast process.

1.5.3 The Diffusion Layer

Diffusion control is responsible for the effect which causes a drop in the current as seen in the typical cyclic voltammogram, and hence a peak. This is a part of the mass transport effects that were outlined earlier and is one of the factors responsible for controlling the currents we observed[29]. If we take the oxidative current example, when the positive potentials are high enough, all of species X near the electrode surface is quickly oxidized resulting in no X being present at the surface of the electrode, thus setting up a concentration gradient moving away from the electrode. At the electrode surface, the concentration of X is zero, and as we move away from the electrode surface, the concentration starts to increase until it eventually reaches the original bulk concentration of species X. This creates a diffusion layer, and this layer will become larger as more time passes with the applied potential[29], this is illustrated in figure 15. The diffusion layer will eventually reach a maximum size, but cannot grow indefinitely (due to the inevitable mixing effects that will occur within the solution), thus an equilibrium is reached, balanced by the amount of mixing that the solution experiences[27].

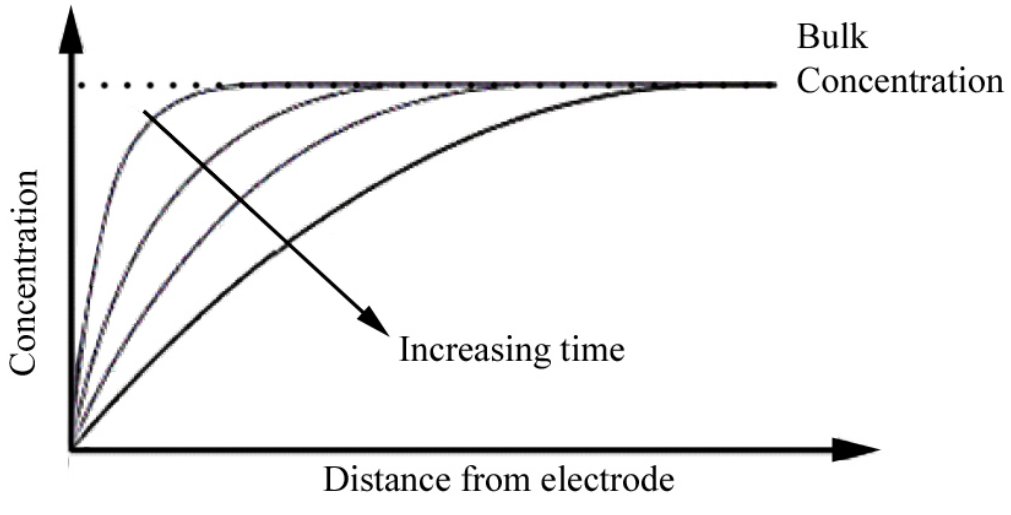

Figure 15– Graphical illustration showing the growth of the diffusion layer as a result of time

Once the potential has reached E2, it is returned back to the starting value of E1. Provided that the reaction is reversible, an inverted (negative) current peak, (labelled in figure 13 as i_{pa}), is seen in the opposite direction, which corresponds to X^+ being reduced back to the starting species X. A similar fall from the peak height will be observed as the current tends towards zero; this is due to the same reasons outlined for the oxidative process [25].

1.5.4 Effect of Scan Rate

Thus far we have only looked at a single scan rate, the typical cyclic voltammogram for a reversible species as shown earlier in figure 13 will change as a result of varying the scan rate. Varying scan rate simply means varying the speed at which the potential is swept from E1, to E2 and then back again. A faster scan rate means going through the cycle at a faster rate. Performing the experiment at a faster scan rate has an impact on the voltammograms recorded, and this is seen as an increase in peak height for the signals observed- i.e. a higher current-[29][31]. This is illustrated in figure 16[29][31].

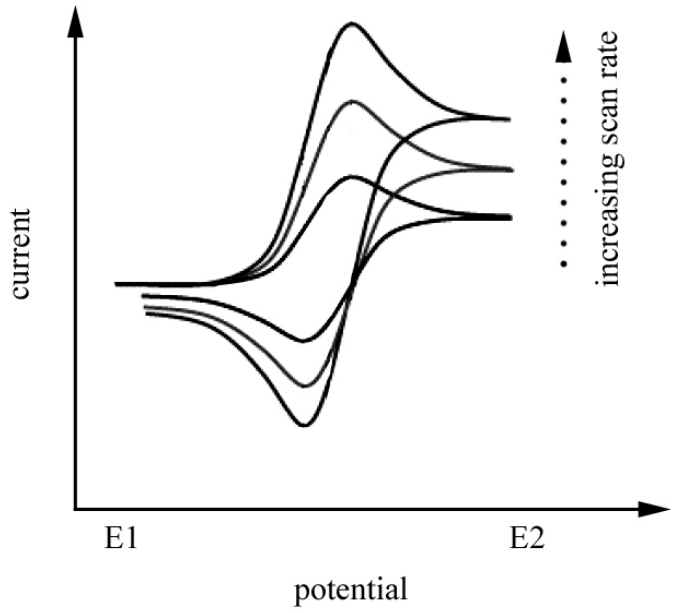

Figure 16 - Illustration of how increasing scan rate affects cyclic voltammetry scans

This effect of increasing peak current can be attributed to the growth and size of the diffusion layer. The longer a scan takes to run, the more time the diffusion layer has to grow into the bulk, and therefore the larger the size of the diffusion layer. A large diffusion layer as a consequence of a slow scan rate will mean that the flux to the electrode surface will be considerably smaller than the flux to the electrode surface during a fast scan rate, which would only produce a comparatively small diffusion layer. The current that is observed during a voltammetry experiment is proportional to flux *(vide ante*, equation 7), therefore slow scan rates cause large diffusion layers, meaning shallower concentration gradients. These is turn lead to less flux to the electrode surface, which in turn corresponds to smaller peak currents for the current voltage curves that are obtained[(27)].

1.5.5 Electrochemical Reversibility

It should be noted that the positions of all the peaks along the potential axis in figure 16 do not change as a result of increasing scan rate, only the peak height is seen to increase. This is typical of a reversible system. A reversible system is one that has fast electron transfer kinetics, and the corresponding cyclic voltammograms have well defined characteristics. The peak to peak separation of such a system is 59mV, it has no peak position change as a result of increasing scan rate, only an increase in the peak height which is proportional to the square root of scan rate, and finally the magnitude of both the forward and back peak are equal [(29)(31)]. If the electron transfer kinetics are slow in comparison, more over potential will be required in order to facilitate electron transfer. This is termed an irreversible electron transfer reaction. The increase in current as a result of oxidation will be observed at higher potential

values than those observed for a reversible system. This is illustrated in figure 17[27].

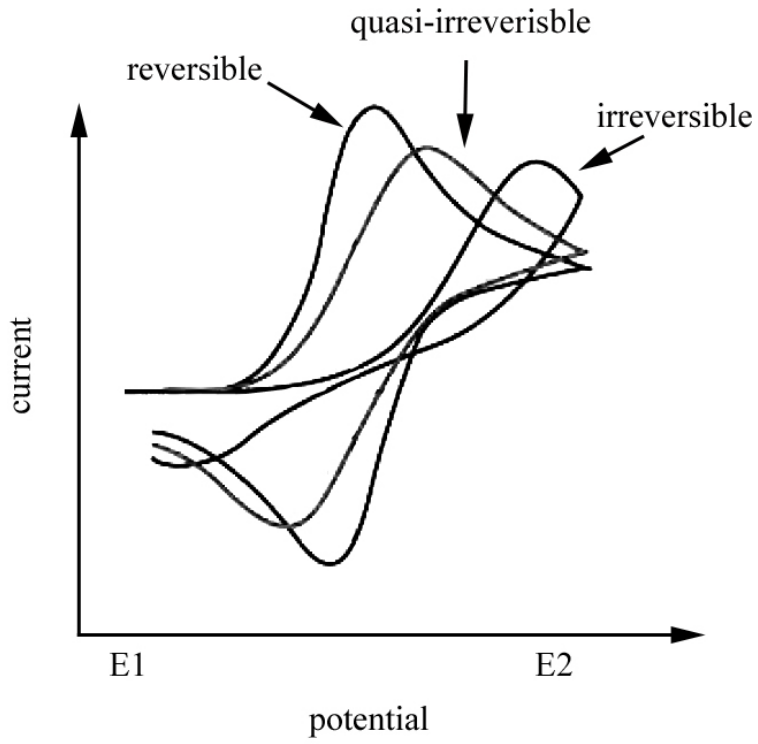

Figure 17 – Illustration of cyclic voltammograms obtained for reversible, quasi-irreversible, and irreversible electron transfer reactions.

The term quasi-irreversible refers to an electron transfer reaction which is neither limiting case, but somewhere in between. In these cases both the mass transport and the electron transfer rates will affect the surface concentration of the species at the electrode surface, and hence the observed voltammogram. For processes that are not reversible the peak height does not increase as a function of the square root of scan rate, and also we see that the peak positions are dependent on the scan rate, which is not observed for reversible systems[31].

1.5.6 - Surface Attached Reversible Electrochemical Signals

Up until now, only the voltammetry of a species in solution reacting at an electrode surface has been considered. When a species is specifically adsorbed onto the surface of an electrode it will profoundly change the voltammetric signals obtained. In this section we will consider the voltammetry of a species that is adsorbed onto the surface, undergoes reduction, stays adsorbed on the surface, and then undergoes re-oxidation. A typical cyclic voltammogram for a reversible one-electron transfer where both reduced and oxidized forms remain on the surface is shown in figure 18. The first thing which is immediately obvious as a difference from the voltammograms that have been explored thus far is the symmetrical nature of the reduction and oxidation peaks([31].

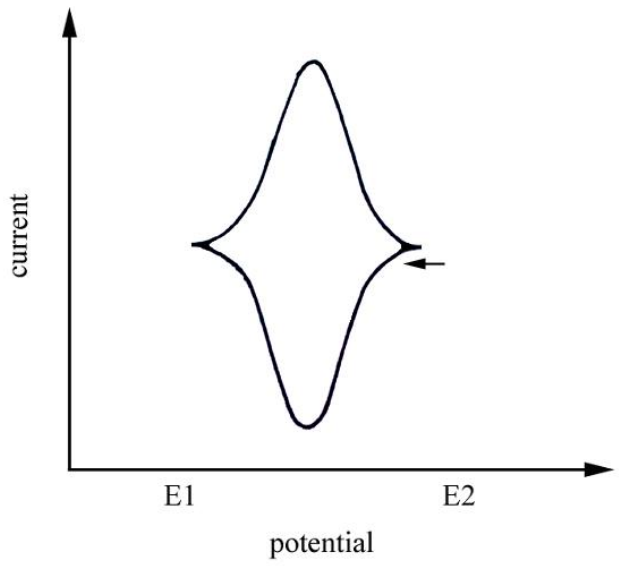

Figure 18 – Typical cyclic voltammogram for a reversible one-electron transfer where both reduced and oxidised materials are surface adsorbed.

The current is seen to drop back down to zero quite soon after the reversible potential. This occurs because, as a surface adsorbed species, there is a limited quantity available on the surface that can undergo reduction, and once this has been converted to the products there is simply no more which can undergo reduction. Due to the fact that there is no diffusion hysteresis for this reaction, it is therefore governed by the electron transfer kinetics of the reaction. This is why the reduction and oxidation peaks both overlap and are symmetrical about the zero current axis. The peaks will only remain symmetrical as long as the surface adsorption is stable. For this type of system, as there is a finite quality of material on the surface, the area of the voltammograms peak can be used to calculate the charge and hence provide a quantitative analysis for the amount of material on the surface [27] [31].

1.7 – Identifying Chemical Reactions by Voltammetry

The final section of this introduction to voltammetry deals with any chemical reactions or steps that may occur alongside the Faradaic electron transfer processes within a given electrochemical experiment. These types of reactions are often known as EC mechanisms, where E refers to an electrochemical redox process, and C to a chemical reaction step that occurs after the electrochemical process. These types of reaction, for example, can occur when the electrochemical process generates an unstable product which then goes on to react in a chemical reaction[31]. Depending on how unstable the generated product is and the rate constant of its decay via the chemical step, one can try to outrun this chemical step by increasing scan rate (such as when running a cyclic voltammetry experiment)[27][31].

EC would refer to a system where no more electrochemical steps occur after the chemical reaction, however these are possible depending on what product was yielded from the chemical step. If another electrochemical reduction/oxidation is possible, the mechanism would be referred to as an ECE mechanism[31].

1.7.1 The EC Mechanism

A good example of an EC mechanism would be the electrochemical oxidation of 1,4-aminophenol (figure 19)[31]. This molecule undergoes a two-electron oxidation forming the quinone imine, which then in turn undergoes a chemical hydrolysis reaction where it forms benzoquinone. The final generated species does not undergo oxidation or reduction at the potentials utilized for voltammetry of the original aminophenol species. We therefore see an irreversible voltammogram for the cyclic voltammetry experiment[29][31].

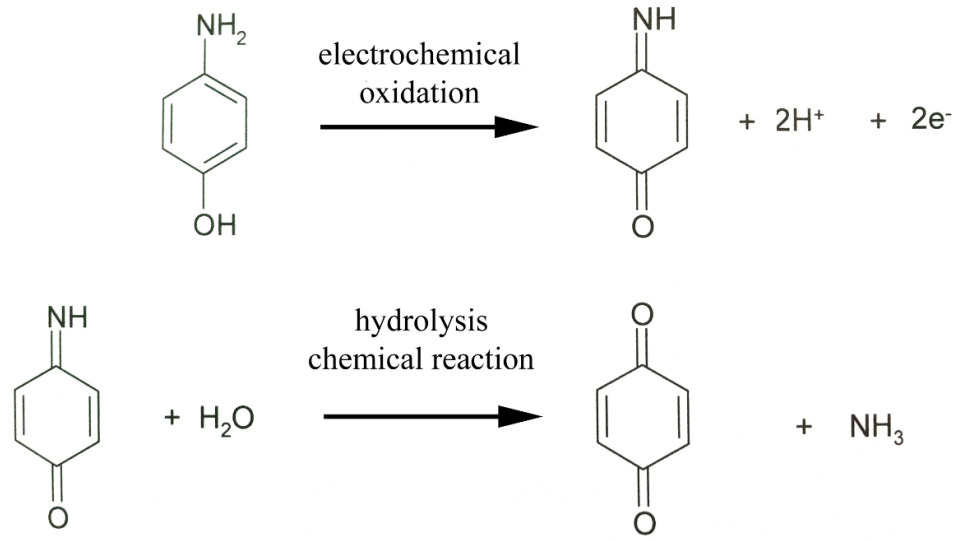

Figure 19[31] – Example mechanism for a EC process.

In the case where an EC mechanism occurs during a cyclic voltammetry experiment, and where the product of the chemical step is not able to be reduced or oxidized at the potential window of the experiment, the rate constant for the chemical step will determine whether it is visible at the scan rate being run. Faster scan rates may be able to 'outrun' the chemical reaction and one would be able to see a reversible signal for the voltammogram[31]. At intermediate speeds (relative to the speed of the chemical step) the reversible signal for the reduction would be of a lesser magnitude than the oxidation, as the scan rate is not fast enough to completely outrun the chemical step, nor is the rate constant high enough to consume the material before the potential can begin to start reducing it again[31]. Finally, at slow scan rates, the chemical step occurs at a fast enough rate to consume all the material from the electrochemical oxidation, and thus there is nothing left to reduce electrochemically so we see an irreversible voltammetry signal.

An illustration of how scan rate would affect the visibility of the chemical step for an EC reaction is shown in figure 20 [31]; it should be noted that the peak height in the voltammograms will increase with scan rate, although this is not illustrated in the figure as it is the ratios and relative magnitudes between the oxidative and reductive peaks that are of interest for the purposes of this figure.

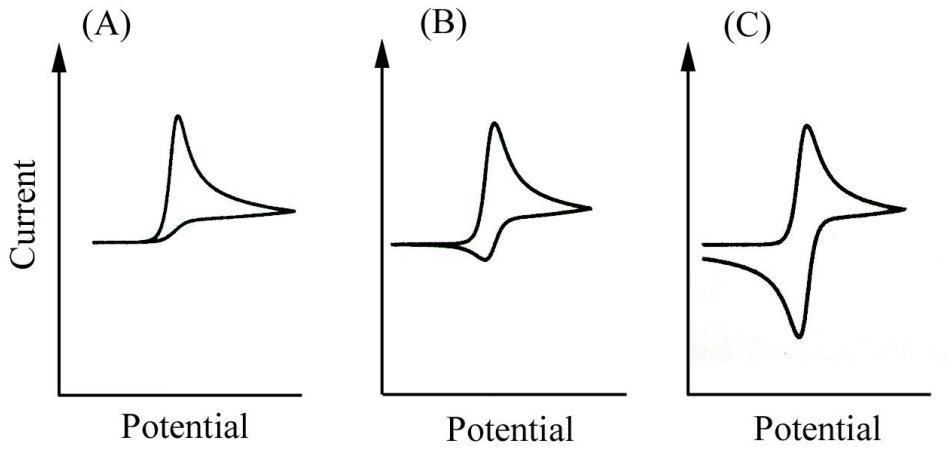

Figure 20[31] - Illustration of how scan rate would affect the visibility of a chemical step in a voltammogram, for the purposes of this figure, the magnitudes of the currents across the different scan rates have been shown as equal in order to view the information more easily. (A) slow (B) intermediate (C) fast scan rate

1.7.2 The ECE Mechanism

An ECE mechanism proceeds in a slightly different fashion. This is when the chemical reaction yields a product which is then able to be electrochemically reduced/oxidised within the given potential window. This will often yield a product which can be reduced back one step, but not back to the original starting material as the chemical step has precluded this. A generic reaction scheme for an ECE process is given below [31].

$$A + e^- \rightleftharpoons B$$

$$B \rightarrow C$$

$$C + e^- \rightarrow D$$

Assuming that the rate constant for the process B $\rightarrow$ C is fast enough to allow complete oxidation of C, we would see two oxidations followed by only one reduction current corresponding to the reduction of D. An illustration of the produced voltammogram is shown in figure 21[31].

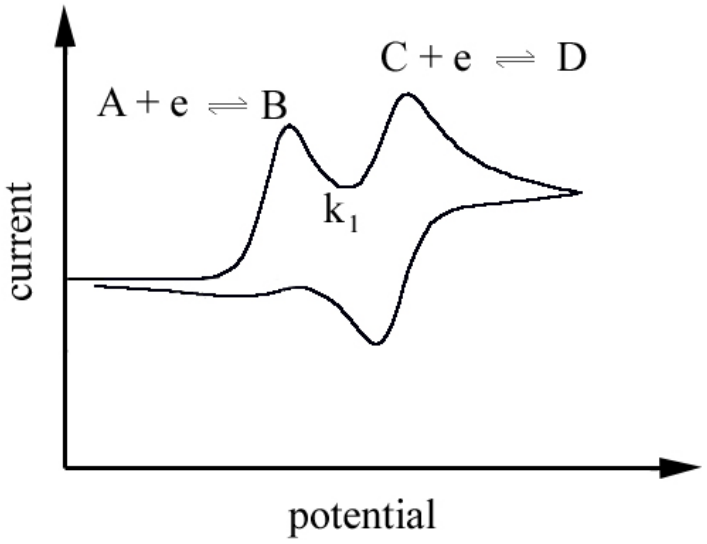

Figure 21[31] – Illustration of a voltammogram for an ECE process with k_1 of the chemical conversion occurring at a rate fast enough to completely convert the B to C. Note there is no back peak for the reduction of B

1.8 - Liquid | Liquid and Triple Phase Boundary Electrochemistry

Thus far, the scope of this introduction has been limited to solid electrodes, however there are many other types of electrodes that can be utilized in voltammetric study. The ones employed in this report utilize liquid oils to form microdroplets on electrodes. The following section is concerned with some of the background information dealing with liquid | liquid interfaces as well as triple phase boundaries.

We see liquid | liquid interfaces and droplets occurring quite often both in nature and in man made products and also arising within biological systems. Cells can be considered vesicles, and these themselves contain other tiny droplets, or vesicles. The surface of these is composed of a lipid-bilayer membrane, they are enclosed by a fluid, and normally filled with another fluid, hence forming the liquid | liquid boundary[33]. Knowledge of how these boundaries work, and their processes, has been essential in various medical applications such as the creation of artificial vesicles which are employed in the transfer of drugs to cells [33] or an understanding of events like proton pumping [34]. In another example, biosensors require an understanding of how membranes bind to different substrates[35]. An ability to mimic the photosynthetic process that occurs within plant cells and harvest light energy has been a driving force in energy research. Much of the work so far has concentrated on semi-conductors but recent work has looked into various bio-inspired systems including photo-electrochemical devices [36].

1.8.1 – Four-Electrode Cell

Electrochemistry conducted using liquid | liquid boundaries, is not a new technique and its origins can be traced back to work carried out by Nernst and Riesenfeld in the early 1900's [37], but it was not until much later on in the late 1960's [38] that the development of the four-electrode electrochemical cell (figure 22) opened the door to truly better understand the processes that occur between two immiscible phases. The four-electrode electrochemical cell involved a reference electrode and a working electrode placed in each phase. The interface could then be polarised by the electrodes and this allowed for the exploration of many avenues, from biological applications such as drug transfer and reactions exploring lipophilicity within cells [39], to electro-analysis [40], ion transfer [41] and sensing applications [42].

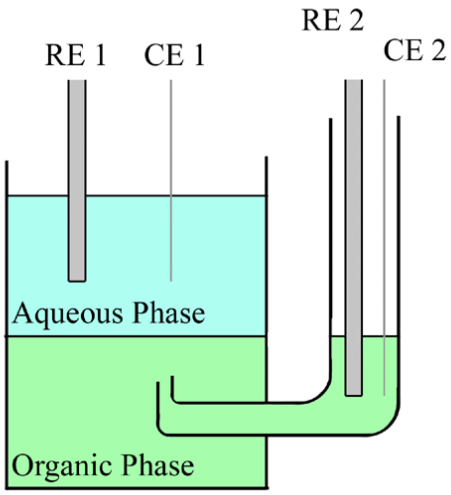

Figure 22 - Schematic representation of a four electrode electrochemical cell showing the phase boundary between two immiscible liquids

The four-electrode cell was, however, not without its difficulties. The two phases both needed to have an intentionally added salt, both of which needed to be capable of dissolving effectively in the specific environment of either the aqueous or organic phases. Both salts had to be carefully selected in order to effectively facilitate the polarization of the interface, and it was not always easy to find a suitable candidate [(43).] The nature of the interface itself was also difficult to describe adequately, with questions over whether the interface was better described as sharp or diffuse being raised. Subsequently, we now know that the answer to this question is dependant on the time scale that one observes the interface for[(44)]. Experimental methods such as capillary wave experiments conducted using neutrons or X-rays[(44)(45)] have been applied to the interface between two immiscible liquids, but thus far a complete portrayal of the interface has not been possible, and the current models are based on computer simulations and models utilizing molecular dynamic simulations[(44)(46)].

When this interface was successfully polarized, surface tension experiments and capacitance data showed that the potential was distributed between the two back to back diffuse layers[(47)(48)]. It was suggested that the space-charged regions did not interact with each other, and other publications show that the thickness of the interface actually becomes smaller as polarization increases [(49)]. Although these types of systems had their disadvantages and unknowns, one significant advantage they had over standard solid metal electrodes was the interfacial dynamics, and this could be used to probe the diverse and varied range of charge transfer reactions that can be induced such as ion transfer (*vide infra*), assisted ion transfer and electron transfer [(44)].

1.8.2 - Towards Triple Phase Systems

With the boundary between two liquids proven to be of scientific interest, new directions were taken from the four-electrode system. One of these new novel systems was employed by *Scholz et al*[50] and provided an evolution of liquid | liquid chemistry which overcame several of the problematic issues of the four electrode cell mentioned. The first key difference was that with this work there were three phases, instead of two. Using an aqueous electrolyte, modification of a solid electrode surface with a single droplet of organic electro-active media allowed the experiments to do away with the problematic four electrode system, and simply trade this for a simpler three electrode set up.

As long as the droplet was small enough in size, one could omit the need to have a salt present within the organic phase, neatly circumventing the afore mentioned issues of finding a suitable salt for the four-electrode set ups and also adding the cost saving advantage of only utilizing a very small amount of the organic media[50]. When immersed in the aqueous electrolyte, the boundary at the oil droplet's edge and the electrode -providing that the edges of the droplet did not completely obscure the electrode surface- creates a triple phase boundary that allows for the facilitation of the electrochemical reactions. This is shown schematically in figure 23.

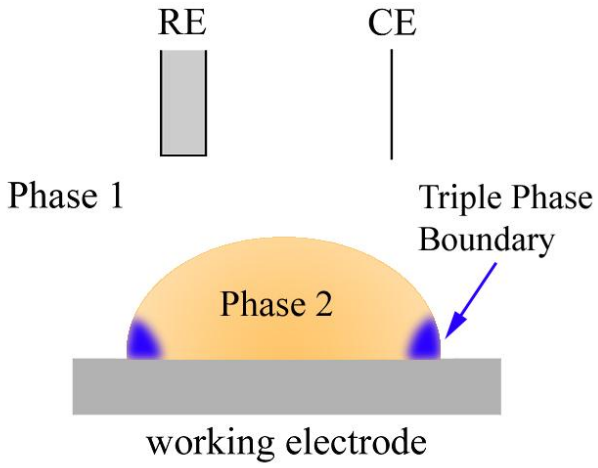

Figure 23 – Schematic representation of an electrochemical set up for a liquid | liquid | solid triple phase boundary utilizing a single electro active droplet.

1.8.3 – Microdroplets

Further work in this field by Marken *et al* led to a new method of creating these triple phase boundaries in biphasic media, and involved the creation of an array of random microdroplets on an electrode surface. Using this technique, the individual droplets created were in the order of femtolitres in volume with a total deposition volume in the order of nanolitres[51]. The approach by *Marken et al* also involved not necessarily having an electrochemically active oil phase, but instead could employ an electrochemically inert oil, and dissolve electrochemically active compounds within. These microdroplets carried some advantages over the single droplet triple phase systems. If using single droplets in the three-electrode system (as shown in figure 23), care must be taken in order to avoid large capacitive currents which could overwhelm the desired signal as a result of a large area of bare electrode not being covered by the organic media. Another advantage of the microdroplet array is that they have a significantly increased active triple phase boundary area, allowing for larger currents to be observed. The miniaturization of the system compared to previous work also

allows glimpses into understanding biological processes, for example those that occur within cells [52].

An elegantly simple method of microdroplet deposition is provided by *Marken* [53], and involves depositing oils containing an electrochemically active molecule dissolved within, onto an electrode surface. This is accomplished with the aid of a volatile liquid to facilitate the transfer. This is the method that is used throughout the work outlined in this report. It involves taking a solution of the electrochemically active molecule in the oil and dissolving it in a volatile solvent such as acetonitrile or ethanol, this whole mix is referred to as the 'deposition mixture'. An aliquot of the deposition mixture containing the oil, electrochemically active molecule, and carrier solvent is pipetted onto the electrode surface. As evaporation of the solvent takes place, an random array of microdroplets if left behind[53].

Various methods exist for the stabilization and deposition of an array of microdroplets. These range from using mercury droplets, and employing an electrochemically induced nucleation of the mercury to facilitate the droplets [54], to using electrochemical reductions at an electrode surface of a species present in the electrolyte to deposit the microdroplets [55]. The surface upon which a microdroplet array is employed upon has also seen a diverse range of options, there have been studies conducted on electrodes which are highly porous to maximize the triple phase area [56], or even lithographically modified surfaces [57]. Another interesting and novel approach to using droplets was employed by utilization of a hanging oil droplet in conjunction with a wire electrode, which pierced the droplet. This acted as a means to control the triple phase boundary area [58][59]. It is important to note that the size of the

triple phase boundary area in any of these systems will affect the observed current during electrochemical analysis. In the case of *Marken* style droplets, studies have shown that smaller droplets (and hence larger triple phase boundary area) lead to increased currents being observed[60].

1.8.4 - Ion Transfer

One important thing to note is that whenever electron transfer occurs at an unsupported oil in the liquid | liquid | solid interface, simultaneous transfer of a counter ion will happen in order to conserve charge neutrality[61]. This has been exploited in a vast range of different systems ranging from electro-synthetic projects [62], electrochemical sensing [62] to biphasic-electro luminescence[63]. This ion transfer is illustrated in the diagram figure 24. In a droplet of electrochemically inactive oil containing a redox active molecule, reduction of the redox active molecule will impart a movement of cations from the aqueous phase into the organic oil microdroplet in order to maintain electro neutrality[64]. The cation transferred will depend on what is present in the aqueous electrolyte used, and which cation is transferred can have an impact on the redox processes that occur within the microdroplet. It is therefore important to understand which ion transfers will occur for a given system[64].

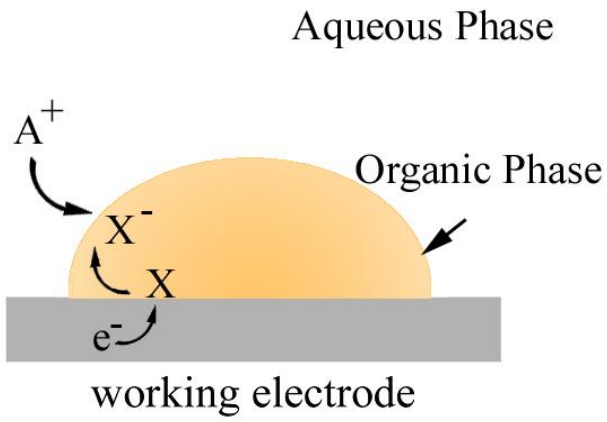

Figure 24 – Schematic representation of reductions of species within the organic droplet followed by transfer of cation from the aqueous phase in order to maintain electroneutrality.

1.8.5 Other Approaches to the Voltammetry of the Triple Phase Boundary

Thus far, a simple evolutionary timeline has been outlined for how the triple phase methods employed in this report evolved. There are however many other methods, strategies and equally novel processes that utilize the triple phase boundary for electrochemical study.

One of these other methods builds on the development of a novel and easily made junction electrode with a well-determined, customisable gap size in the order of micrometer to sub-micrometer in size[(65)]. These are created by growing two separate gold hemispherical electrodes in close proximity[(66)]: the potentiostat is then programmed to cut off automatically at a pre-set current value which determines junction size. One part of the junction -the generator- can induce electrochemical reactions, and the collector can be used to both characterize the junction and information on the electrochemically active species[(67)]. Instead of just using the

junction in a homogeneous solution to perform the electrochemistry, a droplet of an electrochemically active, water-immiscible liquid is deposited onto the junction where it creates a triple phase boundary with incorporation the junction itself into this. Oxidation can be induced at the generator electrode, which will be coupled with anion exchange from the aqueous phase. A driving force is set up between the generator and collector electrodes, finally resulting in expulsion of the anion at the collector electrode site. This system set-up can yield information on rates of transport of the anion and oxidized form of redox system through the electrode gap [68].

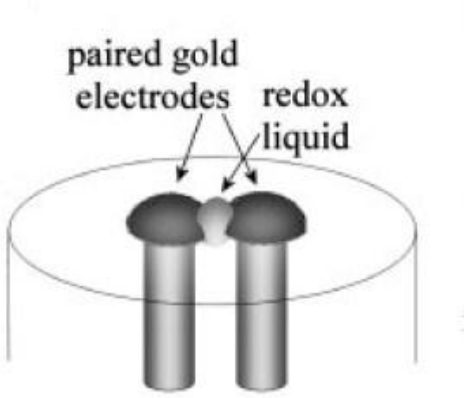

Figure 25 [68] – Schematic representation of a paired gold junction electrode, with electrochemically active, water immiscible liquid deposited and immobilized in the junction.

Another good example of triple phase electrochemistry, and approached in a completely different way to the work done on the junction systems, is microfluidic reactors for electro-synthesis[69]. Microfluidic reactors are of interest as they can potentially be a clean synthetic approach, minimizing waste, cost and issues such as contamination [70, 71, 72]. Recent approaches have seen attempts to omit the role of the supporting electrolyte in the organic phase, and this has led to several experimental methods [73, 74]. These include a method which sees a parallel, immiscible, two-phase

flow system of organic media and supporting electrolyte; the flow channel incorporates an area of a working electrode over which both the aqueous phase and the organic phase flow, hence creating the triple phase boundary [75].

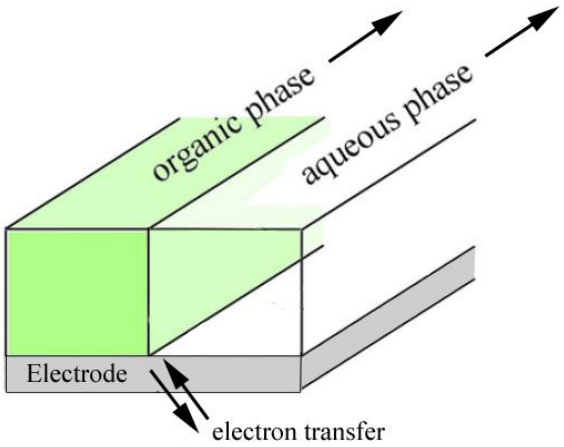

Figure 26 – [76] Schematic representation of a two-phase flow microfluidic system.

Synthetic methods are not limited to flow systems, and other novel approaches utilizing sonication have been employed towards the goal of synthesis. An oil containing electrochemically active molecules of interest for synthesis can be placed on an electrode surface and exposed to ultrasound. This has the effect of breaking up the droplet of oil and creating an acoustic emulsification [77]. This effect is caused by the ultrasound breaking up the single droplet and creating a dynamic emulsion of droplets with a high triple phase boundary area. Studies have shown that these emulsions can have droplet sizes in the range of 1μm, with relatively tight standard deviation[78].

Other types of biphasic systems have been employed by other groups and do not necessarily strive towards synthesis, but can be more analytical in nature, such as one employed by *Fisher et al.* This system did not see a continuous flow of each phase across an electrode, but rather utilized a pulsing system whereby droplets of one phase were created within the other phase and both flowed down a channel. These then passed over the working electrode in pulses. This triple phase boundary electrochemical process has been proposed for use as a substitute to optical imaging when characterizing moving droplets in a channel [(79)].

So far we have outlined a variety of methods for examining and exploiting the liquid | liquid | electrode triple phase boundary. For the sake of completeness, it would be remiss not to briefly mention other triple phase approaches that have been employed. Solid | liquid electrolyte | solid electrode boundaries have been utilized in electrodeposition experiments, where various types of nano-structures have been grown successfully[(80)], as well as solid deposits of electroactive, yet insulating molecules undergoing isomerization reactions as a result of electrochemical redox processes[(81)]. The gas phase has also been utilized in triple phase studies with an interesting approach being reported utilizing plasma in a gas (plasma) | liquid electrolyte | solid electrode system[(82)(83)]. Another variation on the triple phase boundary is the gas | solid electrolyte | solid electrode. This provides an interesting and useful variation, allowing for implementation in areas we might not consider 'traditional' electrochemical environments, with applications in sensing[(84)] and catalysis[(85)] being reported.

1.9 - Photo-Electrochemical Reactions at the Triple Phase Boundary

Perhaps a good place to start for the final section of the introduction is simply to ask, why are we interested in photo-electrochemical reactions at the triple phase boundary?

1.9.1 Light Harvesting

Photo processes are of particular interest and relevance at present with the need for renewable energy sources becoming a growing concern. The most commonly used energy source based on solar energy is the standard silicon photovoltaic cell; this consists of a direct conversion of solar energy into electricity. These systems typically have an efficiency (solar to current conversion) of approximately 20%. A promising contender is the dye-sensitized solar cell, this is a comparatively recent development and has not been implemented in large-scale use, however it is a system that shows great promise with average efficiencies of approximately 10% being reported [(85a)]. Another method that has attracted interest is light harvesting [(86)].

The term light harvesting has been popularised in recent years and essentially denotes utilizing the Sun's energy to drive a reaction that will ultimately create a fuel. This is in contrast to standard solar cells employed in general use, in that the power comes from storage of the energy into a chemical bond rather than direct conversion into current. This has several advantages: Humanity's energy requirements are vast, and any global energy replacement would have to be based on a dense power source (such as chemical bonds) and the corresponding breaking of these bonds to release energy. Also storage of the energy obtained via chemical bonds would mean that the power source is able to be used when and where it is needed, being harvested in locations

around the globe with good solar energy reception to be transported elsewhere for use[87]. So, in essence, this type of work is similar to creating an artificial form of photosynthesis. This is a hugely complicated task, and although working models have been achieved they have always been plagued by problems such as degradation of the materials within the system, difficulties in synthesis of component molecule and poor quantum yields[87][88].

The overwhelming majority of the work in this field is based on semi conductors and utilization of a solid | liquid interface[86]. This report will however, will be concerned with the possibility of light harvesting from a triple phase liquid | liquid | solid interface, achieved through a random microdroplet array.

The liquid | liquid interface has been identified as a potentially good route to explore the possibility of light harvesting as it mimics factors in natural photosynthetic process environments. It could therefore produce a feasible bio-mimetic model for light harvesting due to a similarity in design of a cell membrane to the liquid | liquid interfaces[89][90]. It has only been recently however, that pioneering work performed by *Wadhawan et al*, has focused on photo-reactions at microdroplets This work saw some initial non-illuminated experiments done with microdroplets incorporating vitamin K1, where changes in pH of the buffer system were shown to have radically altered the mechanism, and production of hydrogen being reported as a result of the voltammetry carried out[91]. This vein of pursuit was later expanded upon with the first work seen performing illuminated reactions on these types of triple phase boundaries [92][93]. It was shown that the photo reactions which were occurring were

indeed related to the triple phase boundary as well as introducing some of the first preliminary understandings of the ion transfers that occur for these droplets.

As has been discussed in previous sections of this report, electron transfer reactions within microdroplets are coupled to an ion-transfer step as well. This type of process has similarities to the natural photosynthetic system where we see hydrogen ion transfer coupled to electron transfer[87], as well as aspects of its physical structure mimicking those seen in nature. A system which has a resemblance to natural processes is a desirable avenue to pursue, as it has been noted in previous reviews regarding artificial photosynthesises, that a man made system based on the foundations of what we have already observed in nature has the advantage of starting from initial ideas that have already been shown to work in practice[87]. The ion transfer step which is coupled to electron-transfer allows for an added element of control as well as the potential addition of a wide range of electrochemical processes which could be implemented towards the goal of light harvesting[94]. Also microdroplet systems allow for control of the triple phase boundary size; smaller droplets will inherently lead to larger triple phase boundary areas, and it has been shown that these are linked to the extent of the photo process observed[95] [96]. The microdroplet approach will also not require a supporting electrolyte for the organic phase, and thus cuts out any issues one might face in selecting and/or synthesizing an appropriate salt[97].

These factors make the microdroplet approach and utilization of the triple phase boundary, coupled with photo-electrochemical reactions an attractive prospect for novel testing of a light harvesting system. It is hoped that in this report some of the

first tentative steps can be made towards finding whether photo-electrochemical reactions at microdroplets could be a useful, feasible approach towards the ultimate goal of light harvesting or photo-electrosynthetic systems.

The first experimental chapter will look at characterizing and understanding the chemical and electrochemical reactions, both dark and illuminated, that occur for microdroplet arrays of 4-(3-Phenylpropyl)pyridine (PPP) with rhodamine b dissolved within.

Chapter 2

Resolving Triple Phase Boundary Voltammetry of Rhodamine B in PPP Microdroplets

Contents

Published - "Triple Phase Boundary Photovoltammetry: Resolving Rhodamine B Reactivity in 4-(3-Phenylpropyl)-pyridine Microdroplets" in *Chem. Phys. Chem.* 2010, **11**, 2862-2870

2.1 - Abstract

The voltammetry of rhodamine b base (rhodamine b) in microdroplets of 4-(3-phenylpropyl)pyridine (PPP), deposited onto a basal plane pyrolytic graphite electrode immersed in aqueous electrolyte was studied in both illuminated and dark conditions. Under dark conditions, rhodamine b showed a two-electron reduction to leuco-rhodamine b occurring in two separate one-electron steps. The re-oxidation back to rhodamine b. instead occurred as a single consecutive two-electron process. The first reduction step was seen to occur as a one-electron transfer coupled to a sodium ion transfer. In contrast the second reduction was seen to be a one-electron one-proton transfer. The one-electron reduced species was also shown to undergo a chemical reaction step. This occurs as a disproportionation reaction and computer simulations show this to have a rate constant of 3 $mol^{-1}dm^3s^{-1}$.

When light was shone onto the sample of rhodamine b in PPP, a photo-catalytic oxidation process was facilitated, this light driven process was shown to replace the consecutive two-electron oxidation that was observed in the dark scans. This was seen in the voltammetric responses under illuminated conditions as a one-volt negative shift from the original two-electron oxidation to *ca* –0.85V. An insight into the mechanisms of these reactions was done via comparison with a similar molecule, rhodamine b octadecyl, and also computer simulations using Digisim 2.0. This photo process was seen to occur as a photo induced conproportionation reaction, and was shown to have a rate constant of k_{dis} = 0.7 / [rhodamine b *]s^{-1} (at pH 12, [rhodamine b *] represents the steady state concentration of the rhodamine b photo-excited state).

2.2 - Introduction and Previous Work

Rhodamine b is a well-used fluorescent dye molecule with an excited state being induced from an absorption maximum of 550nm; this has a lifetime of approximately 2ns, and produces an emission in the region of 580nm. The normal excited state of rhodamine b is a singlet, although intersystem crossing to a triplet has been reported for rhodamine b in aqueous media[98]. Further studies have also implicated the addition of base in order to help facilitate intersystem crossing to a triplet[99], with some showing rhodamine b to undergo electron transfer reactions in a triplet state[100]. Conversion to triplet states, is however, usual behaviour rhodamine b is normally seen to remain a singlet with the quantum yields for intersystem crossing remaining quite low[101].

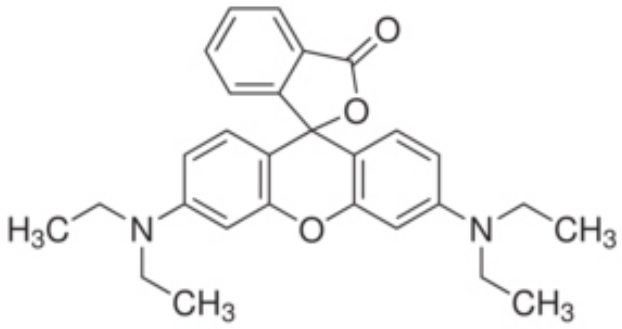

Figure 2.1 – Structure of rhodamine b

The fluorescent properties of rhodamine b are exploited in a variety of uses, ranging from fluorescent pH sensors[102] and other chemiluminescent devices for sensing techniques[103]. It also has applications within dye sensitised solar cells[104], as a laser dye[105], and as probes for structural information on large molecules such as DNA [106].

Rhodamine b has been used in photoelectrochemical reactions before, with some interesting and relevant work being reported on the electron transfer to film electrodes of SnO_2. Rhodamine b was seen to undergo a reduction to a radical anion, where it was then seen to complex with a molecule of the oxidized form of rhodamine b. A disproportionation reaction was expected between the two but not observed in the aqueous basic conditions in the experiment, most likely due to the association that the two molecules underwent[107]. This disproportionation reaction was shown to play an important role in the studies of this chapter.

Rhodamine B has also been employed at a liquid | liquid interface before, with studies at the dichloroethane and water interface showing the behaviour of rhodamine b family molecules adsorbing to the surface of the interface being potential dependant[108]. Rhodamine b has also seen studies within energy producing systems as a sensitizer within a solar cell for injection of electrons into semiconductors [109]. Previous work has shown this molecule to be highly photoactive, and it is employed in this report at the triple phase boundary in PPP microdroplets as a first glimpse into photoreactions occurring in these microphase systems.

In this study rhodamine b will be employed within PPP microdroplets, and the electrochemical and chemical reactions that take place both in dark and illuminated conditions will be explored.

2.3 – Experimental

2.3.1 - Reagents

Rhodamine b (Aldrich 97%), rhodamine octadecylester perchlorate (Aldrich ≥98%), tetra-N-butylammonium hexaflourophosphate, (Aldrich ≥99%), 4-(3-Phenylpropyl)pyridine (PPP) (Aldrich 97%), sodium hydroxide (Aldrich >97%) and phosphoric acid (Fisher Scientific, 85 wt%) were used as received from the supplier without further purification. A Thermo Scientific purification device was used for providing filtered, demineralised water with a resistivity of >18.2 MΩ cm. Laboratory temperature conditions were $20^{o}C \pm 2^{o}C$

2.3.2 - Instrumentation

An Ivium technologies 'compactstat' potentiostat (v1.725) was used for all voltammetric measurements and experiments. A standard three-electrode electrochemical cell was used, employing a quartz glass optical window which was used as necessary when light needed to be shone onto the sample. The working electrode consisted of a basal plane pyrolytic graphite electrode (bppg) and had a diameter of 4.9mm, this was mounted in a Teflon sheath. A different cell was also constructed (figure 2.2) for the purpose of photo measurements consisting of a rectangular design and a channel cut into the top and covered with a quartz window. The bppg electrode could be inserted from the bottom until it was flush with the cut channel, and therefore the electrode could be illuminated from the top through the quartz glass window. This system also employed a flow of electrolyte across the surface of the electrode, *ca* 5 ul min^{-1}, this flow served to circumvent any thermal effects that the light may have had on the voltammetric responses. Both electrochemical cells also consisted of a platinum counter electrode and used a

saturated calomel (SCE REF401, Radiometer) reference electrode with a quartz glass optical window.

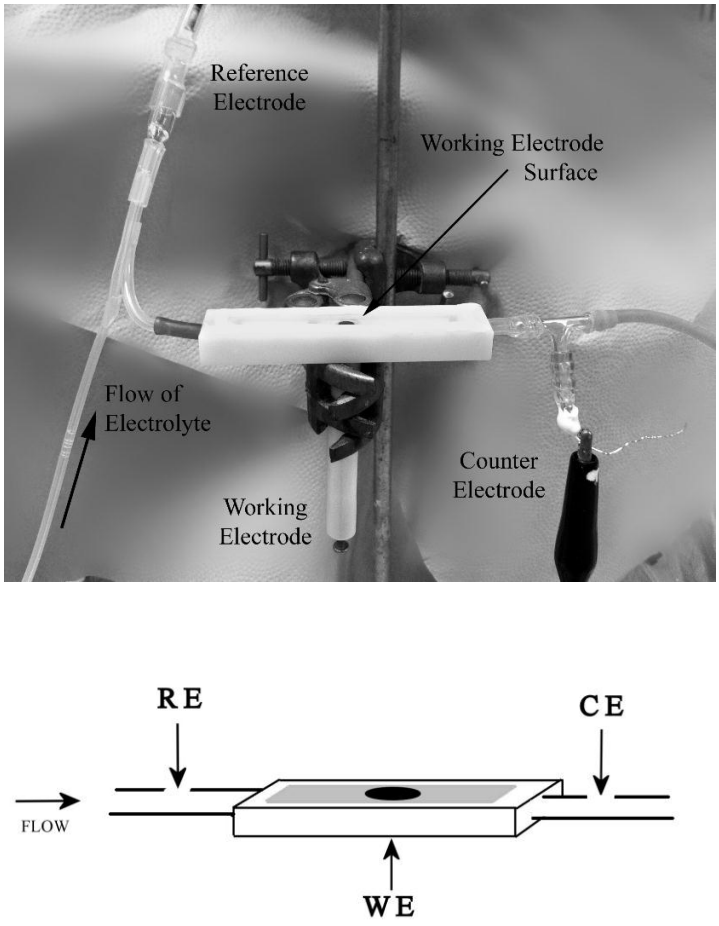

Figure 2.2 – Photographic image, and schematic representation of the photo-electrochemical flow cell constructed

For a white light source, a Fiber-Lite high intensity halogen bulb (MI-150, Dollan-Jenner Industries) was employed. This was shown to have an intensity of approximately 60 $mWcm^{-2}$ at the location of the electrode, (light intensity measurements conducted with an optical power meter, PM100A, Thorlabs Instruments). Pulsing of light was achieved by using a rotating sector blade. Photocurrent spectra were conducted using a monochromatic light source provided by a tungsten lamp, and grating monochromator for specifying the wavelength. This was

pulsed at a frequency of 6Hz, and a lock in amplifier (Stanford Research Systems) was used as a means for detecting the photocurrent. UV Visible spectroscopy was conducted using a Perkin-Elmer Lambda 35 spectrometer.

2.3.3 - Electrode Preparation Procedure

A random microdroplet array of PPP droplets containing rhodamine B base on a bppg electrode was achieved by creating a deposition mixture consisting of rhodamine b, PPP and acetonitrile in quantities of approximately 1-10mg, 80mg and 10ml respectively. An aliquot of this solution, normally between 1-10ul was pipetted onto the electrode surface. As the acetonitrile evaporated off at room temperature, a random array of PPP microdroplets was left behind on the electrode surface; this was normally a volume of 10-100nL of PPP containing rhodamine with a concentration of *ca* 0.28M. The surface of the electrode could be regenerated for a fresh deposit after experiments simply by polishing on fine silicon carbide paper.

2.4 - Voltammetry of Rhodamine b - Dark Processes

For the purposes of this work, rhodamine b was immobilized in microdroplets of 4-(3-phenylpropyl)pyridine (PPP). Due to the rhodamine b's observed ability to be quite soluble in aqueous solutions, a high concentration (0.5M) pH 12 phosphate buffer was used for the electrolyte. This helped promote relatively stable signals and hindered the ability for rhodamine b to leach out of the droplets. It should be noted that the mechanism for this promoted stability of the rhodamine in the droplets is as yet unknown. The phosphate buffer solutions used for the outlined experiments were made by utilizing a 0.5M solution of phosphoric acid, and then adding NaOH as needed to achieve the desired pH.

2.4.1 – Peak Identification and Effect of Deposition Volume

Before attempts at voltammetry under illuminated conditions could be attempted, a thorough understanding of the dark voltammetric process of rhodamine b in PPP microdroplets needed to be understood. Using a solution of 0.28 M rhodamine b in PPP immersed in pH 12 phosphate buffer, the following voltemmetric signals (figure 2.3) were obtained. The first reduction peak (labelled in the voltammogram as P1) of rhodamine b base was seen to occur at a potential of approximately –1.1V *vs.* SCE. If we scanned further negative, the second reduction (P2) could be seen at a potential of approximately –1.4V *vs.* SCE. The consecutive oxidation (P3) was seen at +0.4V *vs.* SCE. These processes are shown in figure 2.3 showing typical cyclic voltammograms for rhodamine b base in PPP microdroplets.

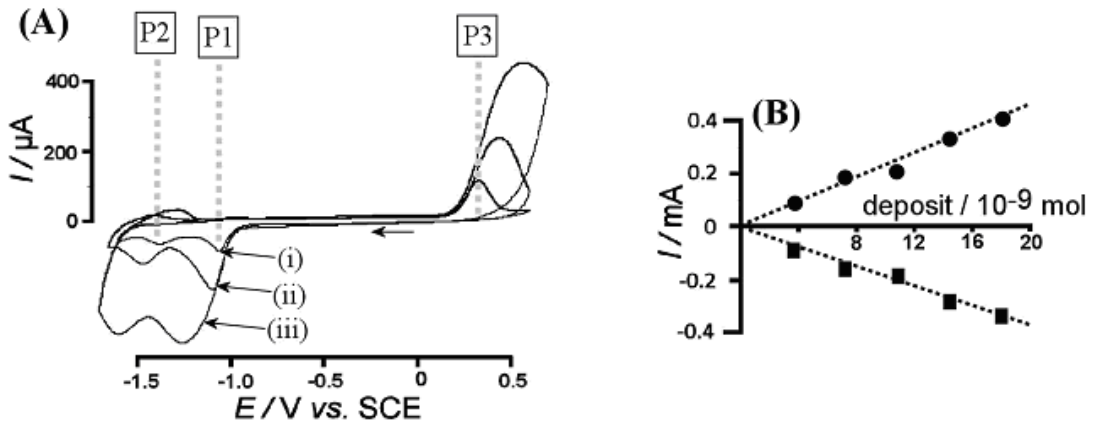

Figure 2.3
(A) Typical cyclic voltammograms at a scan rate of 0.1Vs^{-1} for reduction and oxidation of 0.28 rhodamine B immobilized in microdroplets of PPP deposited onto a 4.9mm graphite disc, immersed in pH 12, 0.5M phosphate buffer solution. The amount of PPP deposited was varied with volumes of (i) 4nL, (ii) 32nL, (iii) 64nL
(B)- Plot of peak currents P1 and P3 vs deposition amounts of the 0.28M rhodamine in PPP solution

Analysis of the area under the voltammetric peaks for rhodamine b in PPP yielded information on the charge, and this in turn was used to calculate the number of moles of electrons that had been transferred for any given reduction or oxidation. Slow scan rates had to be employed in order to ensure that all the rhodamine b molecules had indeed been electrochemically converted. The oxidation peak, having the flattest base line, was used as this provided the most accurate results. A 0.05V/s scan rate used on a 4nL deposit, (which corresponds to $4x10^{-9}$mols of rhodamine b present on the electrode) showed $7.67x10^{-4}$ moles of electrons, suggesting that there were 1.98 times the number of electrons compared to rhodamine b. This confirmed a consecutive two-electron oxidation process. A suggestion for why the experimental number is slightly less than two is because the rhodamine b was not completely stable in the oil and thus

some leaching into the buffer solution occurs. This had the effect of lowering the amount of rhodamine b in the oil compared to the initial concentration.

Experiments were conducted in order to see what effects varying the total deposition volume of rhodamine b in PPP would have on the cyclic voltammograms (figure 2.3). Depositing larger amounts of PPP onto the surface of the electrode would lead to aggregation, and thus result in larger droplet sizes. A larger droplet size would have impacted the size of the total triple phase boundary available for electrochemical reactions. It should be noted that by varying the amount deposited we did not vary the concentration of the rhodamine b present per given amount of PPP, simply the total amount deposited of the rhodamine b / PPP solution.

It was seen that the peak shapes changed as a result of the increasing amounts of PPP on the surface. The current value for the peak height of the signals was shown to increase linearly with the amount deposited, which was to be expected as a result of a greater amount of rhodamine b present on the electrode surface. The signals were also shown to broaden. The reason for this can be assigned to the fact that as the droplet became larger, there would have to be longer conversion times as a result of a decrease in the relative mass transport, and greater rhodamine b present in the bulk of the droplet.

2.4.2 - Effect of Scan Rate

Studies on the effect of scan rate were also conducted and these are illustrated in figure 2.4. A linear increase in peak height as a function of scan rate was observed, until approximately $0.3Vs^{-1}$ at which point the linear correlation started to fail and veered downwards to more negative values. This can be explained as a result of incomplete electrolysis of the rhodamine b -the scan rate was simply too fast to have successfully reduced all the rhodamine b present within the droplet-.

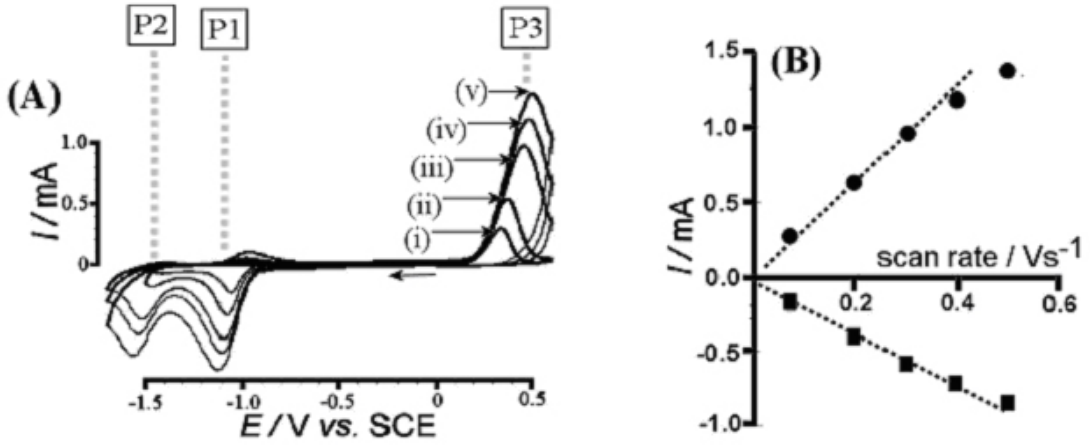

Figure 2.4
(A) Cyclic voltammograms for reduction of 0.28M rhodamine b, immobilized in PPP microdroplets, 16nL, deposited onto a 4.9mm graphite disc, immersed in 0.5M pH12 phosphate buffer. Scan rates were varied at (i)0.05, (ii) 0.1, (iii) 0.3, (iv) 0.4 and (v) $0.5Vs^{-1}$
(B) Plot of peak current P1 and P3 vs scan rate

The experiments in which scan rate was varied yielded some interesting information on the reduction processes. The second reduction peak (P2) was seen to get smaller (figure 2.4) as scan rate was lowered and then to disappear completely at scan rates of approximately 0.005V/s. Also the reduction process P1 was seen to become more reversible at faster scan rates, with a small oxidation peak having formed at approximately –0.1V *vs.* SCE. This was investigated further, and it was found that

when the scan was repeated over a smaller potential window – only encompassing the first reduction- the small oxidation signal at –0.1 *vs.* SCE was seen to become fully reversible *(vide infra).*

The fact that the second reduction became smaller, and then completely disappeared as a result of lowering scan rate suggested a chemical step was taking place, which overtook the electrochemical steps at the slower scan rates. Slower scan rates meant more time for the chemical step to continue before the second electrochemical reduction took place. It is suggested that this chemical step is a disproportionation reaction *(vide infra).* Two molecules of the one-electron reduced rhodamine b, reacted together to form one molecule of the oxidized rhodamine b, and one molecule of the two-electron reduced species.

2.4.3 - Chemical Step - Disproportionation Reaction

It was observed that if the second reduction was not allowed to fully complete, the reduction process P1 became more reversible, this was seen as a small oxidation at approximately -0.95V. When this was further investigated by completely missing out the second reduction by using a smaller potential window, (figure 2.5), P1 was seen to become a fully reversible back peak countering the one-electron reduction. In turn the consecutive oxidation, P3, was seen to become smaller as a result of the reversible signal seen for P1.

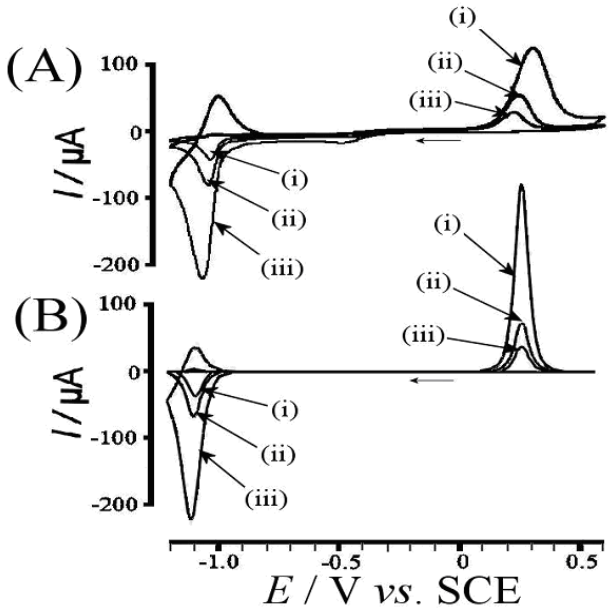

Figure 2.5

(A) Cyclic voltammograms for reduction of rhodamine b, 0.28M, immobilized in PPP microdroplets, 8nL, deposited onto a 4.9mm graphite disc, immersed in 0.5M pH12 phosphate buffer at scan rates of (i) 0.005, (ii) 0.01 and (iii) 0.05 Vs^{-1}
(B) Digisim 2.0 simulation for the reduction of rhodamine at the same scan rates as above, modelled as a thin film without diffusion limitation (assuming sufficiently high diffusion coefficients). The assumed simplified mechanism is given by A + e = B (P1), B + B = C + A, C = D + e (P3), D = F + e (P3), where a disproportionation step is assumed with k_{dis} = 3 $mol^{-1}dm^3s^{-1}$.

As was stated previously, P2 is seen to get smaller as scan rate is slowed down (figure 2.4 and 2.5), this suggests that a chemical reaction step was occurring which was outrunning the slow scan rate. This is thought to be a disproportionation reaction of the one-electron reduced species. Probing of the chemical reversibility of P1 –via scan rate dependence- could be used to help ascertain the reaction process.

Digisim 2.0 was also employed to corroborate findings of the mechanism for this chemical step. Figure 2.5B shows the simulated findings that correlate very well with the experimental data, with overall shapes of the peaks -particularly P1- closely reproduced. The only significant deviation from the experimental data was the

broader aspect of P3. By using the ratio of I_{peak}^{ox} / I_{peak}^{red} for the process P1, a sensitive measure was employed for determining whether it was indeed a second order disproportionation reaction. The plot of this in figure 2.6C follows this theory (*vide infra* equation 2.4), with a k_{dis} (at pH 12) of $3 mol^{-1} dm^3 s^{-1}$.

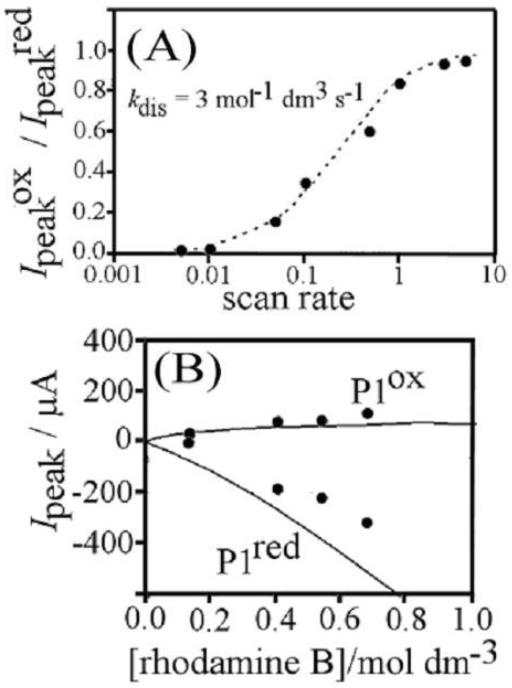

Figure 2.6
(A) Plot of the ratio of peak currents (figure 2.5) I_{peak}^{ox} / I_{peak}^{red} for process P1 versus the scan rate. Simulation data is shown as a dashed line and experimental data points as dots.
(B) Plot of the experimental (dots) and simulated (line) peak currents for process 1 versus rhodamine B concentration for the reduction of rhodamine B in PPP (deposition volume 16 nL) immersed in 0.5 M phosphate buffer solution pH 12

In order to further confirm the disproportionation process, probing the effect that concentration had on the voltammetric signals was needed. Figure 2.6D shows a plot of the peak current of both the oxidation ($P1^{ox}$) and the reduction ($P1^{red}$) as a function of changing concentration. The increasing reaction rate at higher concentrations was confirmed by the behaviour of P1 therefore confirming the theorized disproportionation reaction.

2.4.4 - Suggested Mechanisms

As a result of the triple phase boundary reaction conditions, the redox process is associated with a corresponding ion transfer process. Due to the fact that the reversible response of P1 is unchanged by varying the pH of the electrolyte over a value of 10 and above (vide infra), this suggests that the process is a one-electron one-sodium ion transfer, see (equation 2.1).

(Equation 2.1)

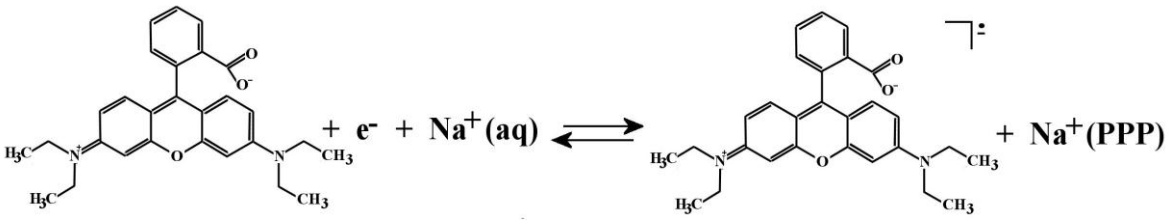

It is seen that the peak current of P2 (relative to P1) becomes larger at faster scan rates where it eventually reaches a similar peak height magnitude to process P1, and smaller at slower scan rates. This is indicative of a one-electron one-proton transfer, see equation 2.2.

(Equation 2.2)

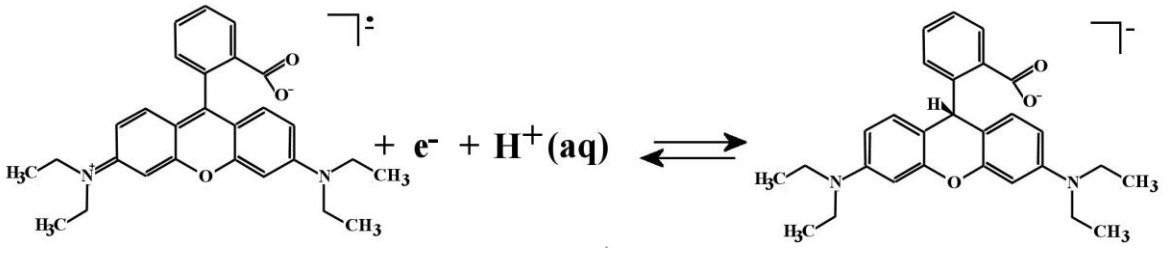

Equation 2.3 shows the mechanism for the overall oxidation seen at ~1.1V. The integration of the oxidation peak P3 corresponds to the P1 + P2 peak integration, illustrating a two electron oxidation.

(Equation 2.3)

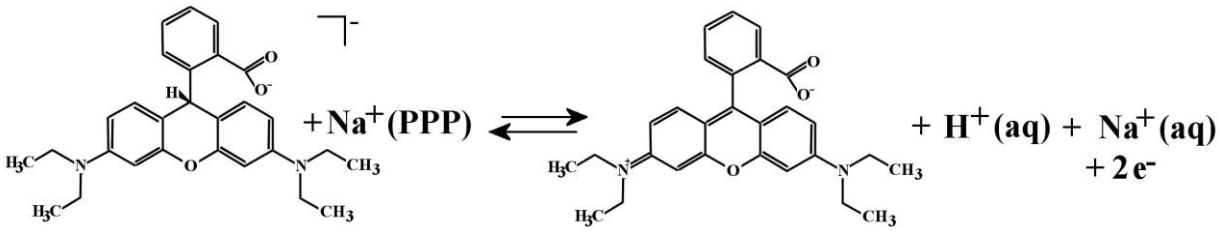

The disproportionation reactions mechanism scheme is shown below in equation 2.4. It involves two molecules of the one-electron reduced rhodamine b, reacting together in a chemical step to form one molecule of the leuco-rhodamine (two-electron reduced species) and one molecule of the oxidized rhodamine b starting material (*vide infra*).

(Equation 2.4)

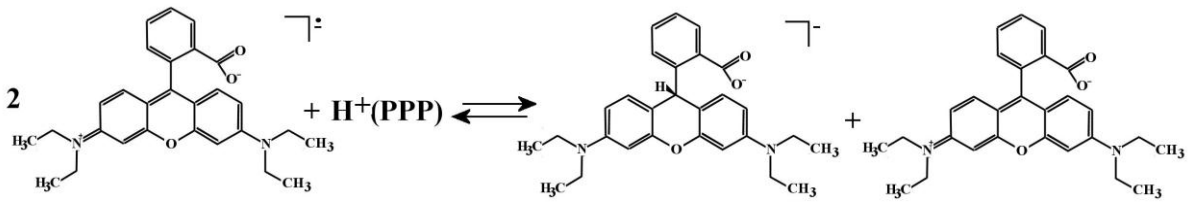

2.4.5 - Effect of pH

Thus far, the disproportionation reaction has only been explored at a constant pH 12. In other cases the rate of such disproportionation reactions has been linked with availability of protons, therefore studies were carried out probing the effect that pH had on the system. The proposed mechanism for the disproportionation reaction (equation 2.4) also included a proton transfer; therefore one would expect a degree of change to be observed in the voltammetry of the disproportionation reaction as the pH is varied.

The pH variance experiments showed that above a value of *ca* pH 10, processes P1 and P3 remained in roughly the same positions along the potential scale. This insensitivity to proton concentration is reflected in the mechanism shown in equations 2.1 and 2.3 where the electron transfer was accompanied by transfer of a sodium ion. However, below pH 10 a clear change was seen as a shift of the voltammetric signals towards more positive potentials. Another interesting observation in the more acidic range is that the second reduction peak, P2, was seen to merge with P1, and seems to become a single two-electron process.

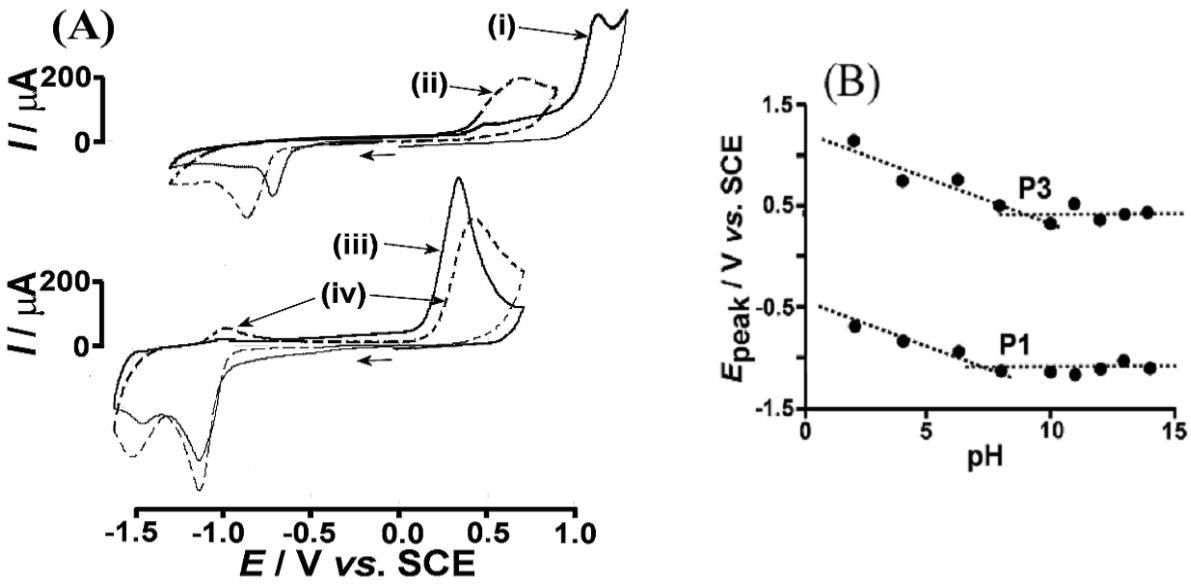

Figure 2.7

(A) Cyclic voltammograms at a scan rate of 0.1 Vs^{-1} for the reduction of 0.28 M rhodamine B base immobilised in microdroplets of PPP, 40 nL, deposited onto a 4.9mm graphite disc, immersed in 0.5 M phosphate buffer solution at (i) pH 2, (ii) pH 4, (iii) pH 12, and (iv) pH 14.
(B) Plot of the peak potentials for the reduction peak P1 and the oxidation peak P3 of rhodamine b at conditions listed above versus pH.

The disproportionation reaction was also seen to undergo change as a result of a change in pH. As seen in figure 2.7, the peak P3 is seen to get larger as a result of increasing pH. This means that the chemical step, in the form of the disproportionation reaction, was loosing ground to the electrochemical step at higher pH's. Further examination of how pH affects the disproportionation reaction was done by looking at the ratios of reduction peaks P1 and P2 and seeing how these were affected across the pH range.

The ratio parameter was taken as $I_{peak,\ P2}/I_{peak,\ P1}$. This process worked as a sensitive measure for looking at the progress for the disproportionation reaction, due to the fact that, as long as a constant scan rate was maintained, the ratios of peaks P1 and P2 will only change depending on how fast the chemical step is proceeding. If at a certain pH the chemical disproportionation reaction was proceeding faster, then the second reduction peak, P2, would be seen to get smaller as a result of the chemical reaction 'using up' the available one-electron reduced material before it can be reduced. This would therefore make the value for our disproportionation ratio parameter of $I_{peak,\ P2}/I_{peak,\ P1}$ become smaller. The graph constructed of $I_{peak,P2}/I_{peak,\ P1}$ plotted against pH, is illustrated in figure 2.8. As the number for the ratio approaches zero, the slower the disproportionation reaction. The graph clearly indicates a trend in that as we progressed to ever more alkaline environments, the disproportionation reaction slowed.

This observation of the activity of the disproportionation reaction as a function of pH would suggest that the chemical step is linked to proton transfer as part of the mechanism, and thus would fit with the suggested scheme for this reaction shown in equation 2.4. It is has not yet been made clear in what way the rhodamine b facilitates this proton transfer, but it is thought to involve the carboxylate functional group which acts as a facilitator/counter ion to the proton. This was explored in experiments involving a sister compound to rhodamine b, *(vide infra).*

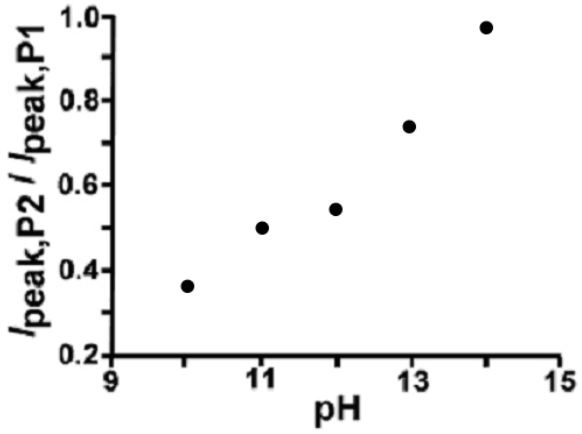

Figure 2.8 - Plot of the ratio of peak currents $I_{peak}^{red}(P2)$ / $I_{peak}^{red}(P1)$ for processes P1 and P2 vs pH, at experimental conditions equal to those stated in figure 2.7

2.5- Voltammetry of Rhodamine Octadecylester Perchlorate, Dark Processes

Rhodamine octadecylester perchlorate was used in order to further ascertain the mechanisms proposed for rhodamine b more fully. Its structure is shown in figure 2.9, and is identical to rhodamine b, save for replacing (and hence protecting) the carboxylate group with a long alkyl chain. The effects of hydrophobicity and determination of whether the carboxylate group played a part in the facilitation of proton transfer were explored by comparing results obtained for the rhodamine octadecylester system, to those already obtained for rhodamine b.

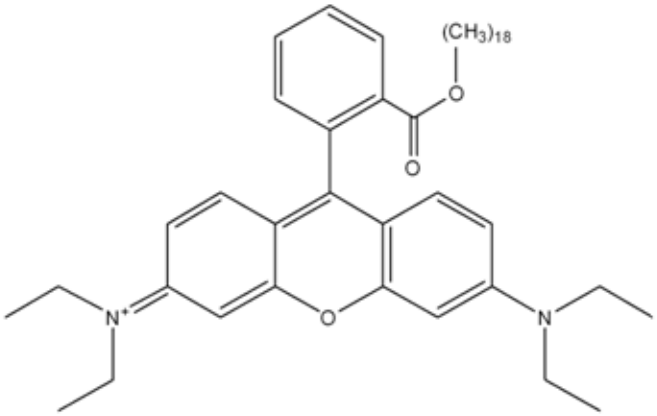

Figure 2.9 – Structure of rhodamine octadecyl perchlorate

The cyclic voltammograms shown in figure 2.10 show the reduction and re-oxidation of the rhodamine octadecylester. The resulting CVs were almost identical to those observed for the rhodamine b system, both in terms of positions and magnitude, with the processes P1, P2 and P3 being easily identified. This would seem to indicate very similar mechanisms occurring for the electrochemical reduction/oxidations in both systems. However, it should be noted that addition of NBu_4PF_6 as a supporting electrolyte directly into the organic phase was found to be necessary in order to significantly enhance the voltammetry signals. The effect of adding electrolyte is shown in figure 2.10A. The addition of the NBu_4PF_6 improved the ionic conductivity of the organic phase and thus will have aided in the electron transfers that take place. It is not fully understood why the addition of adding electrolyte enhanced the signals so significantly.

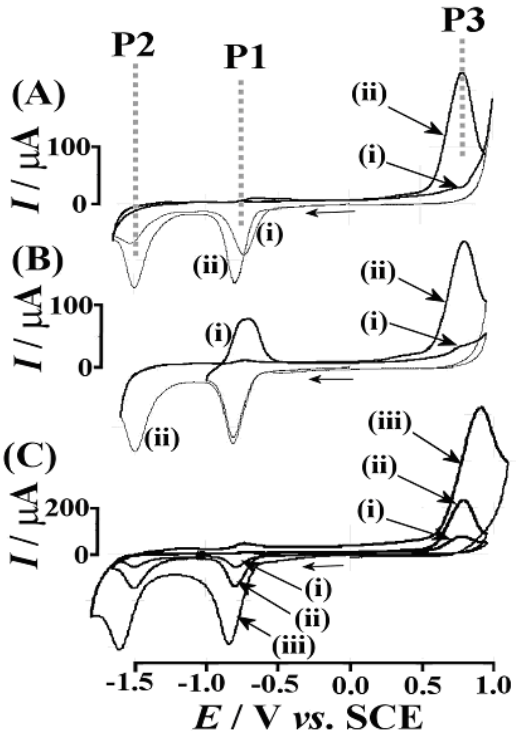

Figure 2.10
(A) Cyclic voltammograms at a scan rate 0.1 Vs^{-1} for the reduction and re-oxidation of 32mM rhodamine b octadecyl ester immobilised in PPP microdroplets, 62 nL, in 0.5 M phosphate buffer solution pH 12 (i) without and (ii) with 0.1 M NBu_4PF_6 added into the organic phase.
(B) Cyclic voltammograms (scan rate 0.1 Vs^{-1}) for the reduction and re-oxidation of 32mM rhodamine b octadecyl ester immobilised in PPP (deposition volume 62nL nL, with 0.1 M NBu_4PF_6) in 0.5 M phosphate buffer solution pH 12 recorded over (i) a small and (ii) a wider potential window.
(C) Cyclic voltammograms (scan rates (i) 0.05Vs^{-1} (ii) 0.1Vs (iii) 0.5Vs^{-1}) for the reduction and re-oxidation of 032m M rhodamine b octadecyl ester immobilised in PPP (deposition volume 62nl nL, with 0.1 M NBu_4PF_6) in 0.5 M phosphate buffer solution pH 12.

Figures 2.10B and C show cyclic voltammetry scans using the same potential window as was used on the rhodamine b system (see figures 2.4 and 2.5 for equivalent rhodamine b voltammograms). These include encompassing the whole range of processes (P1, P2 and P3), and also just encompassing the first reduction, (P1, and returning for re-oxidation). When a smaller potential window was used for the cyclic voltammetry on rhodamine octadecylester, it could be seen that process P1 was fully reversible, which is exactly what was seen previously in this report for rhodamine b.

One key difference between the two systems is shown in figure 2.10C. When cyclic scans were conducted with a potential window large enough to allow both P1 and P2 to occur, we see that the ratios of these two peaks remained constant, even throughout the slower scan rates. In contrast to this, the rhodamine b system showed the second reduction peak, P2, getting smaller at slower scan rates as a result of the chemical step, in the form of the disproportionation reaction. The evidence from the rhodamine octadecylester voltammograms would suggest that since the reduction peak ratios of P1 and P2 remain contrast throughout the scan rates, then the disproportionation reaction was not occurring, or if it was, occurring imperceptibly slowly at the studied scan rates. There are several suggested possibilities as to why this may be the case. One possibility is that the steric bulk of this species was hindering the ability for the molecules to approach and react with one another; and that the one-electron reduced species for rhodamine octadecylester is relatively stable under bi-phasic conditions.

Another possible reason for the disproportionation reaction not occurring is the carboxylic group present within the rhodamine b system, it is this functional group which is likely to be responsible for facilitating the transfer of protons from the aqueous phase, as needed for the disproportionation reaction. With the octadecylester group in place of this carboxylic group the transfer may simply be non-existent, and hence no evidence of a disproportionation reaction was recorded for this system.

2.6 - Photo-Electrochemical Processes for Rhodamine B Base.

We have already outlined how light driven processes occurring at interfaces between two immiscible liquids could be of importance towards the goal of light harvesting [110]. With a reasonable understanding of the dark electrochemical processes of rhodamine b, it is possible to move on to examine the effect that light would have on the system.

A cell was also constructed in order to proceed with the photo measurements, with a rectangular design and a channel cut into the top. This channel was covered with a quartz window. Plastic tubing entered from either side to feed in and out of the channel, and it was in these tubes that the reference and counter electrode were also situated to allow connection with the working electrode. The bppg working electrode could be inserted from the bottom until it was flush with the cut channel, the electrode was then illuminated from the top through the quartz glass window (figure 2.11). This system also employed a flow of electrolyte across the surface of the electrode, at around a value of approximately 5 ml min^{-1}, this flow served to circumvent any thermal effects that the light may have had on the voltammetric responses.

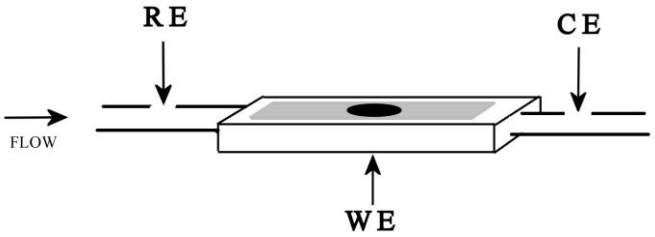

Figure 2.11- Schematic representation of the Photo-electrochemical flow cell constructed.

The light was pulsed as this allowed a clear characterisation of any photocurrents that may have been observed. It also served to allow information on the response time of the photocurrents to be determined. Under illuminated conditions, microdroplets of rhodamine b in PPP showed a clear change when compared to voltammograms that had been run under dark conditions. The resulting voltammograms showed a new oxidation peak taking place (figure 2.12). This new photo-induced oxidation was seen at approximately -0.85V *vs.* SCE. It is also important to note that as a result of the new photo-induced oxidation, the oxidation we previously observed for leuco-rhodamine, P3, was seen to disappear. It was interesting to note that this new photo oxidation was seen at the same potential to the reversible oxidation of the one-electron reduced rhodamine b species (P1). Because of this and other evidence (*vide infra*) it has been suggested that the mechanism involved in the photo process is the result of another chemical step, this time in the form of a conproportionation reaction. This step is thought to form the one-electron reduced species, which was then electrochemically oxidized back to the starting species.

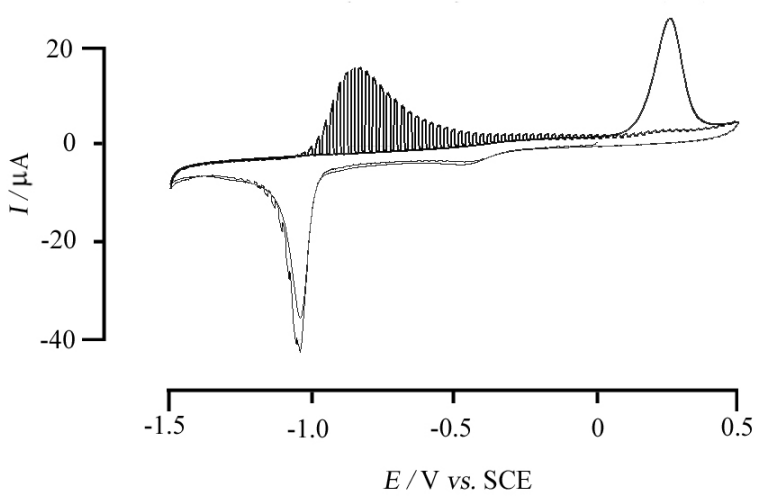

Figure 2.12 - Comparative CV's showing photocatalysed oxidation (seen at approximately -0.8V) and a regular voltammogram of rhodamine b base at the same scan rate. 64nl deposit, 0.28M rhodamine:PPP, 0.01V/s

2.6.1 - Photocurrent Spectroscopy

In order to gain further details about the photo-induced oxidation that was observed, experiments utilizing photocurrent spectroscopy were carried out. These involed conducting chrono-amperometry scans as a function of wavelength with the incident monochromatic light chopped by a rotating sector blade; a lock-in amplifier was then employed to detect both the presence and magnitude of any pulsed currents that occurred at that frequency.

A graph could then be constructed plotting the magnitude of the observed photocurrents against the incident wavelength of the chopped light. Figure 2.13 shows the results of the photocurrent spectroscopy where a clear absorption at 550nm was seen. When we compare this with values in the literature [(104)] as well as UV-visible measurements conducted with rhodamine b in PPP, it shows that the species which undergoes photo-excitation is the oxidized form of rhodamine b. This species is still present within the droplets, as the scan rates are slow enough to allow the disproportionation reaction to take place, which creates the starting species along with the two-electron reduced species.

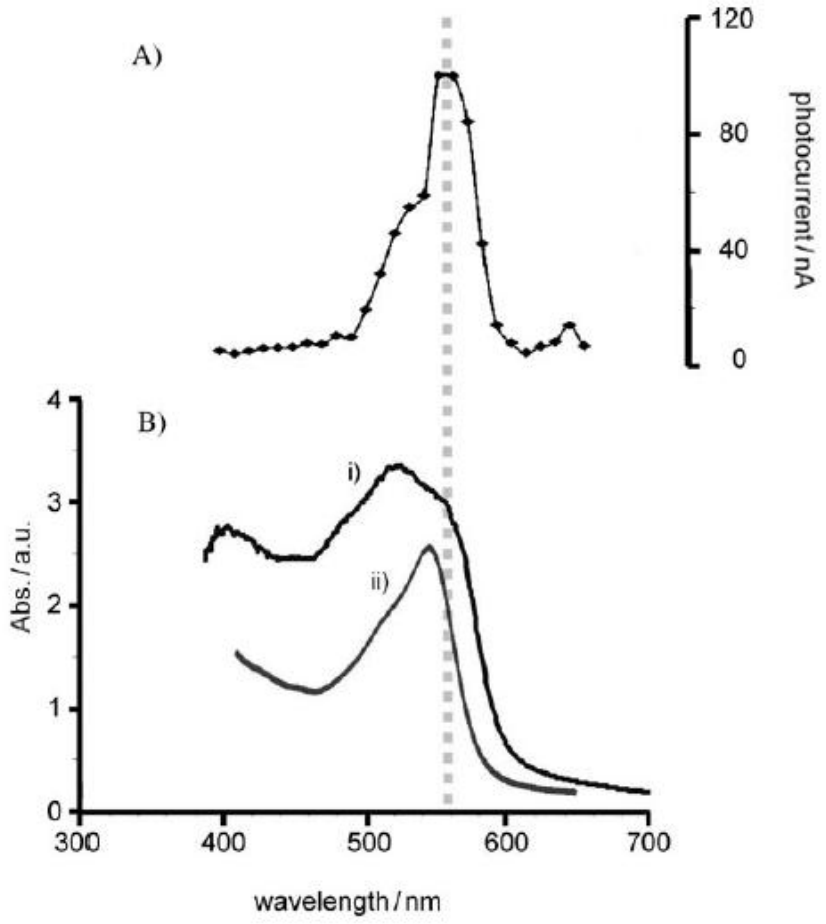

Figure 2.13
(A) Photocurrent spectroscopy spectrum for the photo-induced oxidation of rhodamine b, immobilized in PPP microdroplets on a graphite disc inmmersed in 0.5M pH 12 phosphate buffer.
(B) UV/Vis spectra of a rhodamine b / PPP solution shown both before (i) and after (ii) contact and equilibration with phosphate buffer, 0.5M pH 12

2.6.2 – Photo Induced Conproportionation Reaction

Using the data gathered, a scheme for the photo-induced oxidation mechanism is proposed. It is suggested that a conproportionation chemical step reaction takes place between the photo-excited starting species and the two-electron reduced species, leuco-rhodamine b. One mole of each reacted together in a chemical reaction step forming two moles of the one-electron reduced species.

The proposed mechanism for this is illustrated in equation 2.5. As it is the one-electron reduced species that is formed as a result of the photo-excitation and subsequent chemical conproportionation step, it is now clear why we observe the photo-oxidation response, as a reversible signal for the process P1 –as P1 corresponds to a one-electron reduced species-.

(Equation 2.5)

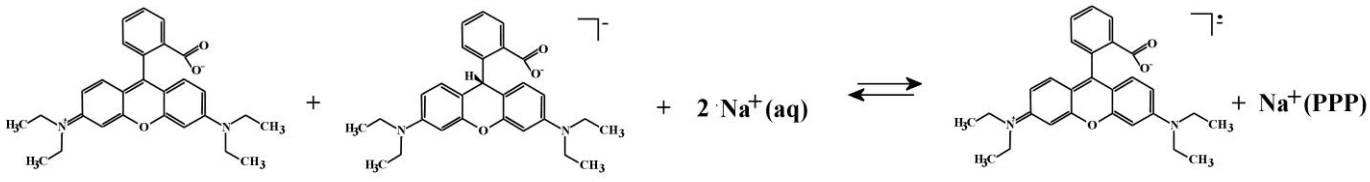

2.6.3 - Effect of pH on the Photo Processes

The effect that pH has on the photo-induced oxidation was also studied, this is shown in figure 2.14. The data shows that the optimum pH range for the conproportionation reaction to take place is basic conditions above pH 10. A suggested rational for this is that at pH ranges of 10 and above, there may a competing mechanism in the form of the disproportionation reaction. The presence of protons as a result of a more acidic environment would have caused the disproportionation reaction to occur more quickly relative to the conproportionation reaction, and thus be responsible for the loss of the photo-induced mechanism, due to less one-electron reduced material being present.

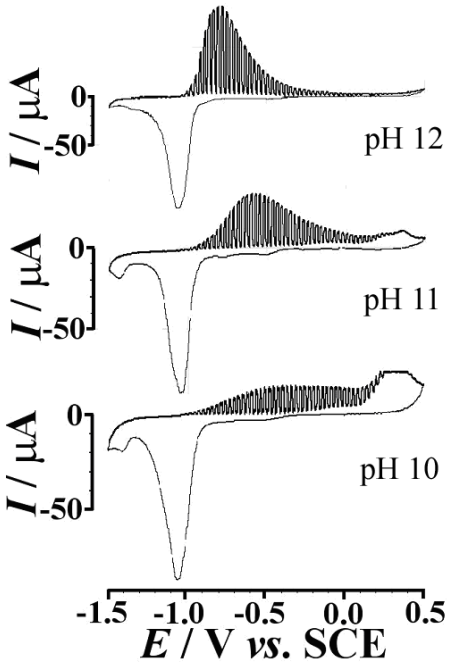

Figure 2.14 - Cyclic voltammograms for reduction of 0.28M rhodamine b at a scan rate of 0.01 Vs^{-1} immobilised in PPP microdroplets, 64 nL on a 4.9mm graphite disc immersed in 0.5 M phosphate buffer solution

2.7 - Computer Simulation Corroboration of Proposed Mechanisms

2.7.1 - Effect of Light Intensity

In order to further study the proposed mechanism, experiments were conducted studying the photo-effect, and the influence that scan rate and light intensity had upon it. Computer simulations of these experiments were then executed using the proposed mechanism for the conproportionation reaction and then compared to experimental values.

Variation of light intensity showed a clear effect (figure 2.15) on the photo-induced oxidation. As the light source was dimmed, the peak corresponding to the photo-process weakened significantly, as well as gradually shifting to more positive potentials, until dark conditions were approached, when only the original consecutive two-electron oxidation, P3, was observed.

The mechanism for the conproportionation reaction was programmed into a DigiSim computer simulation, and the photo-excited state formation was modelled as a reversible pre-equilibrium. The multiplication value of the equilibrium constant, rhodamine b concentration, and the 'concentration' of photons gives the steady-state concentration of the photo-excited state. When compared to the experimental results, good correlation was shown between the experimental data and the simulated voltammograms (figure 2.15), thus providing corroborating evidence for the proposed mechanisms for the photo electrochemistry. The simulation allowed an estimate of the rate constant for the chemical step at a value of $k_{dis} = k_{con} = 3\ mol^{-1}\ dm^3\ s^{-1.}$

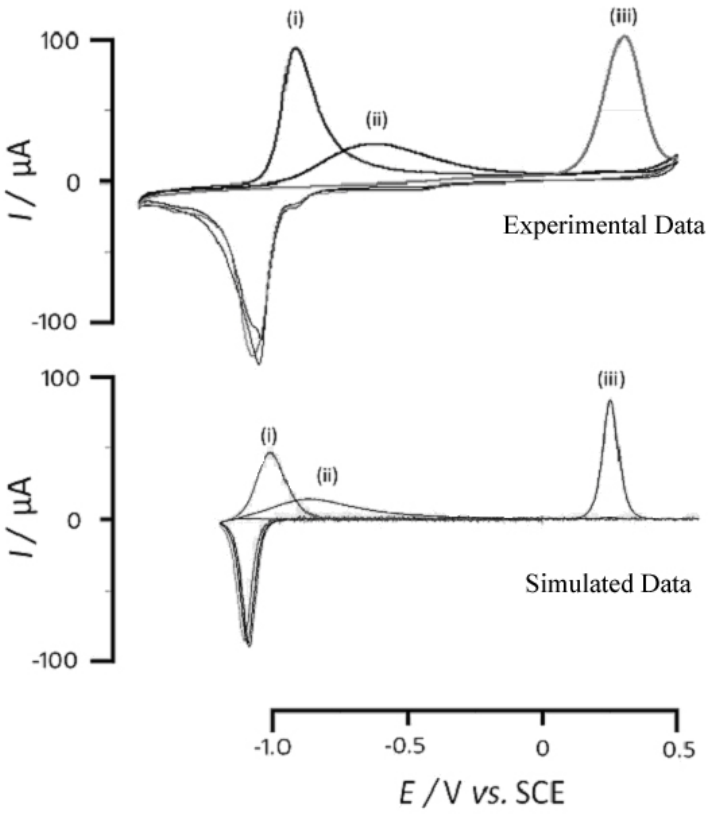

Figure 2.15 – (Experimental data) Cyclic voltammograms conducted at 0.01V/s for a 40nL deposit of 0.28M rhodamine b immobilized in PPP on a graphite disc immersed in pH 12 0.5M phosphate buffer.
(i) Full light intensity, (ii) 30% light intensity, (iii) Dark

(Simulated Data) Digism 2.0 simulation for the reduction of rhodamine B 0.28 M at same scan rates and deposition values as experimental in a thin film without diffusion limitation (assuming sufficiently high diffusion coefficients). The assumed simplified mechanism is given by A + e = B (P1), B + B = C + A, C = D + e (P3), D = F + e (P3), A + P = G (photo excitation), G + C = B (conproportionation) where a disproportionation step is assumed with k_{dis} *= 3* $mol^{-1}dm^3s^{-1}$.

2.7.2 - Effect of Scan rate

The effect that scan rate had on the photo-electrochemical process was also explored in cyclic voltammetry experiments, and these results compared with simulated data (using the same parameters as before for the conproportionation reaction). As the scan rate becomes faster, the voltammetry will start to outrun the photo-electrochemical process, and thus the original consecutive two-electron oxidation peak starts to become apparent again. This causes the photo-induced oxidation to become weaker, and it was seen to move to more positive potentials and merge with the original two-electron consecutive oxidation P3 peak.

Once again simulated data using the proposed mechanisms for the conproportionation and disproportionation reactions show a good fit with the experimental data, corroborating the suggested schemes. The results for scan rate variance on the photo-electrochemical process is shown in figure 2.16.

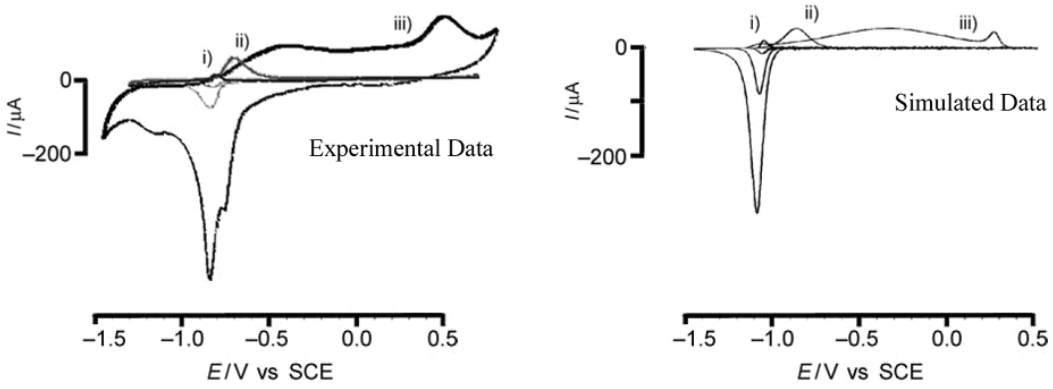

Figure 2.16 - Cyclic voltammograms at scan rates of (i) 0.001 (ii) 0.001 and (ii) 0.05V/s for the reduction of 0.28M rhodamine b in microdroplets of PPP, 40 nL, deposited onto a 4.9mm graphite disc, immersed in 0.5M pH 12 phosphate buffer. Distortion in first reduction peak of (iii) is artefact of pump noise. Simulated data as in figure 2.15 (vide ante).

2.8 - Photo-Electrochemical Processes for Rhodamine Octadecylester Perchlorate

The rhodamine octadecylester was also explored for photo activity, however it displayed no photo-electrochemical reactions, nor showed any evidence of the dark process disproportionation reaction as was seen for the rhodamine b system. It was noted earlier that the absence of the carboxylate functional group was likely responsible for the fact that rhodamine octadecylester was not observed to undergo disproportionation reactions, and it is this which is likely to be the cause of the observed lack in photo-electrochemical activity for the rhodamine octadecylester system.

2.9 - Summary

The work carried out in this section has shown that rhodamine B immobilized in PPP under illumination will undergo a distinct photo-electrochemical process. A chemical step which occurs in dark conditions was shown to be a disproportionation reaction forming leuco-rhodamine b, occurring between two molecules of the one-electron reduced rhodamine b, and was shown to have a rate constant of $k_{dis} = 3\ mol^{-1}\ dm^3\ s^{-1}$.

Under illumination, a photo-electrochemical process is seen to occur in the form of a photo-induced excited state which takes part in a conproportionation reaction. This ultimately photo-catalyses the original consecutive two-electron oxidation, and a new peak is observed at the reversible potential of P1. The dynamic nature of the triple phase boundary area, in which ion exchange occurs in tandem with the electron exchange as a result of the voltammetry, means that the balance between protons and

other cations in the aqueous phase can play an important role in determining which steps of a process will predominate over others.

This research has so far yielded a good understanding of the photo reactions that occur for rhodamine b base immobilised in PPP microdroplets. The next step would be to use this understanding in order to couple the photo processes that occur within the microdroplets to other reactions, for example in order to attempt to harvest the energy from light.

Chapter 3

Triple Phase Boundary Photovoltammetry of Pentoxyresorufin in PPP Microdroplets

Contents

Published - "Liquid|Liquid|Electrode Triple Phase Boundary Photovoltammetry of Pentoxyresorufin in 4-(3-Phenylpropyl)Pyridine" in *Langmuir*, 2011, **27**, 6471-6477

3.1 - Abstract

The voltammetry of pentoxyresorufin in microdroplets of 4-(3-phenylpropyl)pyridine (PPP) immersed in an aqueous electrolyte is studied, both in the dark, and in the presence of light. In the dark, pentoxyresorufin undergoes a two-electron reduction to leuco-pentoxyresorufin. Changes in pH affect this two-electron reduction due to change in proton concentration, but also in that changes occur to the electrolyte | PPP interfacial tension. When voltammetric measurements are conducted with pentoxyresorufin in the presence of light, no net significant photocurrent responses are revealed, however certain transient signals which are observed seem to be suggestive of distinct electron and hole charge carries. This is later confirmed via EPR, suggesting the formation of a long-lived radical intermediate as a result of the illumination.

The pentoxyresorufin voltammetric responses are also investigated with a co-reactant, duroquinone. In PPP microdroplets, duroquinone is shown to have a two-electron two-proton reduction to duroquinol, again no photocurrents are observed for this system. A mixture of pentoxyresorufin and duroquinone in PPP microdroplets yields a different result; the pentoxyresorufin acts as a photo-catalyst for the oxidation of duroquinol back to duroquinone. Wavelength-resolved photo-voltammetry distinctly indicates the pentoxyresorufin as the photo-excited intermediate. A photo-electrochemical mechanism is proposed based on the presumption of a long lived, photo excited intermediate in the PPP phase, evidence also suggests that this intermediate exists as an exciplex of resorufin and PPP.

3.2 – Introduction and Previous Work

Resorufin pentylether is part of a family of dye molecules that are used as a tool for the study of the reactivity and kinetics[112] of enzymes. In a recent electrochemical study, a sibling of pentoxyresorufin –methoxyresorufin- was employed as a probe for the activity of enzyme P450[113]; this study has shown it to undergo a reversible two-electron transfer (at pH 7.4) centred at a mid-point potential of approximately –0.26V *vs*. Ag/AgCl (3M KCl).

Resorufin was chosen for this study due to its highly hydrophobic nature, and therefore stability within PPP microdroplets immobilized on a graphite surface. This study shows interesting effects on the organic phase as a result of pH. Photoreactions are induced with the utilization of a co-reactant molecule, duroquinone, which is employed as an internal quencher. The photoreaction between these two molecules with the microdroplet is the first step towards solidifying an idea utilizing a quinone/quinol system in tandem with photoexcited resorufin towards the goal of light harvesting.

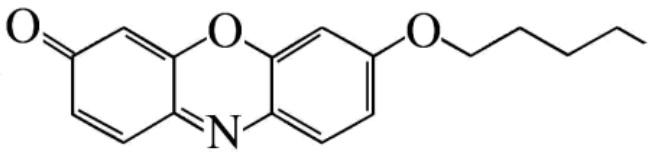

Figure 3.1 – Structure of pentoxyresorufin

In this chapter Electron Paramagnetic Resonance (EPR) is used as an analytical technique to shed light on the products that arise as part of the illuminated reactions. This technique uses microwave spectroscopy in the presence of a magnetic field to detect unpaired electrons in molecules. This is a very powerful technique when radicals and reaction intermediates need to be investigated[114].

Electron posses two spin states; these are either +1/2 or –1/2. When introduced to a magnetic field, these states can absorb energy and jump to higher energy spin states, this gap corresponds to values within the microwave range for the typical fields as used by typical x-band EPR spectromenters[27].

3.3 – Experimental

3.3.1 - Reagents

Pentoxyresorufin (Aldrich), duroquinone (Lancaster >98%), 4-(3-Phenylpropyl)pyridine (PPP) (Aldrich 97%), sodium hydroxide (Aldrich >97%) and phosphoric acid (Fisher Scientific, 85 wt%) were used as received from the supplier without further purification. A Thermo Scientific purification device was used for providing filtered, demineralised water with a resistivity of >18.2 MΩ cm. Laboratory temperature conditions were $20^{o}C \pm 2^{o}C$

3.3.2 - Instrumentation

An Ivium technologies 'compactstat' potentiostat (v1.725) was used for all voltammetric measurements and experiments. A standard three-electrode electrochemical cell was used, employing a quartz glass optical which was used as necessary for any photo measurement. The working electrode consisted of a basal plane pyrolytic graphite electrode (bppg) and had a diameter of 4.9mm, this was mounted in a Teflon sheath. A cell was also constructed with a rectangular design and a channel cut into the top and covered with a quartz window. The bppg electrode could be inserted from the bottom until it was flush with the cut channel, and therefore the electrode could be illuminated from the top through the quartz glass window whilst employing a flow of electrolyte over the electrode surface. This flow was approximately 5 ml min^{-1}, and served to circumvent any thermal effects that the light may have had on the voltammetric responses. Both electrochemical cells also consisted of a platinum counter electrode and used a saturated calomel (SCE REF401, Radiometer) reference electrode.

Light was provided from a variety of sources. For a white light source a Fiber-Lite high intensity halogen bulb (MI-150, Dollan-Jenner Industries) was employed. This was shown to have an intensity of approximately 60 $mWcm^{-2}$ at the location of the electrode, (light intensity measurements conducted with an optical power meter, PM100A, Thorlabs Instruments). Photo-voltammetric action spectra were obtained by use of monochromatic mounted LED's (Thorlabs Instruments) with wavelengths of 405, 455, 530, 590, 625, 660 and 735 nm. Each mounted LED was tested using an optical power meter (PM100A, Thorlabs Instruments) and calibrated to ensure an

equal power output of 2.4 $mWcm^{-2}$ using the LED power supply (LED – Driver, LEDD1B, Thorlabs Instruments). Pulsing of light was achieved by using a rotating sector blade design mounted between the light source and the cell.

UV Visible spectroscopy was conducted using a Cary 50 Probe UV-Vis Spectrophotometer from Varian Inc. Electron Paramagnetic Resonance (EPR) spectra were obtained using a Brucker Biospin X- Band spectrometer (E500, X-Band) which utilized a nitrogen gas flow system for temperature regulation.

3.3.3 - Electrode Preparation Procedure

A random microdroplet array of PPP containing pentoxyresorufin (and/or/duroquinone) on a bppg electrode was achieved by creating a deposition mixture with acetonitrile as the carrier solvent (6 to 10ml). This contained *ca.* 0.1 – 2 mg of the electro-active compound (pentoxyresorufin and/or duroquinone) and approximately 80mg of PPP. An aliquot of the entire deposition mixture (normally between 1-10ul) was deposited onto the electrode surface. As the acetonitrile evaporated off, a random array of PPP microdroplets was left behind on the electrode surface.

3.4 - Voltammetry of Pentoxyresorufin

Following the electrode preparation procedures outlined *(vide ante),* a random array of PPP microdroplets containing pentoxyresorufin was deposited onto a 4.9mm graphite disc and employed as the working electrode in a standard three electrode electrochemical cell. The electrolyte used was 0.1M phosphate buffer with the pH tuned by addition of sodium hydroxide. Basic cyclic voltammetry scans at pH 6 showed one reduction peak followed by one oxidation peak, this was shown to have a mid point occurring at approximately –0.1V *vs* SCE (figure 3.2).

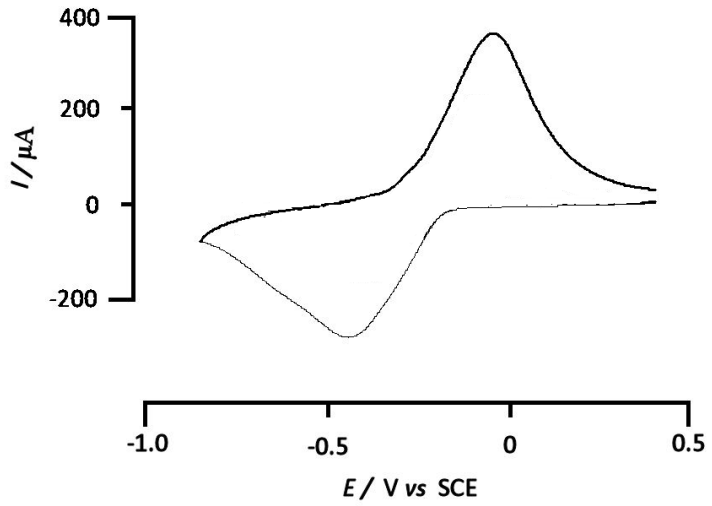

Figure 3.2 – Cyclic voltammogram of 90mM resorufin in PPP (39nL) deposited onto a 4.9mm graphite disc and immersed in 0.1M pH6 phosphate buffer at a scan rate of 100mVs^{-1}.

3.4.1 – Effect of Deposition Volume

Analysis of the area under the peak, corresponding to the charge, was utilized to ascertain the number of electrons transferred. By conducting multiple experiments where the amount of the acetonitrile mixture deposited was varied, it was possible to construct a graph of charge (from area under peak) *vs* deposition volume of PPP. This yielded a graph (figure 3.3) which indicated a two-electron process for both the reduction and oxidation peaks, this was also in concurrence with previous literature reports that have utilized resorufin[113]. The graph of amount deposited *vs* deposition volume of PPP veered off the expected line for a two-electron process as the higher deposition volumes were approached. This was due to the fact that as the droplets of PPP became ever larger, the electrolysis process took longer for full conversion of the pentoxyresorufin within the droplet, and hence veered away from what we would have expected to see for the two-electron process.

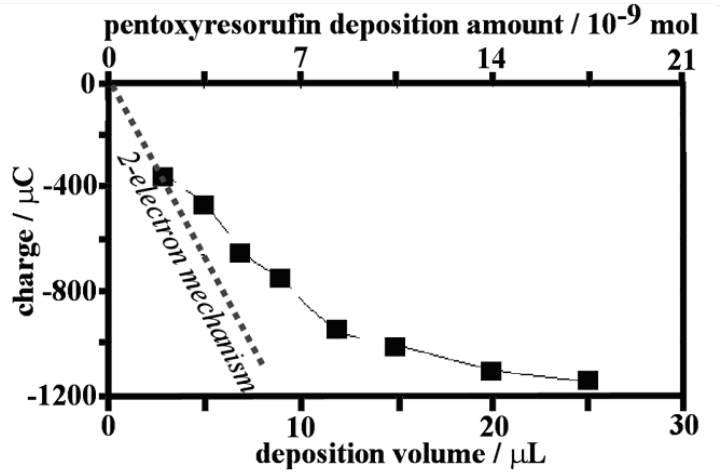

Figure 3.3 – Graph showing plot of area under peak for cyclic voltammograms of pentoxyresorufin in PPP 90mM, deposited onto a 4.9mm diameter graphite disc, immersed in pH 6 phosphate buffer, 0.l M, 0.01Vs^{-1}, vs deposition volume. Dashed line shows the theory line for a two-electron reduction.

3.4.2 – Effect of Scan Rate

Variation of scan rate was also explored; a 39nL deposit of PPP, containing 90mM pentoxyresorufin was immobilized on the surface of the electrode. A scan rate range of $1mVs^{-1}$ to $100mVs^{-1}$ was explored and adapted into a graph, using the area under the reduction peak *vs.* scan rate (figure 3.4). The plot resolved is near linear with a gradient of 0.979. This is consistent with complete conversion of the resorufin.

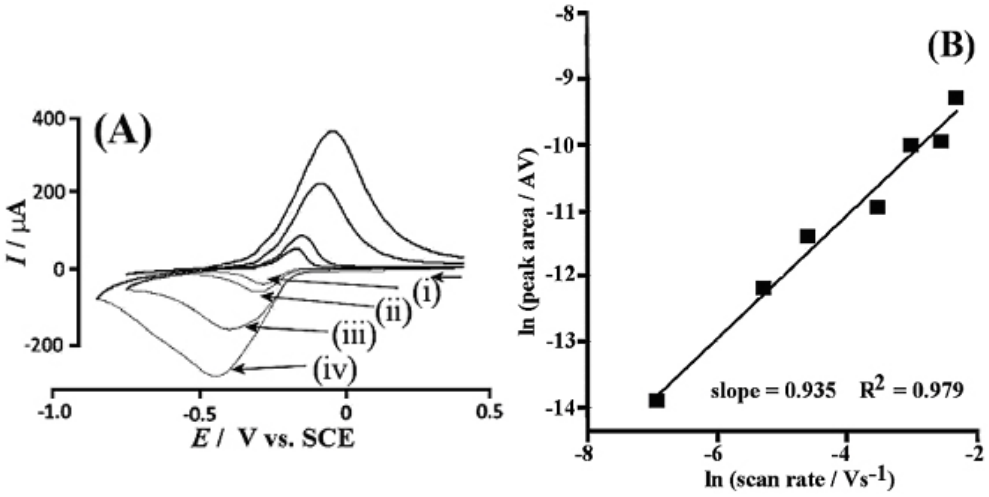

Figure 3.4
(A) Cyclic voltammograms for variation of scan rate of pentoxyresorufin 90mM in PPP microdroplets (39nL), deposited onto a 4.9mm graphite disc, immersed in 0.1M pH6 phosphate buffer, scan rates (i) 5, (ii) 10, (iii) 50 and (iv) $100mVs^{-1}$
(B) Plot of area under reduction peak vs ln scan rate

3.4.3 – Effect of pH

The effect of pH on the voltammetry of pentoxyresorufin in PPP microdroplets was also examined and yielded some surprising results. Using a concentration of 23mM pentoxyresorufin in PPP (140nL), the effects of altering the pH of the phosphate buffer over a range of 2-12 were explored. Figure 3.5 shows three voltammograms within this pH range.

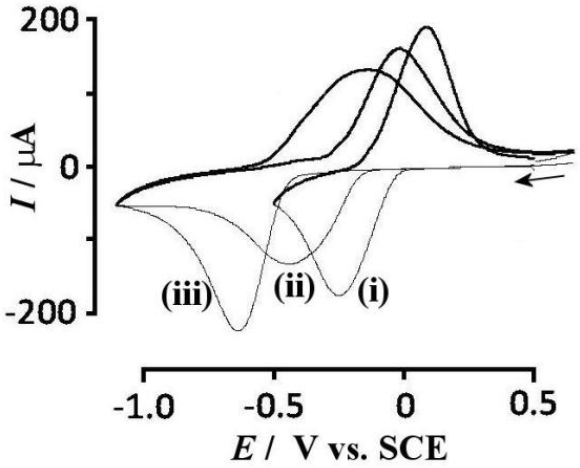

Figure 3.5 – Cyclic voltammograms of 23mM pentoxyresorufin in 140nL PPP, at a scan rate of 50mVs^{-1}, deposited onto a 4.9mm graphite disc and immersed in 0.1M phosphate buffer of (i) pH4, (ii) pH8 and (iii) ph12.

One thing that becomes apparent when looking at figure 3.5 is a shift of the mid point potential as a result of variance of the pH, which clearly indicates proton involvement. Another interesting observation is the voltammogram at pH 12, where the peak to peak separation is higher when compared to the voltammograms at the more acidic conditions. This was an unexpected result, and thus further explored to ascertain the reasons behind the observations. A graph was therefore constructed in

which pH was plotted against mid point potential (figure 3.6). On this graph, the values of the reduction and oxidation peaks are also plotted in order to give a perspective on the peak to peak separation as well. The line produced from the plot of pH *vs* mid point potential had a sharp change in gradient, this is indicative of a change in mechanism, and splits the pH region into two distinct zones, with the change occurring at approximately pH 8.

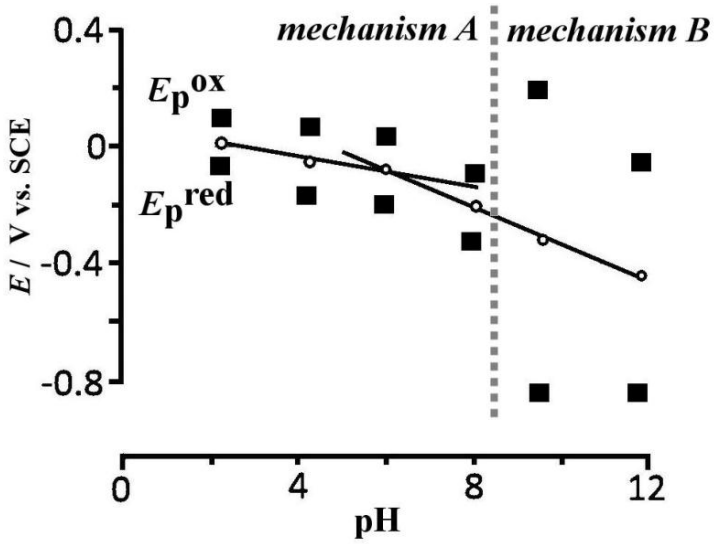

Figure 3.6 – Plot of pH vs mid point potential, $E_{mid,}$ for cyclic voltammograms of 23mM pentoxyresorufin in 140nL PPP, at a scan rate of 50mVs^{-1}, deposited onto a 4.9mm graphite disc and immersed in 0.1M phosphate buffer. The values of the reduction and oxidation peak, $E_{p,\,red,}$ $E_{p,\,ox}$, are also illustrated on this graph in order to give a sense of peak to peak separation.

3.4.4 - Proposed Mechanisms

These mechanism zones are shown on the graph and are named ‘Mechanism A’ and ‘Mechanism B’. These correspond to the pH regions of approximately 2 to 8 and 8 to 12 respectively. If we examine the gradient of the two regions we see that the pH range of mechanism B, corresponding to the more basic region, has a gradient of 60mV per pH unit. This is consistent with a transfer of two-protons from the aqueous electrolyte for every two-electrons transferred as a result of the voltammetry.

Mechanism A, corresponding to the more acidic region, had a gradient of 30mV per pH unit. This is indicative of a two-electron one-proton process, and is in contrast to mechanism b, where we saw a two-electron two-proton system. Curiously, the more acidic conditions showed a lower number of protons being transferred per electron. This result seemed counter-intuitive to what one would expect and therefore further experiments were devised in order to ascertain a reason for this result. A proposed mechanism for the reductions is shown as Mechanisms A and B.

(Mechanism A)

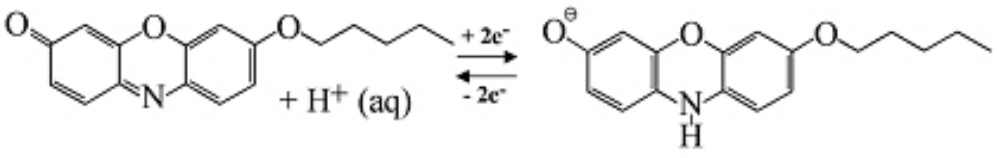

(Mechanism B)

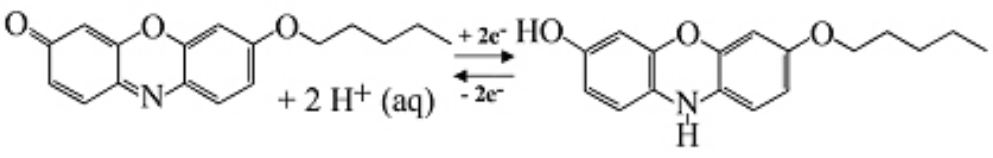

3.4.5 - PPP | Electrolyte Interface Experiments

A preliminary experiment exploring the unexpected change in proton involvement for the two mechanisms involved taking a few millilitres of PPP and putting this in a sample vial containing different pH's of 0.1M phosphate buffer. The result of this is shown in figure 3.7. The PPP reacted in two distinct ways depending on which pH zone it was placed in contact with.

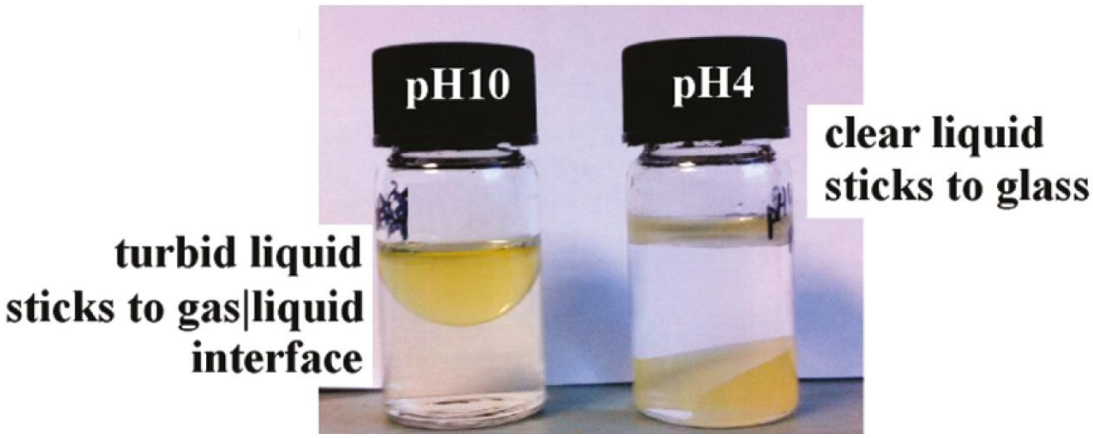

Figure 3.7 – Photographs of PPP mixed with aqueous electrolyte, 0.1M phosphate buffer at pH4 and pH 10

When immersed in 0.1M pH 10 phosphate buffer -corresponding to mechanism B- the PPP floated on the surface of the buffer, and seemed to display a repulsion towards the glass walls of the vial. If the vial was picked up and tilted, the 'mass' of PPP would tip with gravity but seem to resist contact with the glass and slide off the vial wall as opposed to sticking to it. This was in sharp contrast to what was observed with the PPP in contact with acidic pH4 phosphate buffer. In this case the PPP had a clearer appearance and also readily stuck the vial walls.

This clearly indicates that the PPP has different surface interactions depending on the pH of the phosphate buffer it is exposed to. In order to further explore this effect, another experiment was devised to probe the effects that the different pH's of phosphate buffer had on the PPP surface tension [115]. This involved lens angle measurements. A container with glass walls was created in order to photograph the results, and filled with phosphate buffer. A drop of PPP was deposited onto the phosphate buffer surface, where it floated. The contact angle that the droplet created was then measured. This was repeated across a range of pH values and a graph was constructed plotting pH *vs* lens angle. This is illustrated in figure 3.8.

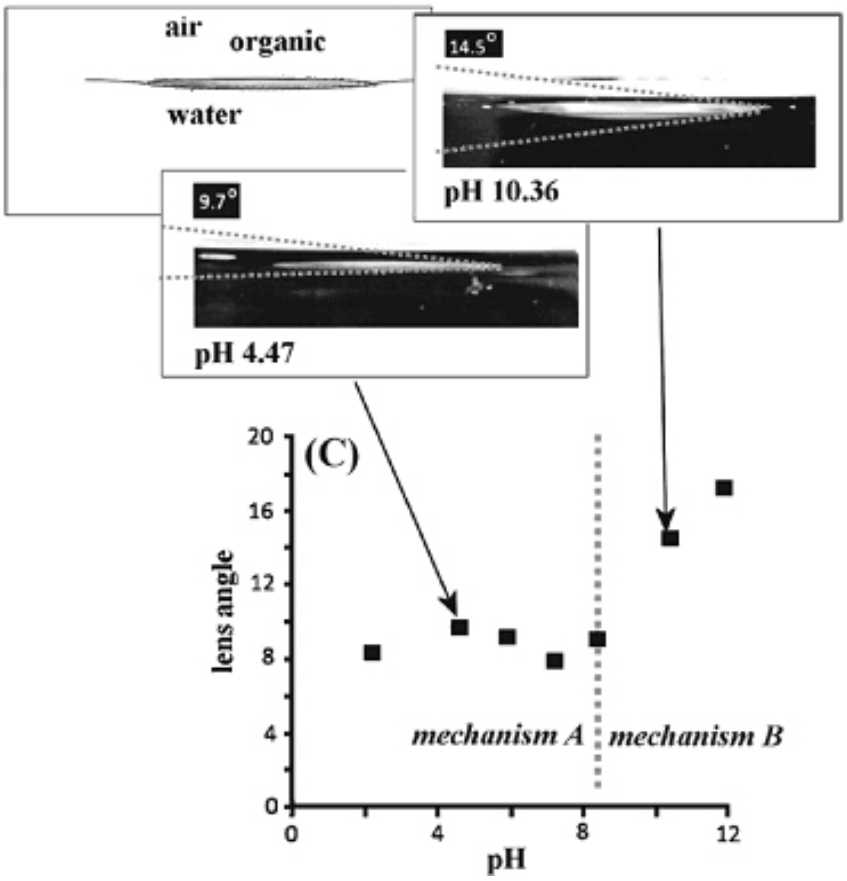

Figure 3.8 - Plot of approximate lens angle of PPP droplets floating on 0.1M phosphate buffer at different pH values.

Again, a distinct change in pattern could be seen as we crossed the pH range. Here we see lens angles of approximately the same values as we proceed from a pH of 2 to *ca* 8, but then a change occurred and the lens angles started to become larger. It is interesting to note that the point at which the change in pattern is seen on the graph occurs at approximately pH 8. This was at the same point in the pH range where we first saw a change in mechanism as a function of pH illustrated in figure 3.6.

From the data gathered it is suggested that protonation of the PPP surface is likely to occur at values at and below approximately pH 8, creating a positively charged surface. We can compare the pH value at which this occurs to the pK_A of a similar molecule, 4-methylpyridine, pK_A = 6.02. This explains the affinity of the PPP surface to the glass surface. This also explains the change in mechanism using fewer protons for the acidic conditions that we observed for 'Mechanism A' as well as the observed change in peak to peak separation. The fact that the PPP surface is charged as a result of the protonation means that the anionic reduction product created in 'Mechanism A' (shown in equation 5) can be stabilized by this protonated interface. Also the smaller peak to peak separation observed for 'Mechanism A' is indicative of a surface process, which again points towards the presence of a charged liquid | liquid interface stabilizing the reduction product as a result of the PPP surface protonation.

3.4.6 - Photo-electrochemistry of Pentoxyresorufin

Figure 3.9 shows two cyclic voltammograms of 23mM pentoxyresorufin in PPP microdroplets (140nL) immersed in 0.1M pH 8 phosphate buffer. One trace is in the dark, and the other is in the presence of pulsed light. The light was chopped to a frequency of approximately 1s on, 1s off, and had a power rating of *ca.* 60mWcm^{-1} at the electrode surface. In the presence of pulsed light a difference in the trace for the cyclic voltammogram was observed, but there was no net photocurrent detection, therefore the light had no overall effect on the path of the reaction. The transient photocurrent signals that were observed could be a result of a radical pair formation as a result of illumination between the PPP and the pentoxyresorufin *(vide infra).* Literature shows that in electronic light emitting polymer devices known as OLED's, poly-pyridine family molecules are shown to act as "electron transporting and hole blocking components" [116]

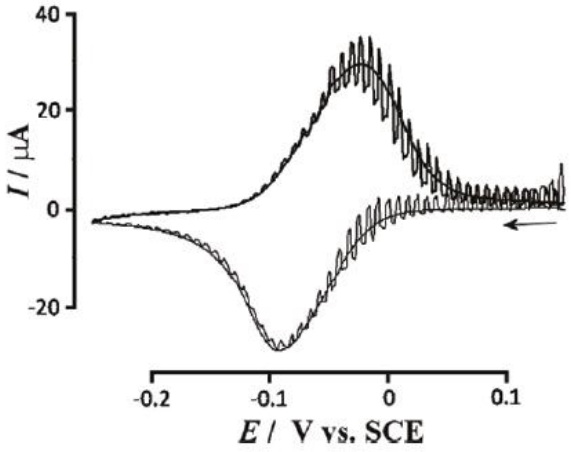

Figure 3.9 - Cyclic voltammograms for the reduction of 23mM resorufin at a scan rate of 50mVs^{-1} in 140 nL PPP deposited onto a 4.9-mm-diameter graphite disk and immersed in 0.1M phosphate buffer at pH 8. The first cycle was recorded in the dark, and the second cycle was recorded with pulsed light (1 s on, 1 s off, ca. 60mWcm^{-2}).

3.5 - Voltammetry of Duroquinone

Duroquinone was chosen as a reaction partner for pentoxyresorufin on the assumption that the duroquinone / duroquinol system would provide a suitable partner for coupled electron / proton transfer with pentoxyresorufin. It is also readily dissolvable in PPP, and does not leach out into the aqueous phase.

3.5.1 - Effect of Scan Rate

Figure 3.10 shows a typical set of duroquinone cyclic voltammetry scans over a selection of scan rates. It shows a single step reduction followed by a single step oxidation. Both occur at potentials that do not obstruct and overlap with the peaks observed for the pentoxyresorufin system. Figure 3.10 also shows a plot of log area under the reduction peak vs. log scan rate; this plot shows a line with gradient value of near one, which is suggestive of a near complete electrolysis of the duroquinone within the droplets. Analysis of the area under the peak is indicative of a two-electron reduction and oxidation.

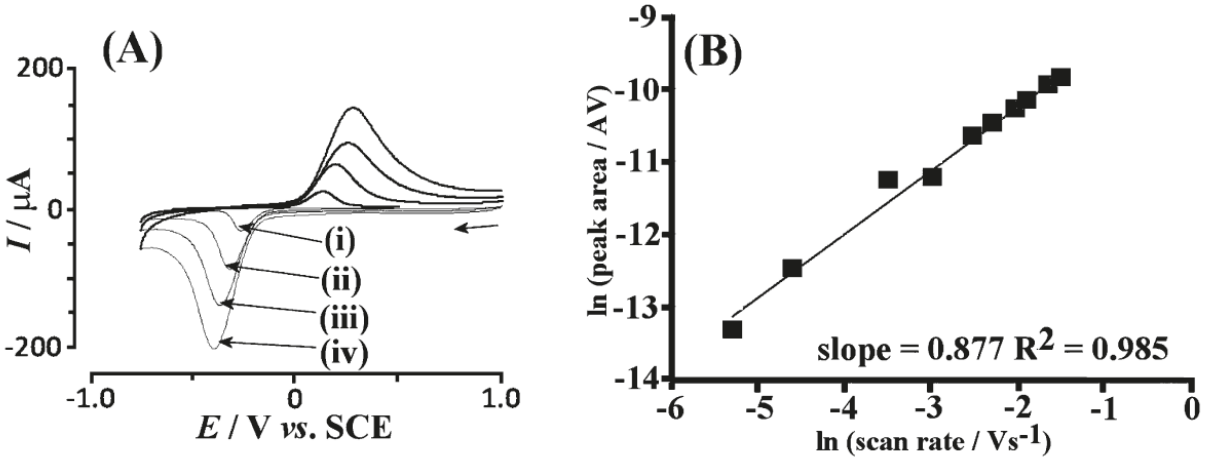

Figure 3.10
(A)Cyclic voltammograms for reduction of 36mM duroquinone in PPP microdroplets, 200nL, deposited onto a graphite disc immersed in 0.1M pH4 phosphate buffer at scan rates (i) 10, (ii) 50, (iii)100 and (iv) 200mVs^{-1} (B) Plot of natural log area under peak vs. natural log scan rate.

3.5.2 - Effect of pH

Investigations into the effect that pH has on the reduction of duroquinone showed no deviation in trend at pH 8 as was seen in the resorufin system when a graph plotting mid point potential vs. pH was produced (figure 3.11). As the graph shows a gradient of $50mVs^{-1}$, it can therefore be assumed that the duroquinone reduction and re-oxidation process followed a two-electron two-proton mechanism across the pH range tested. However, it should be noted that the figure produced for the gradient is sub-Nerstian in value, and slightly below the expected value for a two-electron two-proton system. This most probably indicates that there is some liquid | liquid interface contribution, but is predominantly still in agreement with a two-electron two-proton reduction. The proposed mechanism is shown in equation 3.1.

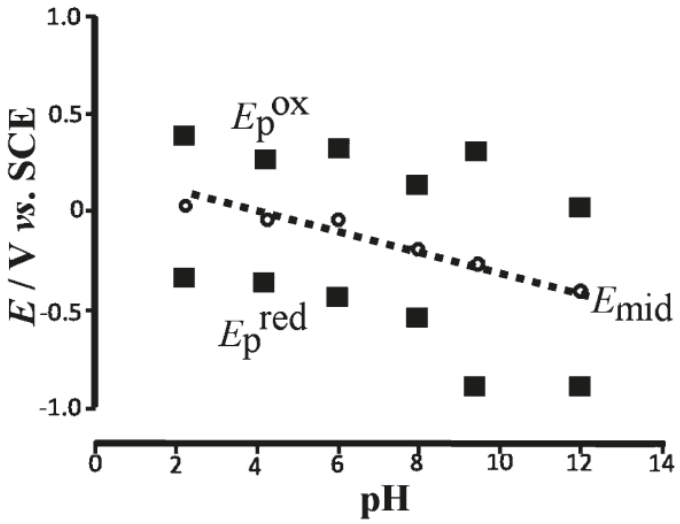

Figure 3.11 - Plot of the mid point potentials, $E_{P\ mid,}$ for 36mM duroquinone in PPP microdroplets (200nL) deposited onto a graphite disc immersed in 0.1M phosphate buffer at a scan rate of $50mVs^{-1}$. The values for the peak potentials $E_{p,\ red}$ and $E_{p,\ ox}$ at each cyclic voltammogram are also shown.

(Equation 3.1)

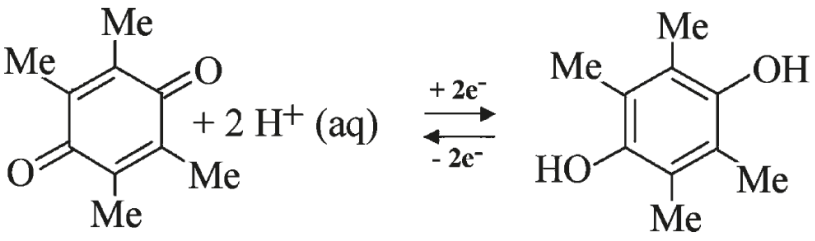

(3)

Investigations into the effect of light on duroquinone was also conducted and it was shown that duroquinone showed no photo activity. In the cyclic voltammogram of duroquinone (36mM in PPP microdroplets, 200nL, in 0.1M pH4 phosphate buffer) under illumination of pulsed light shown in figure 3.12, it can be seen that no photo-currents occurred. There is, however, some thermal effect of the illumination visible in the voltammogram.

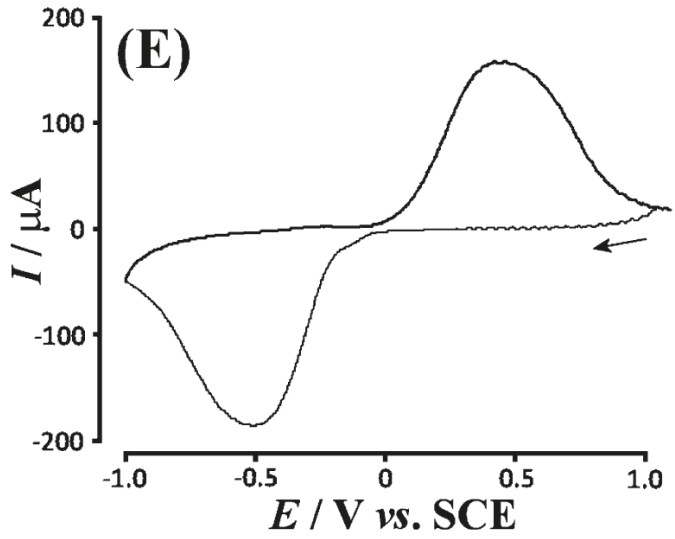

Figure 3.12 - Cyclic voltammogram of 35mM duroquinone in 200nL PPP microdroplets deposited onto a graphite disc, immersed in 0.1M pH4 phosphate buffer at a scan rate of 50mVs^{-1}. Pulsed light shone on sample at an approximate frequency of 1s on, 1s off at ca. 60 mWs^{-1}.

3.6 – Dark Voltammetry of Pentoxyresorufin with Duroquinone as co-reactant

Figure 3.13 shows a cyclic voltammogram, without illumination, for reduction of pentoxyresorufin and duroquinone immobilized in PPP microdroplets. Two separate reduction peaks were seen, followed by two separate oxidation peaks. The position and magnitude of these peaks were in line with where one would expect to see the reduction and re-oxidation of pentoxyresorufin and duroquinone. The two species seemed to undergo separate processes without interference from each other; it is therefore assumed that they proceed autonomously of one another.

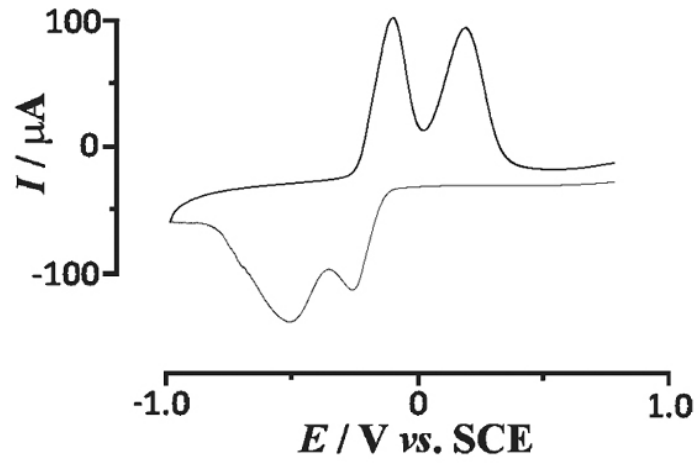

Figure 3.13 - Cyclic voltammogram conducted at a scan rate of 50mVs^{-1} showing reduction and re-oxidation of pentoxyresorufin and duroquinone, 23mM and 40mM respectively, immobilized in PPP microdroplets, 200nL, deposited onto a 4.9mm graphite disc, immersed in 0.1M pH 8 phosphate buffer.

3.7 - Photo-Electrochemistry of Resorufin And Duroquinone

In the presence of light, a distinct change was observed when compared to the cyclic voltammograms recorded for dark scans; this is illustrated in figure 3.14. The peak for the oxidation of duroquinone is clearly seen to shift position towards more negative values, where it is seen to merge and combine with the oxidation peak for pentoxyresorufin. The reduction peaks for both species remain appear to remain unchanged.

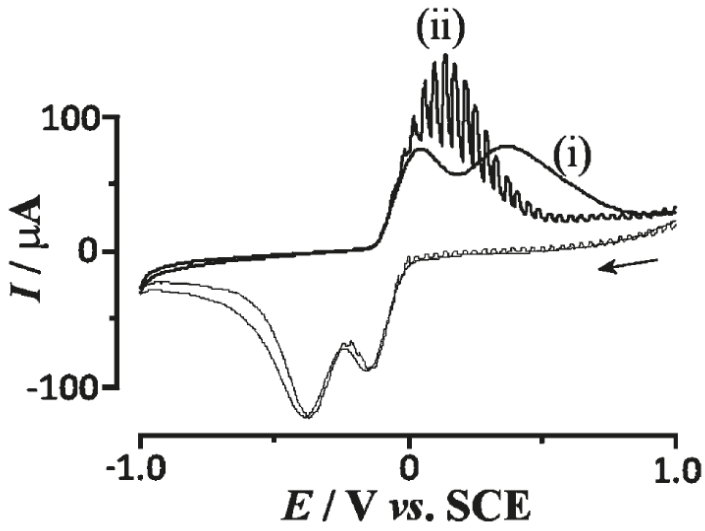

Figure 3.14 – Cyclic voltammograms conducted at a scan rate of 50mVs^{-1} showing reduction and re-oxidation of pentoxyresorufin and duroquinone, 23mM and 40mM respectively, immobilized in PPP microdroplets, 200nL, deposited onto a 4.9mm graphite disc, immersed in 0.1M pH4 phosphate buffer, (i) in the dark and (ii) with pulsed light illumination, ca. 60mWcm^{-1} at an approximate frequency of 1s on 1s off.

3.7.1 - Effect of Light Intensity

Cyclic voltammetry experiments were conducted in which the intensity of the light was varied and the effect on the duroquinone oxidation was noted, these are shown in figure 3.15. It can be seen that the shifting of the duroquinone oxidation process towards that of pentoxyresorufin occurred in a gradual fashion as the light intensity increased, rather that as a sudden shift.

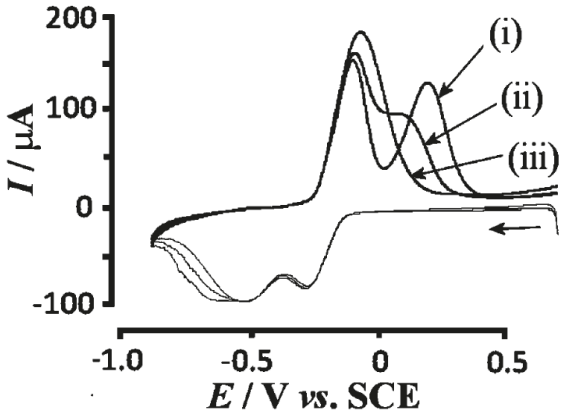

Figure 3.15 – Cyclic voltammograms conducted at a scan rate of 50mVs^{-1} showing reduction and re-oxidation of pentoxyresorufin and duroquinone, 23mM and 40mM respectively, immobilized in PPP microdroplets, 200nL, deposited onto a 4.9mm graphite disc, immersed in 0.1M Ph8 phosphate buffer, at a constant illumination of (i) 0% dark, (ii) 7% and (ii) 23% (where 100% illumination consists of a value of 60mWcm^{-1} at the electrode).

3.7.2 – Effect of pH

Variation of pH was also examined in order to see what effect this had on the oxidation of duroquinone in the presence of light, this was used to aid in determination of the mechanism for the shift of the duroquinone peak. A selection of voltammograms from these experiments is shown in figure 3.16. It can be seen that although the shape of the separate voltammograms for pentoxyresorufin and

duroquinone changed as a result of pH, the photo effect that was observed as a result of illumination did not appear to change in terms of magnitude or direction. It can therefore be assumed that the mechanism responsible for the photo induced process, proceeded independently of pH.

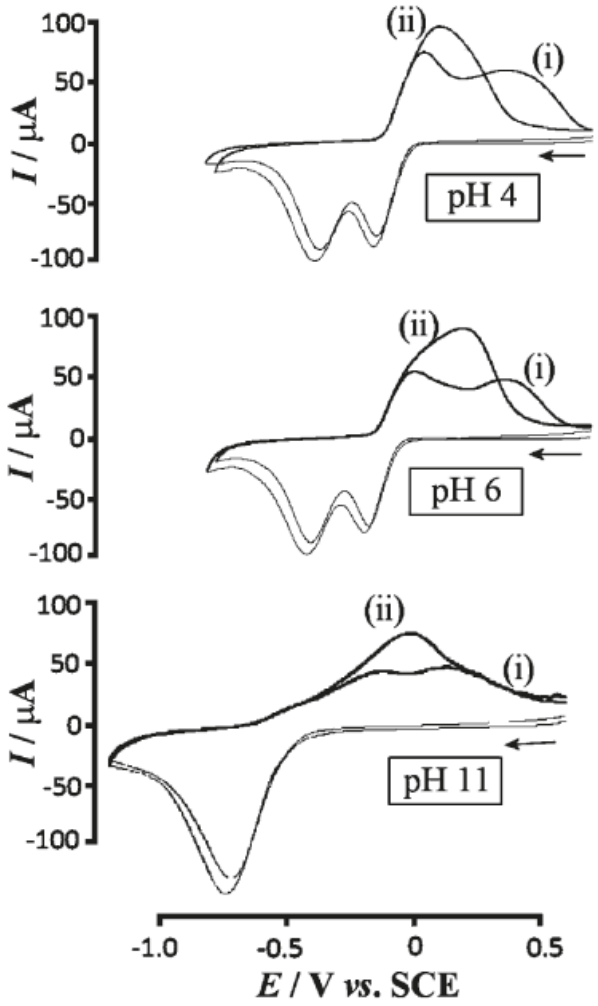

Figure 3.16 - Cyclic voltammograms conducted at a scan rate of 50mVs^{-1} showing reduction and re-oxidation of pentoxyresorufin and duroquinone, 23mM and 40mM respectively, immobilized in PPP microdroplets, 140nL, deposited onto a 4.9mm graphite disc, immersed in 0.1M phosphate buffer.

3.7.3 – Photo Activity as a Function of Wavelength

The effect that wavelength has on the shift of the duroquinone oxidation peak was also examined; these cyclic voltammetry experiments were conducted using high powered, monochromatic, mounted LED's. A selection of cyclic voltammograms from these experiments is shown in figure 3.17. It can be seen that the duroquinone oxidation process in the absence of light occurred at approximately +0.1V vs. SCE. Under illumination, this process shifted to a potential of approximately –0.1V vs. SCE.

The strength of the photo-effect that duroquinone underwent was measured as a function of these two potentials. An action parameter devised for determining this is defined as I_1/I_2, where I_1 is the photo-oxidation which occurred at -0.1V vs. SCE, and I_2 the potential at which duroquinone undergoes its normal, dark oxidation: +0.1V vs. SCE. This action parameter measurement was conducted for each studied wavelength, and therefore shows how effective each wavelength was at stimulating the photo-effect we observed for the oxidation of duroquinone under white light conditions. The action parameter results are shown in figure 3.17.

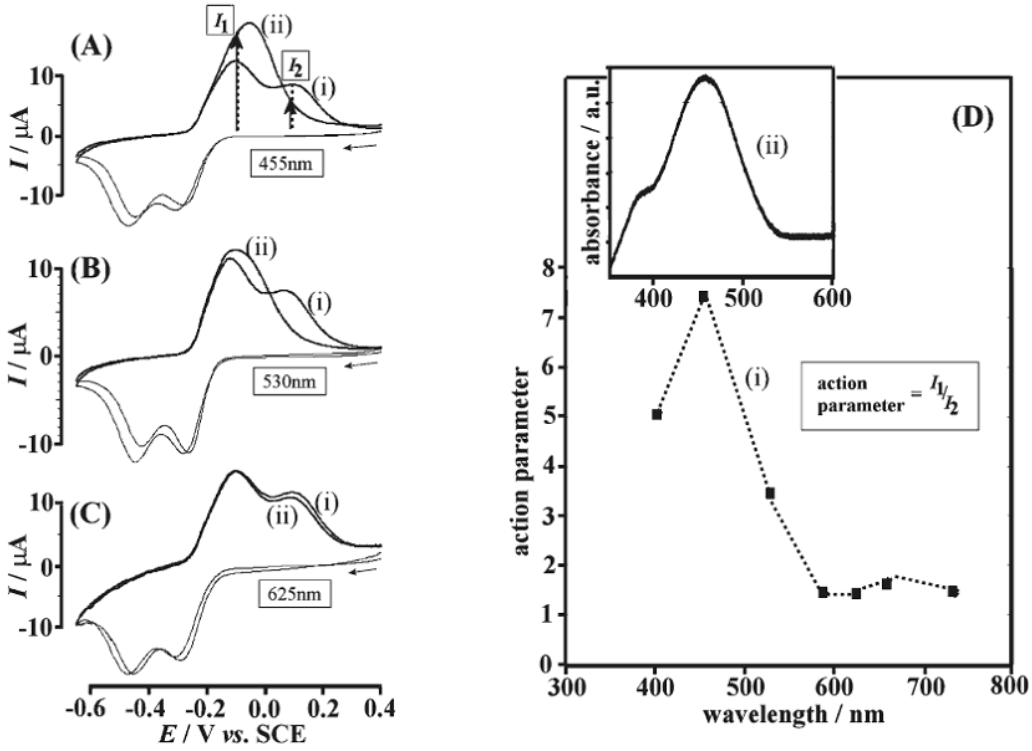

Figure 3.17 - (A, B, C) Cyclic voltammograms conducted at a scan rate of 50mVs^{-1} for the reduction of resorufin and duroquinone, 23mM and 40mM respectively, in PPP microdroplets, 14nL, immersed in 0.1M pH 8 phosphate buffer, illuminated at wavelengths of 455, 530 and 625nm at a power rating of 2.4mWcm^{-1}. (D)(i) Graph showing a plot of action parameter (I_1 / I_2, current at –0.1V vs. SCE divided by current at +0.1V vs. SCE under illumination) as a defining factor for the strength of the photo-effect. (ii) Absorption spectrum of 90mM pentoxyresorufin in PPP vs. wavelength.

3.7.4 - Proposed Mechanisms

The wavelength resolved action parameter data collected on the effect of illumination yielded a plot that bears a significant resemblance to the absorption spectrum of pentoxyresorufin in PPP. This would suggest that it was the pentoxyresorufin that was the photo excited intermediate. Using the information gathered, a scheme (equation 3.2) for the photo-induced effect is proposed based on a pentoxyresorufin photo-excited intermediate.

(Equation 3.2)

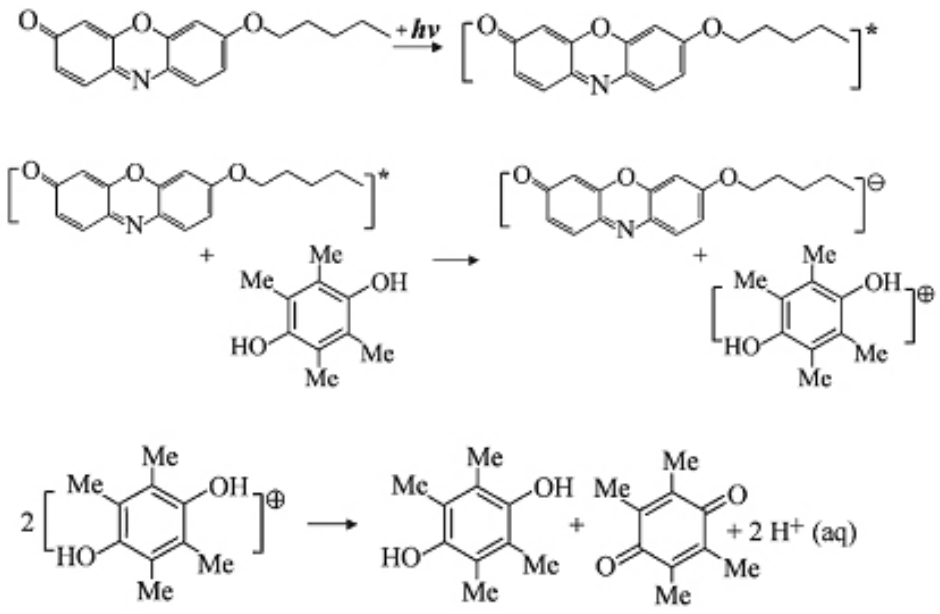

The exact nature of the photo-excited intermediate could not yet be fully resolved using the experimental data thus far gathered, but it is thought to be intrinsically linked to the PPP solvent, perhaps as a charged separated ion pair, or an exciplex. Further exploration of the possibilities of the radical intermediate was conducted with electron paramagnetic resonance (EPR).

3.8 – Exploration of Excited State Using Electron Paramagnetic Resonance

A 1mM solution of pentoxyresorufin in PPP was prepared for EPR examination. Without illumination of the sample, no radical activity was observed; however, upon illumination with a 60mWcm^{-1} halogen white light source, spectra immediately became apparent and were able to be recorded. Once the light source had been deactivated, the signal at once disappeared on a faster than second timescale. Other experiments were conducted using samples containing just resorufin or just PPP but interestingly, neither of these showed any radical photo activity, whether in the dark or under illumination.

It was therefore shown that, in order for any signal to be observed the pentoxyresorufin and PPP needed to be together, there is a need for the presence of both of them together in order for the photo-excited radical intermediate to be observed.

A selection of the EPR spectra recorded are shown in figure 3.18. At room temperature, the spectra observed do not have useful hyperfine coupling information due to solvent broadening that occurred as a result of the PPP's high viscosity. Recording EPR spectra for the sample at a higher temperature (figure 3.18B) circumvented this problem, and allowed hyperfine detail to become visible. With this information, a simulation (WINSIMFONIA) was attempted using a photo-excited system consisting of both pentoxyresorufin and PPP. The EPR spectra simulation was run using coupling assigned to two nitrogens, two methylene protons and 10 aromatic protons, and is shown in figure 3.18C. It can clearly be seen that the simulated data

bares a similar resemblance to the experimental data obtained, lending some credence to the theory of a pentoxyresorufin – PPP pair being responsible for the photo-excited state.

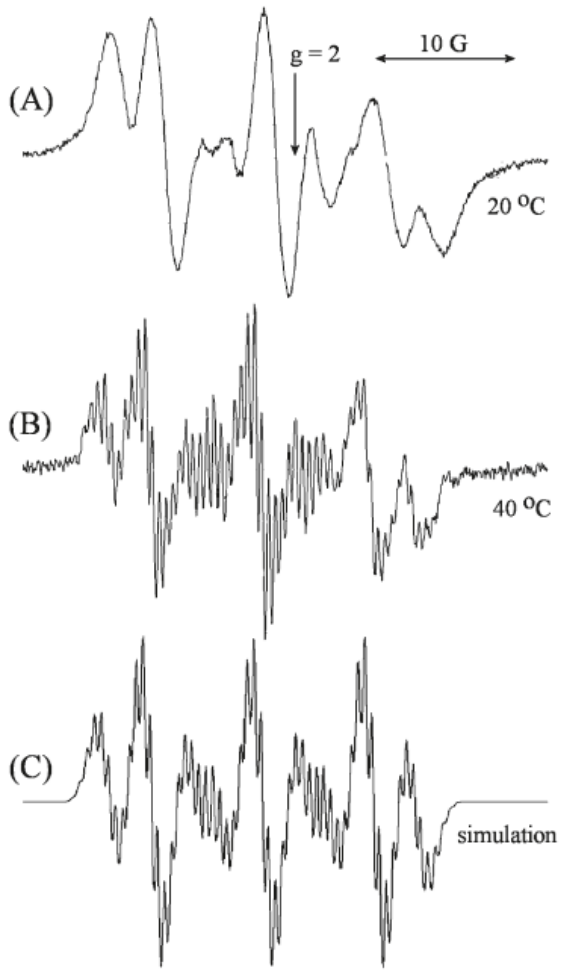

Figure 3.18 – EPR spectra conducted at 9.4466 GHz of a sample of 1mM pentoxyresorufin in PPP at temperatures of (A) 20°C and (B) 40°C, illuminated by a halogen white light source at ca 60mWcm^{-1}. (C) Simulated EPR spectra with hyperfine coupling to ^{14}N (a = 8G), ^{14}N (a = 0.42G), 2 x ^{1}H (a = 3G) and 10 x ^{1}H (a = 0.52G) using a 0.4G modulation.

The photo-voltammetric effects outlined in this report plainly show some interesting photo-activity that occurred within the PPP microdroplets. There are several aspects of what has been outlined which require further investigation in order to fully

understand and resolve. We have an understanding of some of the properties of the photo-excited state, however a full understanding of the interactions between the pentoxyresorufin and the PPP still needs to be achieved, in order to fully understand the contributing role that the PPP plays. The one-electron reaction intermediates also require further understanding before we can proceed forward from the tentative mechanism scheme proposed.

A half field signal seen in an EPR trace is indicative of a triplet. For this system an experiment at a temperature of 4K was attempted in order to see whether a half field signal existed. Such a signal was observed and hence tentatively assigned the excited molecule of the pentoxyresorufin / PPP system a triplet state. This result, was however, not confirmed by re-running the experiment in a different quartz cell to ascertain whether the observed half field signal was indeed a triplet, or an artefact of imperfections in the quartz cell.

3.9 - Summary

Studies of the effect that pH has on the pentoxyresorufin system immobilized in PPP microdroplets have shown a very interesting transition that is observed as a result of a switch that occurs from a bulk process in the microdroplet, to one that occurs at the surface instead. A two-electron two-proton mechanism having a wide peak-to-peak separation denotes the bulk process, whilst the surface process is composed of a two-electron, one-proton scheme with a small peak-to-peak separation. Results indicate that it is a protonation of the PPP microdroplet surface that is the cause of these

observations, and other cases may exist where this process could have a profound impact on mechanism and rates.

Pentoxyresorufin in microdroplets of 4-(3-Phenylpropyl)pyridine (PPP) are shown to undergo a photo-excitation, in which the excited species was shown to react with duroquinol. This process was not affected by pH, and hence the photo process proceeded independently of any changes in pH. EPR studies detected a radical intermediate, and studies show that it is likely composed of a pentoxyresorufin-PPP pair, though thus far it has not been possible to fully understand and characterize the behaviour that pentoxyresorufin and PPP exhibit in combination under illumination. This is an important aspect of the system to understand as the PPP clearly plays a very important role, and a thorough understand of it would be beneficial in employing it in future systems

A future target would be to use what has been learned throughout this work and drive it towards having a system which sees a charge transfer driven by energy absorbed from light at the liquid | liquid interface. An example of this could be a system composed of a water-soluble quinone and oil soluble quinol derivative with a reversible potential at a more positive value. This would see the oxidized quinone partition into the aqueous phase. This sort of system would hopefully provide a light harvesting process producing energy from illuminated microdroplets.

Chapter 4

Driven Liquid | Liquid | Electrode Anion Transfer into 4-(3-Phenylpropyl)-Pyridine

Contents

Published - Spectroelectrochemical Investigation of TPPMn(III/II)-Driven Liquid | Liquid | Electrode Triple Phase Boundary Anion Transfer into 4-(3-Phenylpropyl)-Pyridine: ClO4-, CO3H-, Cl-, and F- ” in Electroanalysis , 2012, **24**, 2, 246-253

4.1 – Abstract

Electrochemically driven ion transfer chemistry of perchlorate, fluoride, chloride and bicarbonate is investigated for a system of tetraphenylporphyrin-Mn (III) chloride (TPPMn) dissolved in microdroplets of PPP. Perchlorate and chloride transfer is shown to be a simpler process; however, effects observed for bicarbonate and fluoride are more complex. For the case of a sodium bicarbonate electrolyte, results seem to implicate a combination of $HCO3^-$ and $CO3^{2-}$ transfer. In order to more fully explore these ion transfers, an *in situ* UV/Vis spectro-electrochemical experimental set-up was developed using mesoporous ITO conducting film electrodes. This set-up showed that the fluoride ion was seen to associate with the $TPPMn(III)^+$. It is also shown that vacuum heating allows improved ITO conductivity and allows for a viable transparent electrode for voltammetric ion-transfer studies.

4.2 - Introduction

Ion transfer processes at microdroplet deposits [117] provide a useful methodology for the examination of ion transfer coupled to electron transfer[118]. Both cation transfer [119] and anion transfer[120] processes have been observed in the literature, and from these, facilitated transfer systems have been developed; an example would be as seen for a-hydroxy-carboxylates facilitated by boronic acids [121] .

In previous studies new types of porous and mesoporous electrodes have been developed in order to increase the extent of the triple phase boundary region, and therefore, the efficiency of ion-transfer processes. A variety of these types of surfaces have been suggested, such as porous metal[122] and carbon surfaces[123]. Tin-doped indium oxide (ITO) nano-particles have been shown to make conductive mesoporous films when deposited onto ITO glass slide electrodes[124]. This effectively creates a transparent electrode, which was utilized for the UV/Vis spectroelectrochemical measurements.

Coupling UV/Vis with electrochemical techniques is useful as it can provide information on reaction intermediates. Voltammetric responses can sometimes be interpreted as more than one mechanism, so coupling with another technique such as *in-situ* UV/Vis can provide complementary data to the voltammetric analysis [114]. *Scholz* has previously used this technique for triple phase boundary characterization as a method for proving the assumption of progressive activation of the working electrode[125].

This report focuses on the transfer of a variety of anions, some of which have been shown to undergo simple transfers such as perchlorate, chloride, fluoride; and those which exhibit a more complex transfer reaction, such as those seen for a solution of bicarbonate leading to bicarbonate and carbonate transfer. The *in situ* spectroelectrochemical method is employed to discern the ion-transfer mechanism and to start to develop a new electro-analytical tool. This method could be of benefit for a wider range of systems consisting of liquid | liquid interfaces with immobilized oils and ion transfer.

Previous voltammetric reports have shown that for the TPPMn redox system dissolved within 4-(3-Phenylpropyl)pyridine (PPP), highly nucleophilic anions are likely to undergo an axial coordination with TPPMn[(126)]. Weak facilitation was shown for ions such as cyanate, as this was described as likely due to coordination with Mn(III). Voltammetric techniques for these types of observations have their limitations, and it is hoped that the spectroelectrochemical technique discussed in this chapter will be able to provide more detailed information on the system, with insights into ligand exchange and coordination to the metal centre, as well as the kinetics of triple phase boundary reactions.

4.3 – Experimental

4.3.1 – Chemicals

The reagents 4-(3-phenylpropyl)-pyridine (Aldrich, 97%), tetraphenylporphyrin-Mn (III) chloride (TPPMn) (Aldrich 95%), ITO nanoparticles (diameter ca. 20 nm, dispersion in water, Nanophase Technologies Corp. USA), phosphoric acid (Fischer Scientific, 85% wt), sodium hydroxide (Aldrich >97%), methanol (Aldrich) were used without further purification. Filtered and demineralised water was taken from a Thermo Scientific purification system with resistivity not less than 18.2 MOhm cm. Experiments were conducted at a temperature of 20 ± 2^{o}C.

4.3.2 – Instrumentation

An Ivium Technologies 'Compactsta' 'potentiostat (release v1.725) was used as the potentiostat for electrochemical experiments. A standard three electrode cell was used with the working electrode consisted of a basal plane pyrolytic graphite (bppg) electrode with a diameter of 4.9 mm (mounted in Teflon®) and used in conjunction with a platinum wire counter electrode and a KCl - saturated calomel reference electrode (SCE, REF401, Radiometer). Spectro-electrochemical experiments were conducted with a mesoporous ITO coated ITO working electrode, platinum wire counter electrode, and a Dri-Ref reference electrode (World Precision Instruments). The UV/visible spectroscopy was carried out on a Cary 50 Probe UV-Vis spectrophotometer (Varian Inc.).

4.3.3 - Electrode Preparation Procedures

The deposition of random microdroplet arrays was achieved by evaporation of an acetonitrile solution containing TPPMnCl and PPP (typically 4mg and 80 mg respectively in 6 ml of acetonitrile) onto a freshly polished bppg electrode. Room temperature evaporation of the acetonitrile resulted in a random array of PPP microdroplets on the graphite electrode surface. The final volume of PPP varied with deposition volume but is typically 10 nL on a 4.9 mm diameter disc. The electrode surface was renewed by removing the top layer of graphite by polishing on P1000 silicon carbide polishing paper.

The mesoporous ITO coated electrode was prepared by first cleaning (sonication of the ITO in an ethanol/water solution and then heating in air for one hour at 500^{o}C), the ITO was then heated for two hours in a vacuum furnace (500^{o}C). Once cooled, this ITO was dipped into a solution of ITO nanoparticles in methanol (commercial ITO nanoparticle solution was evaporated close to dryness and then re-dispersed in methanol). After removal from the solution and drying, the dip and dry step was repeated. Finally, the mesoporous ITO electrode was again heated in a vacuum furnace at 500^{o}C for 2 hours. Figure 4.1 shows SEM images taken of the modified ITO surfaces. A reasonably uniform particulate coating is clearly visible. This coating is approximately 80 nm thick for a two-step coating [127] and opaque; however, coloured oil deposits on this substrate give well-defined UV/Vis absorbance spectral data.

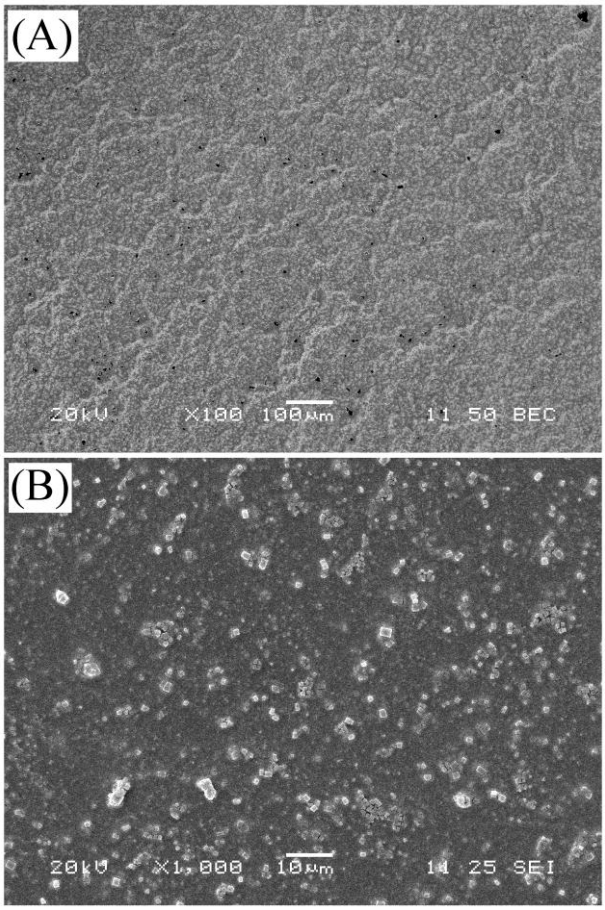

Figure 4.1 - SEM images (showing lower (A), and higher (B) resolution) of a film of approximately 80 nm thickness composed of ITO nanoparticle of ca. 20 nm diameter.

4.4 - Ion transfer Voltammetry for the TPPMn System in PPP Microdroplets

The voltammetric responses for TPPMn reduction and re-oxidation and coupled anion transfer were first studied with a 70nL deposit of TPPMn in PPP on a 4.9mm graphite disc immersed in a 0.1M solution of the given anion being studied. These were sodium perchlorate, sodium bicarbonate, potassium fluoride and sodium chloride. The cyclic voltammograms for these experiments are shown in figure 4.2. Also displayed is a selection of voltammograms for each ion transfer conducted over a range of scan rates.

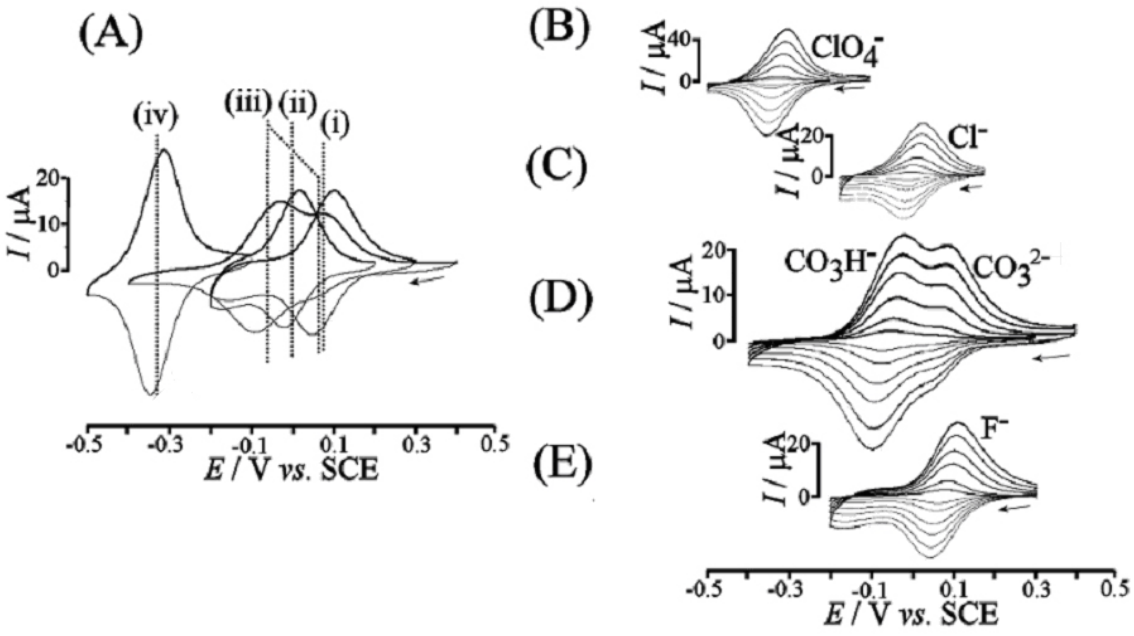

Figure 4.2

(A) Cyclic voltammograms at a scan rate of 50mVs^{-1} for the reduction and re-oxidation of 18 mM TPPMn(III) in PPP microdroplets, 70 nL, deposited on a 4.9 mm diameter graphite disc, immersed in 0.1 M aqueous solution of (i) KF, (ii)NaCl, (iii) $NaHCO_3$, and (iv) $NaClO_4$
(B-E) Effect of scan rate (5, 10, 30, 50, 75, 100 mVs^{-1}) on voltammetric responses for transfer of ClO_4^-, Cl^-, HCO_3^-, and F^-, respectively.

For the perchlorate system, $ClO4^-$ (shown in figure 4.2 A and B), we see a simple transfer into the organic phase from the aqueous electrolyte where Nerstian conditions prevail. For this a mid-point potential of -0.3V *vs.* SCE is observed (where $E_{mid} = ½ (E_p^{ox} + E_p^{red})$). From figure 4.2 B we can see that at slower scan rates the reduction and oxidation peaks are seen to get closer together; this increasing symmetry is in line with what one would expect of thin layer electrolysis and complete conversion of the electroactive material within the deposit. A proposed mechanism for the reduction of TPPMn with perchlorate ion transfer is shown in equation 4.1.

(Equation 4.1)

$$Mn(II)_{(org)} + ClO_4^-{}_{(aq)} \rightleftarrows Mn(III)^+{}_{(org)} + ClO_4^-{}_{(org)} + e^-$$

A range of scan rates for the sodium chloride electrolyte system, using a 0.1M solution, is illustrated in figure 4.2 C. This shows transfer of a chlorine anion with the voltammograms showing a midpoint potential of 0 V *vs.* SCE, it is shown to be a reversible system. It is worth noting the small reduction shoulder that occurs at approximately –0.2V *vs.* SCE, most probably indicating some form of weak interaction with the Mn centre, but the predominant process is described in equation 4.2.

(Equation 4.2)

$$Mn(II)_{(org)} + Cl^-{}_{(aq)} \rightleftarrows Mn(III)^+{}_{(org)} + Cl^-{}_{(org)} + e^-$$

Figure 4.2 D shows the voltammograms for a range of scan rates for redox voltammetry of TPPMn in a 0.1M Sodium Bicarbonate ($NaHCO_3$) electrolyte, with a pH of approximately 8.4. This system has a more complicated ion transfer, as there are two processes that are possible. The process corresponding to transfer of bicarbonate is shown in equation 4.3 and is seen at a potential of approximately –0.08V *vs* SCE. This process is dominating at slower scan rates. The other process seems to take over at higher scan rates, and corresponds to the transfer/expulsion of a proton from the organic phase into the aqueous phase as a result of oxidation; this process is seen at 0.07V *vs*. SCE, and the proposed mechanism for it is shown in equation 4.4. This is discussed in further detail in chapter 4.4.1.

(Equation 4.3)

$$Mn(II)_{(org)} + HCO_3^-{}_{(aq)} \rightleftarrows Mn(III)^+{}_{(org)} + HCO_3^-{}_{(org)} + e^-$$

(Equation 4.4)

$$Mn(II)_{(org)} + HCO_3^-{}_{(org)} \rightleftarrows Mn(III)^+{}_{(org)} + CO_3^{2-}{}_{(org)} + H^+{}_{(aq)} + e^-$$

The final ion transfer that is studied in this section is fluoride, as part of a 0.1M solution of KF. This shows a mid point potential of 0.07V *vs.* SCE and upon initial observations the transfer of the fluoride seems to be a simple process very similar to that observed for the chloride transfer, however this was later shown to be a more complex case, and is further examined in chapter 4.4.2.

(Equation 4.5)

$$Mn(II)_{(org)} + F^-{}_{(aq)} \rightleftarrows Mn(III)^+{}_{(org)} + F^-{}_{(org)} + e^-$$

4.4.1 – Ion Transfer with Sodium Bicarbonate Electrolyte

We noted that the sodium bicarbonate solution resulted in a less than straightforward ion transfer, with two competing processes occurring. We have already inferred that scan rate seems to play a part in which ion transfer takes place, with bicarbonate transfer into the oil dominating at slower scan rate. However, there are other factors which heavily influence the chemistry taking place and these were further explored. Figure 4.3 shows how exploration of two other factors, (deposition volume and the pH of the sodium bicarbonate solution) affect the voltammetric signals of TPPMn.

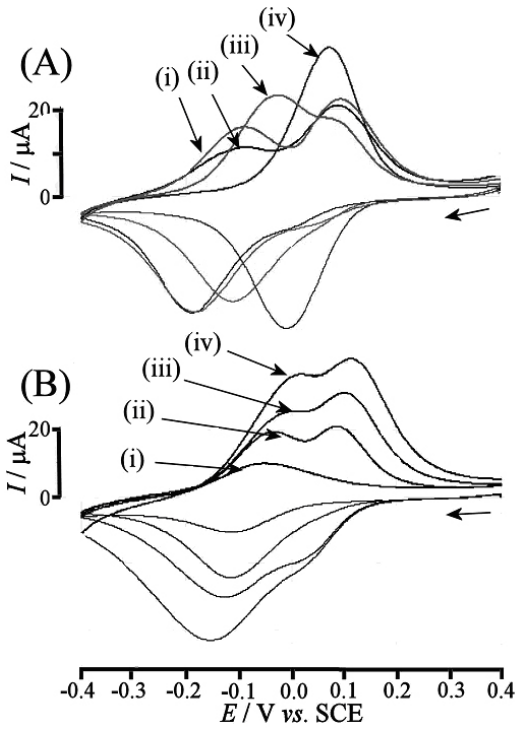

Figure 4.3 - Cyclic voltammograms at a scan rate of 50 mVs^{-1} for the reduction of 18mM TPPMn deposited in PPP microdroplets, 70 nL, deposited on a 4.9 mm diameter graphite disc immersed in 0.1 M aqueous electrolyte solution.
(A) Comparison of current responses for the carbonate transfer at pH (i) 11.1, (ii) 10.4, (iii) 8.4, and (iv) 6.8.
(B) Voltammograms illustrating how deposition volume of PPP affects observed carbonate transfer at pH 8.4 with deposition volume (i) 7nL, (ii) 35nL, (iii) 70nL, and (iv) 140nL.

Small deposition volumes, and hence smaller droplets, show a complete domination of the more negative reduction process, corresponding to the transfer of bicarbonate from the aqueous phase into the organic phase. This would seem to indicate that under the conditions of small deposition volumes the bicarbonate transfer can go to completion, without competition from the energetically unfavourable second process occurring.

The pH is also seen to have a profound and somewhat unexpected effect on the voltammetry. Alteration of the pH of the sodium bicarbonate solution to more acidic conditions was achieved by the bubbling of CO_2 into it. At more alkaline conditions, in the range of pH 8-11, we see the double peak indicating both processes are occurring. However at acidic conditions only one peak is observed, corresponding to the bicarbonate transfer we saw dominating at slower scan rates and smaller deposition volumes. These voltammograms over a range of pH's showed the very unexpected result of seeing a shift in mid point potential as the pH range was traversed; this would seem to indicate that the process occurring under acidic conditions is a more difficult transfer. Acidic conditions would mean a lower concentration of $HCO3^-$, however this alone does not explain this definite shift to more positive potentials. It is proposed that a considerable solubility of the H_2CO_3, and absence of the carbonate transfer within the PPP phase, allows for a change in mechanism towards that of the proton expulsion, as shown in equation 4.6.

(Equation 4.6)

$$2\ Mn(II)_{(org)} + H_2CO_{3(org)} \rightleftarrows 2\ Mn(III)^+_{(org)} + CO_3^{2-}{}_{(org)} + 2\ H^+_{(aq)} + 2\ e^-$$

4.4.2 – Ion Transfer with Potassium Fluoride Electrolyte

It was alluded to earlier, that the fluoride system underwent a more complicated ion transfer, prompting further observation in order to more fully understand the process. It was noted over the course of the initial experimentation with this system that even slight variations in the conditions led to different voltammograms being observed.

In order to more fully observe these effects, a set of experiments was devised whereby the cyclic scans were not started until a 300s pre-equilibration time at the starting potential had been completed. These voltammograms were also recorded starting at both a positive potential and a negative potential. The resulting cyclic voltammograms from these experiments are shown in figure 4.4.

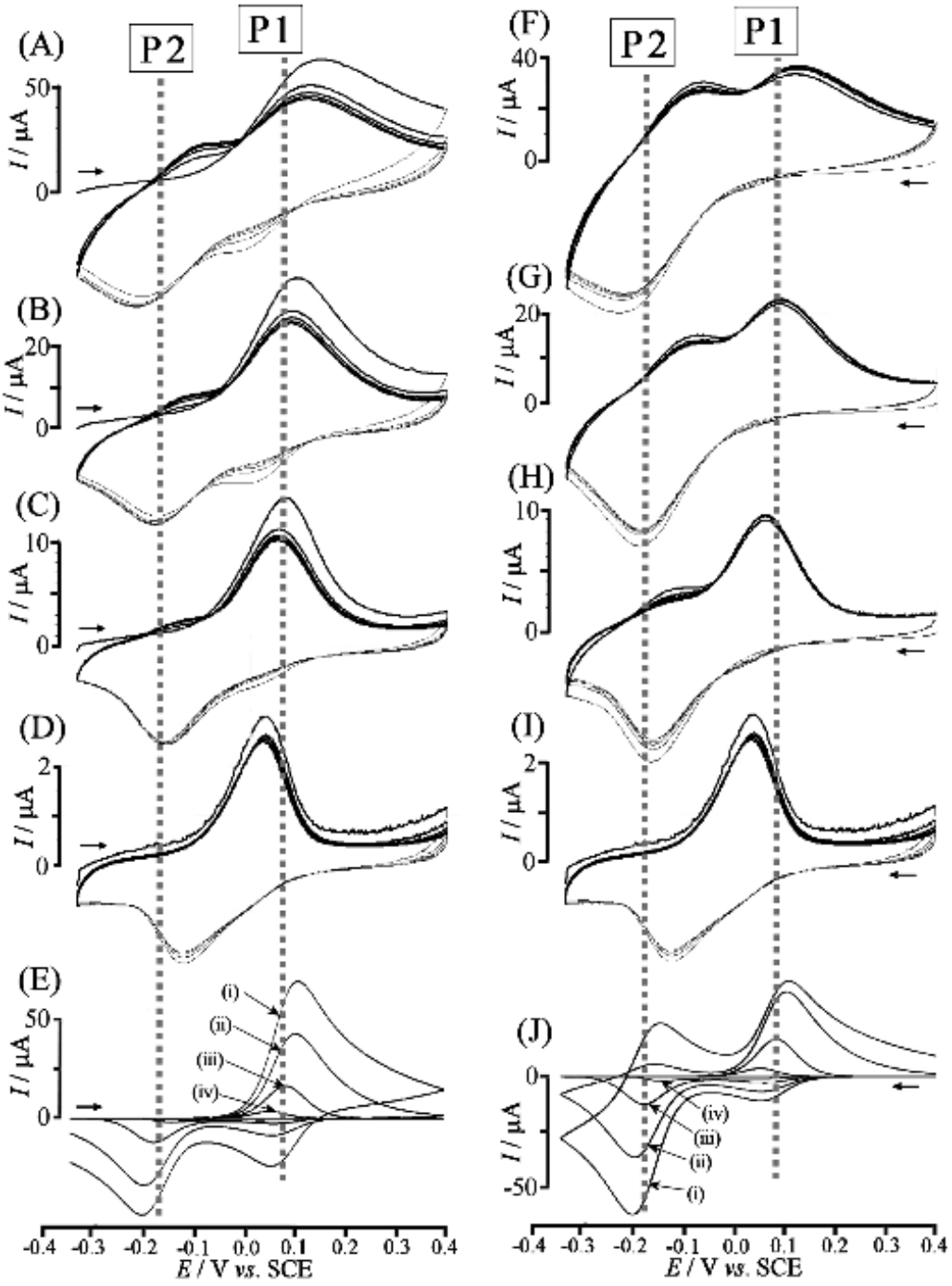

Figure 4.4 - Cyclic voltammograms at scan rates of (A,F) 10, (B,G) 50, (C,H) 200, and (D,I) 500 mVs^{-1} for 18 mM TPPMn(II) in PPP microdroplets, 70 nL, deposited onto a 4.9 mm diameter graphite electrode, immersed in aqueous 0.1 M KF electrolyte solution. For (A-E) the start potential is negative and for (F-J) the start potential is positive. In (E,J) a Digisim simulation output is shown, this is shown for the first cycle at scan rates of (i) 500, (ii) 200, (iii) 50, and (iv) 10 mVs^{-1}, the computer model is for a thin film case

Looking at the voltammograms shown in figure 4.4, A to D show scans that start at a negative potential, whilst F to I show scans started from a positive potential. In both sets of cases, the scans were only started after a 300 second equilibration time at the starting potential. It can be seen that two distinct processes emerged. One occurred (P1) at approximately 0.07V *vs* SCE, corresponding to the initial fluoride transfer shown in equation 4.5. The other process, (P2), was seen to occur at approximately –0.18V *vs* SCE, and corresponded to the proposed process outline in equation 4.7, involving a cation transfer. This new process arising with the fluoride system was seen to be particularly prevalent as a result of starting and holding at a positive potential and hence creating a 'pre-oxidized state' of the TPPMn within the oil droplets at the electrode surface.

(Equation 4.7)

$$Mn(II)F^-_{(org)} + Na^+_{(org)} \rightleftharpoons Mn(III)F_{(org)} + Na^+_{(aq)} + e^-$$

The voltammograms of these experiments starting at different potentials show five cycles. Over the course of these cycles it can be seen that a slow conversion is taking place towards a dynamic steady state. At the slower scan rates, $10mVs^{-1}$, the responses seen in the voltammograms start to become impossible to tell apart.

As a means to confirm and corroborate the proposed mechanism for the rather more complex case of the fluoride transfer, DigiSim computer simulations of the system were attempted. As was the case when last utilized, a thin layer diffusion (1μm) case was assumed, and the diffusion coefficient was set at $10^{-8}cm^2s^{-1}$ in order to attempt to

replicate the onset of diffusion control at the faster scan rates. From the voltammograms illustrated in figure 4.4, particularly those at higher scan rates, it is assumed that the equilibrium constant for the complexation of the fluoride to the $TPPMn(III)^{+}$ had to be quite high, and that for the complexation of the fluoride to the TPPMn(II) had to be fairly low. These were defined in the simulations as KMn(III) = $2000 mol^{-1}dm^{3}$ and KMn(II) = $0.08\ mol^{-1}dm^{3}$ respectively.

For the simulation, the individual rate constants were manipulated in order to satisfactorily reproduce the observed experimental data. In particular it was important to reproduce the ratio of the peaks observed at the faster scan rates as well as the observed fact that the signals obtained were seen to merge at slower scan rates. The rate constants which were seen to best fit the experimental data were $k_{Mn(III)ass}$ = 100 $mol^{-1}\ dm^{3}\ s^{-1}$, $k_{Mn(III)dis}$ = 0.05 s^{-1} and $k_{Mn(II)ass}$ = 0.1 $mol^{-1}\ dm^{3}\ s^{-1}$ and $k_{Mn(II)dis}$ = 1.2 s^{-1}. The simulated data is shown as part of the earlier figure 4.4, parts E and J.

4.5 - Ion Transfer Voltammetry at Mesoporous ITO electrodes

The utilization of a spectroelectrochemical set-up -that is being able to run UV-Vis spectra as a function of potential- was envisaged as a process to allow additional insights into the mechanism that occur as a result of charge transfer. In the case of these experiments interesting observations were made of the changes within the ligand sphere of the Mn centre. A set up based on a transparent ITO electrode modified with a thin film of ITO nanoparticles was used to allow for UV/Vis measurements to be recorded whilst conducting voltammetry. This film was slightly opaque, but allowed for enough light to pass to see through with the naked eye. This

film was also optimal for the deposition of PPP microdroplets, allowing even distribution and an extension of the triple phase boundary area.

Figure 4.5 shows a typical cyclic voltammogram for a 70nL deposit of PPP with 18mM TPPMn, which would normally spread over approximately $1cm^2$ of the ITO nanoparticle electrode. The electrode was immersed in 0.1M sodium perchlorate. From the figure, it can be seen that the reduction and re-oxidation peaks observed are in line for what was observed on the graphite electrodes and were consistent with a perchlorate transfer as seen in equation 4.1.

An interesting observation from the ITO nanoparticle electrode was obtained as a result of heating as a pre-treatment. The voltammetric responses were seen to improve when the electrode was vacuum heated at 500^0C for two hours. A comparison of the voltammetric responses from the electrode is shown in figure 4.5, where parts (i) and (ii) corresponded to identical experimental conditions, with the sole difference that (i) was heat treated in air at 500^0C and (ii) was vacuum heat treated at 500^0C. One obvious difference observed between the voltammograms obtained for a graphite electrode and those obtained for the ITO nanoparticle electrode was that the peak to peak separation seen for the ITO electrode was larger when compared to that of graphite. The vacuum treated ITO electrode did show less peak to peak separation but was still higher than those observed for graphite. This may be as a result of slower electron transfer for the ITO electrode triple phase boundary.

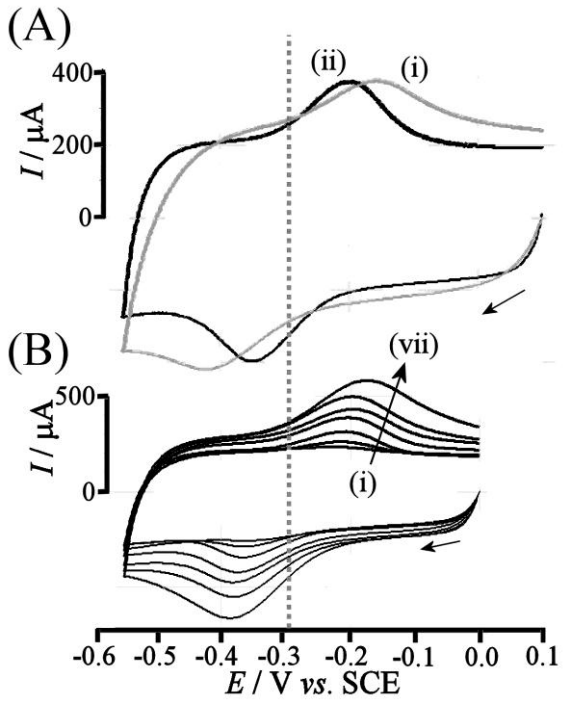

Figure 4.5 - Cyclic voltammograms at a scan rate of 50 mVs^{-1} for the oxidation of 18 mM TPPMn in PPP microdroplets, 70 nL, deposited onto a mesoporous ITO coated ITO electrode, and immersed in aqueous 0.1 M $NaClO_4$ electrolyte solution.
(A) Comparison of current responses for the mesoporous ITO film electrode heat treated at 500 ^oC in air (i) and heat treated at 500 ^oC under vacuum (ii). (B) Effect of the PPP deposition volume (i) 8 nL, (ii) 18 nL, (iii) 35 nL, (iv) 70 nL, (v) 140 nL, (vi) 280 nL, and (vii) 560 nL.

Another effect explored whilst using the ITO nanoparticle electrode was the effect of deposition volume. The voltammetric signals obtained as a result of a variety of deposition volumes is illustrated in figure 4.5 B. It was seen from this that a linear increase of peak current with the deposition volume was observed for volumes of up to 70nL, but the relationship breaks down after this. This is most likely due to the abundance of PPP that floods the mesoporous surface, hence leading to a decrease in available triple phase boundary area.

Shown in figure 4.6 are the typical cyclic voltammograms for the reduction and re-oxidation of TPPMn on an ITO nanoparticle electrode immersed in the same four 0.1M electrolytes that were used for the graphite ion transfer experiments.

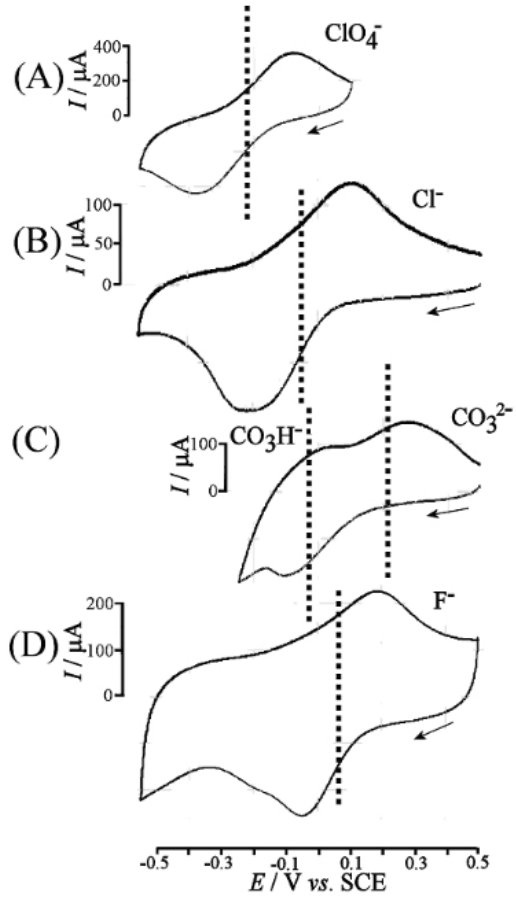

Figure 4.6 - Cyclic voltammograms at a scan rate of 50 mVs^{-1} for oxidation of 36 mM TPPMn in PPP microdroplets, 45 nL, deposited onto a mesoporous ITO electrode, immersed in aqueous 0.1 M electrolyte solution: (A) $NaClO_4$, (B) NaCl (C) $NACO_3H$ pH 8.4, and (D) KF

It can be seen from the experimental data from the mesoporous ITO, that the distortions on the voltammograms have an adverse effect on any quantitative extrapolations that one might be able to make from these. It is, however, still clear from the data obtained that the characteristics of the ion transfers we observed on graphite are still prevalent.

4.5.1 – Spectroelectrochemical Experiments

The mesoporous ITO nanoparticle electrodes were placed in a standard cuvette for conducting the spectroelectrochemical experiments. The results of the in-situ UV/Vis measurements as a function of potential are illustrated in figure 4.7. These show the optical absorbance of the TPPMn in PPP (144mM in 45nL) at the ITO nanoparticle electrode immersed in 0.1M electrolyte. In order to effectively obtain an absorbance scan from the UV/Vis spectrometer, the potential was stepped in approximately 0.1V intervals across the potential range, and held at each potential for 60 seconds.

For the reduced form of TPPMn immersed in the perchlorate, chloride and bicarbonate systems, a single well-defined absorption is seen at 440nm with an extension coefficient of 140000mol^{-1} dm^3 cm^{-1}. This figure was obtained from the assumption of a concentration of 0.144 mol dm^{-3} and a path length of 0.45μm. This is consistent with the soret band and hence the dark green colour of the TPPMn [(128).] As the potential tended towards more positive values the absorption band too shifted, until it reached a new value of 473nm (e = 48000 mol^{-1} dm^3 s^{-1}). This was attributed to the TPPMn (III) species with two axial ligands.

The case of the potassium fluoride electrolyte is slightly different and its oxidized species saw an absorbance at 435nm (e = 50000 mol-1 dm3 s-1). This was attributed to the coordination of fluoride to the Mn centre, as was shown for equation 4.7.

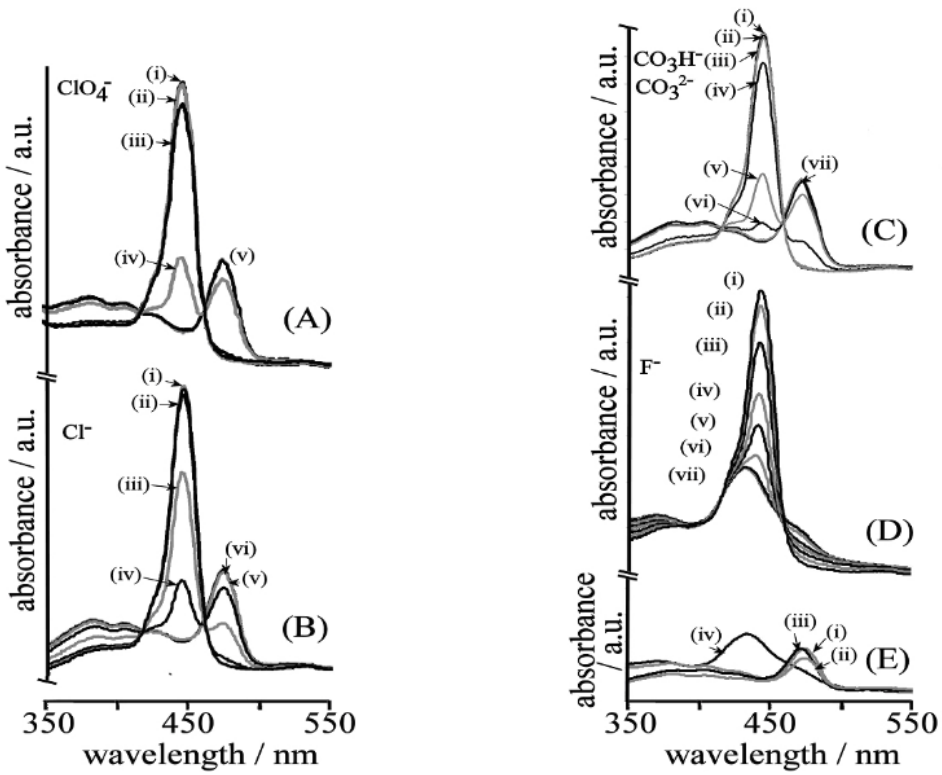

Figure 4.7 - UV/Vis data for in situ spectro-electrochemical oxidation of 45 nL of 144 mM TPPMn(II) in PPP immobilised onto a mesoporous ITO film electrode and immersed in aqueous 0.1 M electrolyte in a 1 cm path length cuvette. The potential was stepped in 60 s intervals: (A) ClO_4^-, (i) -0.5, (ii) -0.4, (iii) -0.3, (iv) -0.2, and (v) 0.0 V vs. SCE; (B) Cl^-, (i) -0.4, (ii) -0.3, (iii) -0.1, (iv) 0.1, (v) 0.2, and (vi) 0.3 V vs. SCE; (C) HCO_3^-, (i) –0.4, (ii) –0.3, (iii) –0.2, (iv) –0.1, (v) 0.0, (vi) 0.1, and (vii) 0.2 V vs. SCE; (D) F^-, (i) -0.4, (ii) -0.3, (iii) -0.2, (iv) -0.1, (v) 0.0, (vi) 0.1, (vii) 0.2, and (viii) 0.3 V vs. SCE; (E) comparison of the fully oxidised cases for (i) ClO_4^-, (ii) Cl^-, (iii) HCO_3^-, and (iv) F^-.

4.6 - Summary

It has been shown that anion transfer for ClO_4^-, Cl^-, and HCO_3^- from the aqueous electrolyte phase into PPP microdroplets can be driven by the TPPMn(iii/ii) redox system. Some of these systems are more reversible than others, with Cl^- and ClO_4^- being close to reversible systems. The case for HCO_3^- is slightly different and a second process corresponding to the expulsion of a proton arises; this is therefore a net process of CO_3^- transfer. A mesoporous thin film ITO nanoparticle electrode was employed in spectroelectrochemical measurements. This electrode was optically transparent and could therefore be used to obtain data on the UV/Vis absorption of the TPPMn as a function of potential. Using this method, the potassium fluoride electrolyte system proved to behave in a different fashion to the others, showing a direct complexation of a fluoride anion to the Mn metal centre. This preliminary work with the ITO nanoparticle electrode illustrates its potential in other uses where mechanistic aspects of ion transfer need to be more fully understood. This type of system could also be used as a spectroelectrochemical sensor- one of similar design [(129)] is a TPPMn based sensor for the detection of perchlorate using chromomeric ion transfer reactions to operate.

Chapter 5

Electrochemical Bicarbonate and Carbonate Capture Facilitated by Boronic Acids

Contents

Published - "Liquid|Liquid Electrochemical Bicarbonate and Carbonate Capture Facilitated by Boronic Acids " in Chemical Communications, 2011, **47,** 43, 12002-12004

5.1 - Abstract

For a tetraphenylporphyrin-Mn (III) chloride (TPPMn) system dissolved within microdroplets of 4-(3-phenylpropylpyridine) (PPP), reversible transfer of bicarbonate and carbonate across the liquid | liquid interface is driven electrochemically and shown to be facilitated across a wide pH range by the utilization of 2-napthylboronic acid. The bicarbonate transfer was shown to have a potential of –0.08V *vs.* SCE and a binding constant of $K_{AB} = 10^2$ mol^{-1} dm^{-3}, whilst the carbonate dianion was seen to have a transfer potential of 0.07V *vs* SCE and a binding constant $K_{AB2} = 2 \times 10^{10}$ mol^{-2} dm^6.

5.2 - Introduction

We have seen how at the triple phase boundary of microdroplets in an aqueous electrolyte there is an ion transfer accompanying the transfer of electrons[130]. This has been shown to be useful for such applications as sensing[131], and in medical applications such as screening and product development[132]. Recent studies have shown that voltammetric techniques can be utilized to study facilitated transfer; this is when the ion transfer process is paired with a complexation in the microdroplet organic phase[133,134]. A range of facilitated ion transfer is known from the literature[135], and for this study boronic acid is used. Boronic acid has been used in previous studies as a facilitator for a wide range of transfers[136], from sugars and diols[137] to some more complicated molecules such as α-aminocarboxylates and α-hydroxycarboxylates[136]. In this report, the napthylboronic acid was utilized for the complexation to the carbonate dianion, and the results obtained for the system were analysed, resulting in quantitative results.

The redox system dissolved within the microdroplets that underwent electrochemical reduction and oxidation was tetraphenylporphyrin-Mn(III) chloride (TPPMn). Previous work in this field utilizing this molecule has shown transfer of a variety of ions including nitrate, perchlorate and thiocyanate[138], and a range of carboxylates[139].

5.3 – Experimental

5.3.1 - Chemicals

The reagents 4-(3-phenylpropyl)-pyridine (Aldrich, 97%), tetraphenylporphyrin-Mn (III) chloride (TPPMn) (Aldrich 95%), Napthylboronic acid, phosphoric acid (Fischer Scientific, 85% wt), sodium hydroxide (Aldrich >97%), were used without further purification. Filtered and demineralised water was taken from a Thermo Scientific purification system with resistivity not less than 18.2 MOhm cm. Experiments were conducted at a temperature of 20 ± 2^{o}C.

5.3.2 - Instrumentation

An Ivium Technologies Compactstat potentiostat (release v1.725) was used as the potentiostat for electrochemical experiments. A standard three electrode cell was used with the working electrode consisting of a basal plane pyrolytic graphite (bppg) electrode with a diameter of 4.9 mm (mounted in Teflon®) and used in conjunction with a platinum wire counter electrode and a KCl - saturated calomel reference electrode (SCE, REF401, Radiometer).

5.3.3 - Electrode Preparation Procedures

The deposition of random microdroplet arrays was achieved by evaporation of an acetonitrile solution containing TPPMnCl and PPP (typically 4 mg and 6 mg respectively in 6 ml of acetonitrile) onto a freshly polished bppg electrode. Room temperature evaporation of the acetonitrile resulted in a random array of PPP microdroplets on the graphite electrode surface. The final volume of PPP varied with deposition volume (typically 10 nL on a 4.9 mm diameter disc). The electrode surface was renewed by removing the top layer of graphite by polishing on P1000 silicon carbide polishing paper.

5.4 – Voltammetry of TPPMn in Sodium Bicarbonate Solution

An 80mM solution of TPPMn in PPP was prepared and deposited onto a graphite disc and then immersed in a solution of 0.1M sodium bicarbonate ($NaHCO_3$). Figure 5.1 shows a typical cyclic voltammogram for TPPMn for this system and showed two processes occurring. One occurred with a mid-point potential of approximately –0.08V *vs.* SCE and was consistent with bicarbonate transfer from the aqueous phase to the organic phase, as shown in equation 5.1.

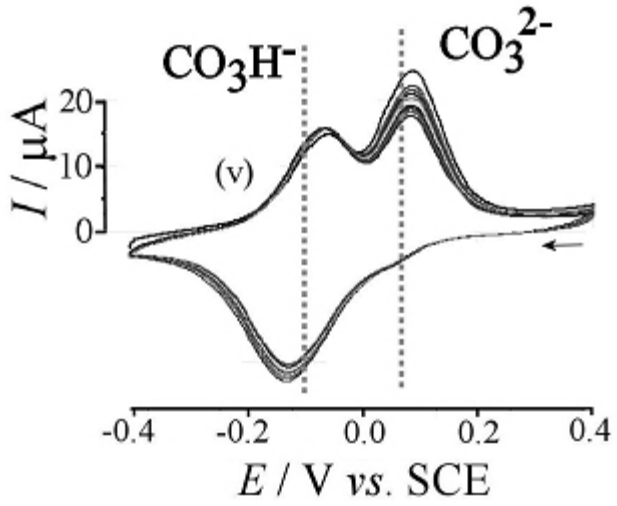

Figure 5.1 - Cyclic voltammograms at a scan rate of 50 mVs^{-1} for 80 mM TPPMn(III) in PPP, 70nL,deposited onto a graphite disc, immersed in 0.1 M carbonate solution ($NaHCO_3^-$) at pH 6.

(Equation 5.1)

$$Mn(II)_{(org)} + HCO_3^-{}_{(aq)} \rightleftarrows Mn(III)_{(org)} + HCO_3^-{}_{(org)} + e$$

A second process would be seen to occur at more positive potential with a mid point of 0.07 *vs.* SCE. This process corresponded to an expulsion of a proton from the organic phase.

(Equation 5.2)

$$Mn(II)_{(org)} + HCO_3^-{}_{(org)} \rightleftarrows Mn(III)_{(org)} + CO_3^-{}_{(org)} + H^+_{(aq)} + e$$

These two mechanisms together create a net process of carbonate dianion tranfer (equation 5.3). The second process, which entails the expulsion of a proton from the organic phase is an energetically unfavourable process and hence will only be seen when it is able to successfully compete with the first process -this occurs at high scan rates and larger droplet sizes-. It is proposed that due to the larger droplet sizes, and hence decreased triple phase boundary (as a result of aggregation of the droplets), the less energetically favourable expulsion of a proton occurs, as the electrochemical reactions are simply less effective. At slow scan rates however, there is sufficient time for the most energetically favourable process to dominate.

(Equation 5.3)

$$2\ Mn(II)_{(org)} + H_2CO_{3(org)} \rightleftarrows 2\ Mn(III)^+_{(org)} + CO_3^{2-}{}_{(org)} + 2\ H^+_{(aq)} + 2\ e^-$$

5.4.1 – Facilitation of Ion Transfer with Napthylboronic Acid

Addition of the 2-napthylboronic acid as a facilitator caused a few interesting observations in the voltammograms. Figure 5.2 shows cyclic voltammograms of TPPMn with increasing amounts of the boronic acid added into the PPP droplets alongside the TPPMn.

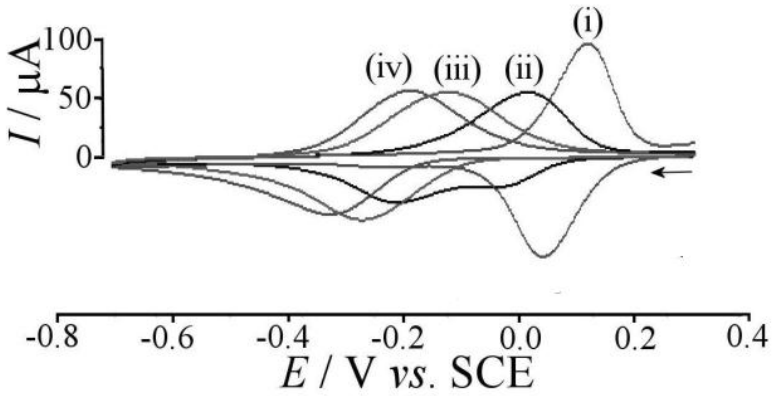

Figure 5.2- Cyclic voltammograms at a scan rate 50 mVs^{-1} for 80mM TPPMn in PPP, 70nL, immersed in 0.1 M carbonate solution (i-iv) at pH 9.9 with (i) 0, (ii) 0.35, (iii) 0.85, and (iv) 2.5 mol dm^{-3} 2-naphthylboronic acid (NBA) added

The voltammograms showed a very clear and distinct shift of the mid point potentials as a function of increasing napthylboronic acid concentration, indicating a complexation of the bicarbonate by the napthylboronic acid. The proposed mechanism for this is shown in equation 5.4 as well as the mathematical expression (Equation 5.5) for the shift in mid point potential.

(Equation 5.4)

$$Mn(II)_{org} + HCO_3^-{}_{(aq)} + NBA_{(org)} \rightleftarrows Mn(III)^+{}_{(org)} + (NBA)HCO_3^-{}_{(org)} + e^-$$

(Equation 5.5)

$$E_{rev1/2} = E^{0'} + \frac{RT}{F}\ln\left(\frac{c_0}{2}\right) - \frac{RT}{F}\ln\left([\mathrm{A}^{-}(aq)]\right) + \Delta E_{mid}$$

Where…

$$\Delta E_{mid} = \frac{RT}{F}\ln\left(\frac{1}{[\mathrm{A}^{-}{}_t(\mathrm{oil})}\left(-\frac{X}{2}+\sqrt{\frac{X^2}{4}+\frac{[\mathrm{A}^{-}{}_t(\mathrm{oil})}{K_{AB}}}\right)\right)$$

And…

$$X = 1/K_{AB} - [\mathrm{A}^{-}{}_t(\mathrm{oil})] + [\mathrm{B}_t(\mathrm{oil})]$$

$$K_{AB} = \frac{[\mathrm{AB}^{-}(\mathrm{oil})]}{[\mathrm{A}^{-}(\mathrm{oil})]\times[\mathrm{B}(\mathrm{oil})]}$$

For the above equations the terms $[A^-(oil)]$ and $[B^-(oil)]$ are defined as the total and known concentration of the anion and boronic acid respectively in the PPP oil phase; these are known from the initial make-up of the deposition mixture. The initial concentration of TPPMn is defined by the term c_0. $E^{0'}$ is the formal potential for the redox system, this includes the contribution that arises from the organic | aqueous phase boundary. F is the Faraday constant, R the gas constant and T the temperature.

The shift observed for the mid point potential as a function of napthylboronic acid concentration is compared to the theoretical values for a mono anion transfer of HCO_3^-. This is illustrated in figure 5.3 with the theory values shown as the solid lines on the graph with the experimental values illustrated as the data points. Three values

of binding constants were selected for the theory lines, (iii) corresponds to K_{AB} = 10 mnol^{-1} dm^3, (iv) to K_{AB} = 100 mol^{-1} dm^3, and finally (v) to K_{AB} = 1000 mol^{-1} dm^3. A good correlation with the experimentally obtained data points is shown when utilizing a binding constant of 100 mol^{-1} dm^3, and thus provides a good value for the interaction of the HCO_3^- anion with the napthylboronic acid in the organic PPP microdroplets.

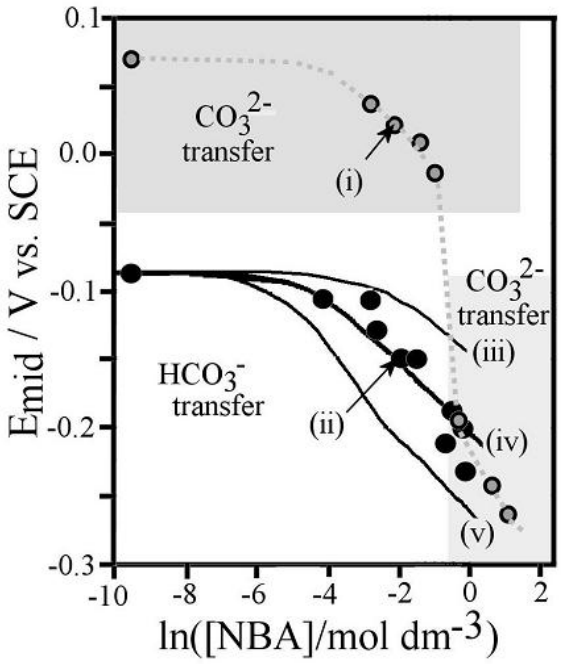

Figure 5.3 - Plot of E_{mid} potentials versus NBA concentration for (i) pH 9.9 and (ii) pH 6. Theory lines for K_{AB} = (iii) 10 (iv) 100, (v) 1000 mol^{-1}dm^3.

It is worth noting that a deviation from the good fit with this binding constant was seen when higher concentrations (0.5M and above) were utilized within the PPP microdroplets. This was seen as a further shift to more negative potentials. A net double complexation was proposed for the amalgamation of the data from the CO_3^{2-} and HCO_3^-, this is shown in equation 5.6.

(equation 5.6)

$$2\ Mn(II)_{(org)} + CO_3^{2-}{}_{(aq)} + 2NBA_{(org)} \leftrightarrow 2\ Mn(III)^{+}{}_{(org)} + (NBA)_2CO_3^{2-}{}_{(org)} + 2e^-$$

Analysing this net double complexation through a spreadsheet is possible, however requires the use of Matlab in order to solve the cubic equation that arises. Elimination of the cubic term for $[B_t(oil)] >> 2[A^{2-}{}_t(oil)]$ allows for the approximate mathematical expression for the mid point potential shift to be expressed.

(Equation 5.7)

$$E_{rev1/2} = E^{0'} + \frac{RT}{2F}\ln\left(\frac{c_0}{4}\right) - \frac{RT}{2F}\ln\left([A^{2-}(aq)]\right) + \Delta E_{mid}$$

Where

$$\Delta E_{mid} = \frac{RT}{2F}\ln\left(\frac{1}{[A^{2-}{}_t(oil)}\left(-\frac{Y}{2}+\sqrt{\frac{Y^2}{4}-Z}\right)\right)$$

$$Y = \frac{4K_{AB_2}[A^{2-}{}_t(oil)]^2 - 4K_{AB_2}[B_t(oil)][A^{2-}{}_t(oil)] + K_{AB_2}[B_t(oil)]^2 + 1}{4K_{AB_2}[B_t(oil)] - 8K_{AB_2}[A^{2-}{}_t(oil)]}$$

$$Z = \frac{[A^{2-}{}_t(oil)]}{8K_{AB_2}[A^{2-}{}_t(oil)] - 4K_{AB_2}[B_t(oil)]}$$

$$K_{AB_2} = \frac{[AB_2{}^{2-}(oil)]}{[A^{2-}(oil)]\times[B(oil)]^2}$$

Using the experimentally derived data points from the facilitated transfer of carbonate (as shown in equation 5.7, using an assumed transfer potential for the CO_3^{2-} of 0.07V *vs* SCE which is consistent with other di-anionic carboxylate transfers) [140] a value for the binding constant is estimated as $K_{AB2} = 2 \times 10^{10}$ mol^{-2} dm^6. This shows a much stronger binding of this dianion when compared to that of the mono-anion. The second binding constant can be derived as $2 \times 10^{10} / 100 = 2x\ 10^8$ mol^{-1} dm^3. This can be compared with the bascisity in water $K_{B1} = 10^{6.3}$ mol^{-1} dm^2 and $K_{B2} = 10^{10.3}$ mol^{-1} dm^2 and $K_{B1} \times K_{B2} = 10^{16.6}$ mol^{-2} dm^6 for carbonate in water[141].

5.5 - Summary

This work has shown, and quantified, the facilitated reversible ion transfer of bicarbonate and carbonate using napthylboronic acid as the facilitator. This facilitation occurs strongly in the pH ranges of 6 to 11. Using this premise one can envision future work based on boronic acid containing membranes which would be able to sift out bicarbonates and carbonates from systems. For a more biological application of this within lipophilic systems, synthesis of the boronic acid derivative would need to be performed in order to create more suitable molecular structures.

Final Comments

The first two experimental chapters of this report yielded interesting and important information of microdroplets and the photo-electrochemical reactions that occur within. Characterization of how processes occur within the droplets for both dark and illuminated conditions were explored for rhodamine b and pentoxyresorufin. This also yielded information on the various chemical steps that occur within the droplets such as the disproportionation of rhodamine b, or the photo catalysis of duroquinone's oxidation by pentoxyresorufin. Using a variety of techniques, some of these chemical steps were able to be fully characterized also providing quantitative data on the rate constants.

Perhaps one of the most surprising results from these chapters was the role that the PPP played within the system. Initially it was assumed that the PPP acted as merely a bystander, simply being the solvent for the droplets. Evidence from both the rhodamine b and pentoxyresorufin systems however, clearly implicated the PPP as an active player in the photoreactions, with EPR evidence tentatively suggesting an excited pair between the pentoxyresorufin and the PPP. This has implications for other work in this field, as the ability to switch on photo reactions (as we have observed PPP to do), could be very useful in any light themed liquid | liquid research. It was also found that the PPP surface could be protonated, which led to changes in mechanism for the voltammetry of pentoxyresorufin dissolved within. This could be

utilized if one wanted a further element of control over what reactions and ion exchanges took place across the liquid | liquid interface.

Throughout the research conducted for this report, various alternative methods have been applied to help discern and account for the data produced, for example utilizing surface tension to investigate PPP surface effects, later attributed to protonation. One of the most useful to be utilized however was *in situ* UV/Vis of the microdroplet arrays whilst conducting voltammetry as a method for gaining further information on ion exchange and other such processes. When paired with an ITO nanoparticle electrode, a powerful tool is created for any triple phase work where additional information is required on mechanistic aspects on ion transfer that voltammetry on its own simply cannot provide.

A firm platform has been built with this work, however more needs to be done in future in order to drive this vein of research forward. A full and thorough understanding of the pentoxyresorufin / PPP excited pair effect that was observed would be essential and once understood in more detail, this could hopefully be used to further the research, perhaps even pointing in the direction of other solvents and oils which can facilitate photoreactions. With an understanding of the mechanism that caused the observed effect of the photoexcited pair, one can also envisage more experimental control over how photoreactions take place and the possibility to tune a system to desired specifications.

Acknowledgements

There are many people who deserve thanks for seeing me through the last few years;

At the University of Bath, everyone in the Marken Group, both past and present, and MChem student Xiaohang Zhang. Funding bodies EPSRC and NSF for financial support, and also specialized help from the EPSRC UK National EPR Service at the University of Manchester. There are some individuals, however, to whom I owe a special thanks.

Prof. Frank Marken, for giving me the opportunity to embark on this journey in the first place, for his knowledge and unflappable optimism, even in the face of experimental disaster.

Abie Wilson, for keeping me on track, for always being there, and without whom this thesis would be riddled with spelling errors and far too many commas, all in the wrong places.

Prof. Gary Blanchard –this project's main collaborator at Michigan State University- for his insights and for making my research visit to Michigan both successful and enjoyable.

John Watkins, for his friendship over the course of this PhD; without him the last few years in the lab would have been nowhere near as fun.

My parents, for their support, and for always keeping a light on at home for me every time I wanted to escape the city and disappear into the mountains for a few days.

References

(1) H. Karami, F. Taala, *Journal of Power sources,* 2011, 196, **15,** 6400-6411
(2) Z.M. Xue, B. H. Zhao, C.H. Chem, *Journal of Power Sources,* 2011, 196, **15**, 6478-6482
(3) Y.C. Lu, D.G. Kwabi, K.P.C. yao, J. R. Harding, J.G. Zhou, L Zuin, Y. Shao-Horn, *Energy and Environmental Science,* 2011, 4, **8**, 2999-3007
(4) A. Heller, B. Feldman, *Accounts of Chemical Research,* 2010, 43, **7**, 963-973
(5) B. Oregan, M. Gratzel, *Nature,* 1991, **353**, 737-740
(6) Y. Liu, X.H.Sun, Q.D Tai, H. Hu, B.L. Chen, N. Huang, B. Sebo, X.Z.Zhao, *Journal of Alloys and Compounds* 2011, 509, **37**, 9264-9270
(7) M. Plotkin, I. Hod, A. Zaban, S.A. Boden, D.M. Bagnall, D. Galushko, D.J. Bergman, *Naturewissenschaften*, 2010, 97, **12**, 1067-1076
(8) A. Ghahremaninezhad, E. Asselin, D.G. Dixon, *Journal of Physical Chemistry,* 2011, 115, **19**, 9320-9334
(9) L.M.A Monzon, F. Byrne, J.M.D. Coey, *Journal of Electroanalytical Chemistry,* 2011, 657, **1-2**, 54-60
(10) M.D. Mechada, E.V. Soares, H.M.V.M. Soares. *Enviromental Science and Polution,* 2011, 18, **8**, 1279-1285
(11) J.B. Raoof, R. Ojani, S.M. Golabi, A.E Hamidi, M.S. Hejazi. *Sensors and Actuators B-Chemical,* 2011, 157, **1**, 195-201
(12) A. Ahmadalinezhad, A.C. Chen, *Biosensors and Bioelectronics*, 2011, 26, **11**, 4508-4513
(13) C.V.G. Reddy, S.V. Manorama. *Journal of the Electrochemical Society*, 2000, 147, **1**, 390-393 H2 one
(14) S. Faiardo, D.M. Bastidas, M. Criado, M. Romero, J.M. Bastidas, *Construction and Building Materials*, 2011, 25, **11**, 4190-4196
(15) L. Abosrra, A.F. Ashour, M. Youseffi, *Construction and Building Materials*, 25, **10**, 3915-3925
(16) Q.Y. Cai, Z.M. Gu, T.M. Fu, Y. Liu, H.C. Song, F.S. Li, *Polymer Bulletin*, 2011, 67, **4**, 571-582
(17) C.D. Vectis, M.H. Schnoor, M.S. Rahaman, J.D. Schiffman, M. Elimelech, *Enviromental Science and Technology*, 2011, 45, **8**, 3672-3679
(18) J. Yang, L.D. Zou, H.H. Song, Z. P. Hao, *Desalination*, 2011, 276, **1-3**, 199-206
(19) Electrochemical Methods – Fundamentals and Applications *Second Edition*. A.J. Bard, L.R. Faulkner
(20) R.W. French, A.M.Collins, F. Marken, *Electroanalysis*, 2008, 20, **22**, 2403-2409
(21) J.A. Rodrigues, C.M. Rodrigues, P.J. Almeida, I.M. Valente, L.M. Goncalves, R.G. Compton, A. Aquiles. *Analytica Chimica Acta*, 2011, 701, **2**, 152-156
(22) J. Vacek, E. Vrublova, M. Kubala, M. Janovska, M. Fojita, E. Simkova, J Styskala, J Skopalova, J. Hrbac, J. Ulrichova. *Electroanalysis*, 2011, 23, **7**, 1671-1680
(23) X. Zhao, H.J. Liu, J.H. Qu. *Catalysis Communications,* 2010, 12, **2** 76-79
(24) C.Y. Cummings, G. Zoppi, I. Forbes, P.J. Dale, J.J. Scragg, L.M. Peter, KG Kohn, F. Marken. *Journal of Electroanalytical Chemistry,* 2010, 645, **1**, 16-21

(25) Electrochemistry- Principles, Methods and Applications. C.M.A. Brett, A.M.O. Brett
(26) Modern Electroplating, *fourth edition*. Edited by Mordechay Schlesinger and Milan Paunovic
(27) Electrode Dynamics. A.C. Fisher
(28) Atkins' Physical Chemistry, seventh edition. Peter Atkins, Julio de Paula
(28a) B.A. Howell, V.S. Cobb, R.A. Haaksma. *Journal of Chemical Education*, 1983, **60**, 4, 273-273
(29) Electrochemical Methods – Fundamentals and Applications (*second edition).* Allen J. Bard and Larry R. Faulkner
(30) J. Wang, *Analytical Electrochemistry*, Wiley-VCH, 2nd edition 2000
(31) Understanding Voltammetry. R.G. Compton, C.E. Banks.
(32) R.P Akkermans, S.L. Roberts, R.G. Compton, *Chemical Communications* 1999**, 12**, 1115-1116
(33) M. Richterova, V. Lisy, *Journal of Biological Physics* 2003, **29**, 55-61
(34)L. Stryer, *Biochemistry*, W.H. Freeman and Company, Washington DC, 1995.
(35) U. Seifert. *Advances in Physics*, 1997, **46**, 1, 13-137
(36) L. Chuanhao, F. Wang J. C. Yu, *Energy and Environmental Science.* 2011, **4**, 100
(37) W. Nernst, E. H. Riesenfield, *Annals of. Phyics*. 1901, **8**, 600-608
(38) C .Gavach, T. Mlodnicka, and J. Guastalla, *Comptes Rendus Hebdomadaires des Seances de L'academie des Sciences Serie C*, 1968, **266**, 1196
(39) E. G. Akegemci, B. Haluk, O. Mehmet, E. Mustafa. *Acta Physio-Chimica Sinica*,
(40) C. L. Camara, C. A. Bornancini, J. L Cabrera, M. G. Ortega, L. M. Yudi. *Talanta*, 2010 **83,** 2, 623-630
(41) *C*. Gavach, *Experientia Supplementum, no 18. Biological Aspects of Electrochemistry*, 1971, **18**, 321
(42) D. W. M. Arrigan. *Analytical Letters*, 2008, **41**, 18, 3233-3252,
(43) S. M. MacDonald, M.Opallo, A. Klamt, F. Eckert and F. Marken. *Physical. Chemistry Chemical Physics*, 2008, **10,** 26, 3925-3933
(44) F. raymon, D. Fermin, H.J. Lee, H.H. Girault, *Electrochemica Acta,* 199, **45**, 2647-2662
(45) P.S. Pershan, *Faraday Discussions* 1990, **89,** 231-245
(46) I. Benjamin, *Annual Review of Physical Chemistry* 1997, **48,** 407-451
(47) M. Gros, S Gromb, C. Gavech, *Journal of Analytical Chemistry* 1978, **89**, 29-36
(48) Z Samec, V. Marecek, J. Weber, D. Homolka, *Journal of Analytical Chemistry* 1981, **126,** 105-119
(49) W. Schmickler, *Journal of Electroanalytical Chemistry* 199, **126**, 105
(50) F. Scholz, S Komorsky-Lovric, M.Lovric. *Electrochemistry Communications* 2000, **2**, 112
(51) F. Marken, R. D. Webster, S. D. Bull, R. D. Davies. *Journal of Electroanalytical Chemistry*, 1997, **437**, 209
(52) C. E. Banks, T. J. Davies, R. G. Evans, G. Hignett, A. J. Wain[a], N. S. Lawrence, J. D. Wadhawan, F. Marken, R. G. Compton *Physical. Chemistry Chemical Physics*, 2003, **5,** 4053 – 4069
(53) J. D. Wadhawen, A. J. Wain, A. N. Kirkham, D. J. Walton, B. Wood, R R France, S. D. Bull, R. G. Compton, *Journal of the American Chemical Society*, 2003, **125,** 37, 11418-11429

(54) M. Powell, J. C. Ball, Y.-C. Tsai, M. F. Sua´rez and R. G. Compton, *Journal of Physical Chemistry B*, 2000, **104**, 8268
(55) J. E. Dubois, A. Desbene-Monvernay and P. C. Lacaze, *Journal of Electroanalytical Chemistry*, 1976, **72**, 353
(56) J. Niedziolka, K. Szot, F. Marken, M. Opallo, *Electroanalysis* 2007, **19**, 155.
(57) D. Rayner, N. Fietkau, I. Streeter, F. Marken, B.R. Buckley, P.C. Bulman-Page, J. del Campo, R. Mas, F. X. Munoz, R.G. Compton, *Journal of Physical Chemistry C* 2007, **111**, 9992.
(58) M. Donten, E. Bak, M. Gniadek, Z. Stojek, F. Scholz. *Electrochemica Acta.* 2008, **53**, 5608.
(59) E. Bak, M. Donten, Z. Stojek. *Journal of Electroanalytical Chemistry*, 2007, **600**, 45
(60) U. Schreder, R.G. Compton, F. Marken, S.D. Bull, S.G. Davies, S. Gilmour. *Journal of Physical Chemistry B.* 2001, **105**, 1344
(61) S. Macdonald, M Oppalo, A Klamt, F Eckert, F Marken. *Physical Chemistry Chemical Physics*, 2008, **10**, 3925
(62) S.M. MacDonald, J.D. Watkins, S.D. Bull, I.R. Davies, Y. Gu, K,Yunus, A.C. Fisher, P.C. Bulman-Page, *Journal of Physical Organic Chemistry*, 2009**, 22**, 52-58
(63) C. Lledo-Fernandez, I. Hatay, M.J. Ball, G.M. Greenway, J. Wadhawen. *New Journal of Chemistry*, 2003, **5**, 3748
(64) A.M Kelly, N. Katif, T.D.James, F. Marken, *New Journal of Chemistry*, 2010, **34**, 1261
(65) R.W. French, S.N. Gordeev, P.R. Raithby, Marken F. *Journal of Electroanalytical Chemistry*, 2009, **632**, 206-210
(66) R. W. French, A.M. Collins, F. Marken, *Electroanalysis*, 2008, **20**, 2403–2409.
(67) R. W. French, F. Marken. *Journal of Solid State Electrochem*istry, 2009, **4**, 609-617
(68) R.W. French, Y. H. Chan, P.C. Bulman-Page, F. Marken. *Electrophoresis*, 2009, **30**, 3361-3365
(69) W. Ehrfeld, V. Hessel, H. Lowe. *Microreactors*, Weinheim, 2000. p. 166.
(70) C.A. Paddon, M. Atobe, T. Fuchigami, P. He, P. Watts, S.J. Haswell, G.J. Pritchard, S.D. Bull, F. Marken, *Journal of Applied Electrochemistry*, 2006, **36**, 617.
(71) S. Suga, J. Synth. *Organic Chemistry Japan* 2006, **64**, 1010.
(72) C. A. Paddon, G.J. Pritchard, T. Thiemann, F. Marken, *Electrochemistry Communications, 2002, **4**, 10, 825-831*
(73) T. Tajima, T. Fuchigami, *Angewante Chemie International edition*, 2005, **44**, 4760.
(74) R. Horcajada, M. Okajima, S. Suga, J. Yoshida, *Chemical Communications*, 2005,1303
(75) S.M. MacDonald, J.D. Watkins, Y. Gu, K. Yunus, A.C. Fisher, G. Shul, M. Opallo, F. Marken, *Electrochemistry Communications*, 2007, **9**, 2105.
(76) S.M. MacDonald, J.D. Watkins, S.D. Bull, I.R. Davies, Y. Gu, K,Yunus, A.C. Fisher, P.C. Bulman-Page, *Journal of Physical Organic Chemistry*, 2009**, 22**, 52-58
(77) J.D. Wadhawan, F. Marken, R.G. Compton, *Pure and Applied Chemistry*, 2001, **73**, 12, 1947-1955
(78) O. Behrend, K. Ax, H. Schubert. *Ultrasonics Sonochemistry*, 2000, **7,** 77,

(79) S. Liu, Y. Gu, R.B. Le Roux, S.M. Matthews, D. Bratton, K. Yunus, A.C. Fisher, W.T.S. Huck. *Lab on a Chip*, 2008, **9**¸ 1937-1942
(80) J.D. Wadhawan, F. Marken, R.G. Compton, *Pure Applied Chemistry*, 2001, **73**, 12, 1947-1955
(81) Broadening Electrochemical Horizons, A.M. Bond, Oxford University Press, Oxford, 2002
(82) M. Vannekamp, J. Janek, *Journal of the Electrochemical Society*, 2003, **150**, 723
(83) K. Peppler, M. Polleth, S. meiss, M. Rohnke, J. Janek, *Physical Chemistry Chemical Physics.* 2006, **220**, 1507
(84) W. Vonau, W. Oelssner, J. Zosel, H.Kohler. *TM Technisches Messen*, 2010, **77**, 5
(85) R.M. Lambert, F. Williams, A. Palermo, M.S. Tikhov, *Topics in Catalysis*, 2000, **13**, 91
(85a) M Gratzel, *Journal of Photochemistry and Photobiology C, Photochemistry Reviews*,2003, **4**, 145-153
(86) L. Peter. *Accounts of Chemical Research*, **2009**, 42, 1839
(87) D. Gust, T.A. Moore, A.L. Moore. *Accounts of Chemical Research*, 2009, **42**, 12, 1890-1898
(88) W.J. Youngblood, S-H.A. Lee, Y. Kobayashi, E.A. Hernadez-Pagen, P.G. Hoertz, T.A. Moore, D. Gust, T.E. Mallouk, *Journal of the American Chemical Society*,. 2009, **131**, 926-927
(89) Liquid | Liquid Interfaces, theory and methods. G. Volkov, D.W. Dreamer, CRC London 1996
(90) A.G. Volkov, M. I. Gugeshashvili, D.W. Dreamer. *Electrochemica Acta*, 1995, **40**, 2849
(91) A.J. Wain, J.D. Wadhawan, R.G. Compton, *ChemPhysChem.* 2003, **4¸9,** 974-982
(92) J.D. Wadhawan, A.J. Wain, A.N. Kirkham, D.J. Walton, B. Wood, R.R. France, S.D. Bull, R.G. Compton. *Journal of the American Chemical Society*, 2003, **125**, 37, 11419-11429
(93) J.D. Wadhawan, R.G. Compton, F. Marken, S.D. Bull, S.G. Davies, *Journal of Solid State Electrochemistry*, 2001, **5**, 301-305
(94) F. Marken, J.D. Watkins, A.M. Collins. *Physical Chemistry Chemical Physics*, 2011, **13**, 21, 10036-10047
(95) J.D. Wadhawan, R.G. Compton, F. Marken, S.D. Bull, S.G. Davies, *Journal of Solid State Electrochemistry*, 2001, **5**, 301-305
(96) U. Schroder, J.D. Wadhawan, R.G. Evans, R.G. Compton, B. Wood, D.J. Walton, R.R. France, F. Marken, P.C.B. Page, C.M. Hayman. *Journal of Physical Chemistry C*, 2002, **106**, 8697
(97) A.M. Collins, X. Zhang, J.J. Scragg, G.J. Blanchard, F. Marken. *ChemPhysChem.* 2010, **11**, 2862-2870
(98) V.E. Korobov, A.K.Chibisov, *Journal of Photochemistry*, 1978, **9**, 411-424
(99) S. Becker, I. Gregor, E. Thiel. *Chemical Physics Letters*, 1998, **283**, 350-356
(100) V.E. Korobov, V.V. Shubin A.K.Chibisov, *Chemical Physics Letters*, 1977, **45**, 498-501
(101) R. Menzel, E. Thiel, *Chemical Physics Letters*, 1998, **291**, 237-343
(102) S.W. Hong, W.H. Jo, *Polymer*, 2008, **49**, 4180-4187
(103) S.Q. Han, E.B. Liu, H. Li, *Microchimica Acta*, 2005, **149**, 281-286
(104) J. Huang, D. Stockwell, A. Boulesbaa, J.C. Guo, T.Q. Lian, *Journal of Physical Chemistry C*, 2008, **112**, 5203-5212
(105) Dye Laser Principles. F. J. Duarte and L. W. Hillman, 1990

(106) L.T. Jin, J.K.Choi, *Electrophoresis*, 2004, **25**, 2429-2438
(107) U. Kruger, R. Memming, *Berichte der Bunsen-Gesellschaft-Pysical Cchemistry Chemical Physics*, 1974, **78**, 679-
(108) T. Oskai, H. Yamada, H. Nagatani, T. Sagara, *Journal of Physical Chemistry. C*, 2007, **111**, 9480-9487
(109) L. Bahadur, J.P. Pandey, *Indian Journal of Chemical Technology*,. 1994, **1**, 53-59
(110) A.G. Volkov, M.I. Gugeshashvill, D.W. Deamer, *Electrochimica Acta*,. 1995, **40**, 2849-2868
(112) M.P.N. Bui, C.A. Li, K.N. Han, J. Choo, E.K. Lee, G.H. Seong. *Analytical Chemistry.* 2011, **83**, 5, 1603-1608
(113) A.T.A. Jenkins, H.A. Dash, S. Boundy, C.M. Halliwell, R.H. French-Constant. *Bioelectrochemistry* 2006, **68,** 67
(114) Electroanalytical Methods – Guide to Experiments and Applications. F Scholz, 2nd Revised and Extended Edition.
(115) Molecular Theory of Capillarity, J.S. Rowlinson, B Widom., Oxford University Press. Chapman and Hall, London 1981
(116) G. Hughs, M.R. Bryce, *Journal of Physical Chemistry A*, 2003, **107,** 11587
(117) Electrochemistry of Immobilized Particles and Droplets, F. Scholz, U. Schröder, R. Gulaboski, , Springer, Berlin, 2005.
(118) F. Marken, J.D. Watkins, A.M. Collins, *Physical Chemistry Chemical Physics*. 2011,**13**, 10036.
(119) F. Scholz, R. Gulaboski, *ChemPhysChem* 2005, **6**, 16.
(120) F. Marken, R.D. Webster, S.D. Bull, S.G. Davies, *Journal of Electroanalytical Chemistry* 1997, **437**, 209.
(121) N. Katif, R.A. Harries, A.M. Kelly, J.S. Fossey, T.D. James, F. Marken, *Journal of Solid State Electrochem*istry 2009, **13**, 1475.
(122) M.A. Ghanem, F. Marken, *Electrochemistry Communications*, 2005, **7**, 1333.
(123) J. Niedziolka, M.A. Murphy, F. Marken, M. Opallo, *Electrochimica Acta*, 2006, **51**, 5897.
(124) J. Niedziolka, K. Szot, F. Marken, M. Opallo, *Electroanalysis.* 2007, **19**, 155.
(125) E Komorsky-Lovric, V. Mirceski, C Kabbe, F. Scholz, *Journal of Electroanalytical Chemistry.* 2004, **2**, 566,371-377
(126) M.J. Bonné, C. Reynolds, S. Yates, G. Shul, J. Niedziolka, M. Opallo, F. Marken, *New Journal of Chem*. 2006, **30**, 327.
(127) J. Niedziolka, K. Szot, F. Marken, M. Opallo, *Electroanalysis*, 2007, **19**, 155.
(128) L.J. Boucher, *Coordination Chemistry Reviews*, 1972, **7**, 289.
(129) A.S. Hinman, K. McGarty, C. Tang, B.J. Pavelich, *Canadian Journal of Chemistry*, 1989, **67**, 545.
(130) Liquid-liquid interfaces, theory and methods, A.G. Volkov and D.W. Deamer, CRC Press, New York, 1996.
(131) D.S. Silvester and D.W.M. Arrigan, *Electrochemistry Communications,* 2011, **13**, 477.
(132) G. Bouchard, A. Galland, P.A. Carrupt, R. Gulaboski, V. Mirceski, F. Scholz and H.H. Girault, *Physical Chemistry Chemical Physics,* 2003, **5**, 3748.
(133) F. Marken, J.D. Watkins and A.M. Collins, *Physical Chemistry Chemical Physics*, **13**, 10036.
(134) C.E. Banks, T.J. Davies, R.G. Evans, G. Hignett, A.J. Wain, N.S. Lawrence, J.D. Wadhawan, F. Marken and R.G. Compton, *Physical Chemistry Chemical Physics,* 2003, **5**, 4053.

(135) H.H. Girault and D.J. Schiffrin, *Electroanalytical Chemistry,* 1989, **15**, 1-141
(136) N. Katif, R.A. Harries, A.M. Kelly, J.S. Fossey, T.D. James and F. Marken, J*ournal of Solid State Electrochemistry,* 2009, 13, 1475.
(137) R. Nishiyabu, Y. Kubo, T.D. James and J.S. Fossey, *Chemical Communications,* 2011, **47**, 1106.
(139) S.M. MacDonald, M. Opallo, A. Klamt, F. Eckert and F. Marken, *Physical Chemistry Chemical Physics,* 2008, **10**, 3925.
(140) M.J. Bonné, C. Reynolds, S. Yates, G. Shul, J. Niedziolka, M. Opallo and F. Marken, *New Journal of Chemistry* 2006, **30**, 327.
(141) *Physical Chemistry*, P.W. Atkins and J. de Paula, Oxford University Press, Oxford, 2006, p.1007.